University of North Dakota
UND Scholarly Commons

Theses and Dissertations | Theses, Dissertations, and Senior Projects

2014

Patterns and mechanisms of heat transport in the northern Denver Basin Nebraska, South Dakota and Wyoming

Aaron T. Ochsner
University of North Dakota

Follow this and additional works at: https://commons.und.edu/theses

 Part of the Geology Commons

Recommended Citation
Ochsner, Aaron T., "Patterns and mechanisms of heat transport in the northern Denver Basin Nebraska, South Dakota and Wyoming" (2014). *Theses and Dissertations*. 216.
https://commons.und.edu/theses/216

This Thesis is brought to you for free and open access by the Theses, Dissertations, and Senior Projects at UND Scholarly Commons. It has been accepted for inclusion in Theses and Dissertations by an authorized administrator of UND Scholarly Commons. For more information, please contact zeineb.yousif@library.und.edu.

PATTERNS AND MECHANISMS OF HEAT TRANSPORT IN THE NORTHERN DENVER BASIN: NEBRASKA, SOUTH DAKOTA AND WYOMING

by

Aaron Thomas Ochsner
Bachelor of Science, University of Nebraska-Omaha, 2011

A Thesis

Submitted to the Graduate Faculty

of the

University of North Dakota

in partial fulfillment of the requirements

for the degree of

Master of Science

Grand Forks, North Dakota
August
2014

UMI Number: 1567094

All rights reserved

INFORMATION TO ALL USERS
The quality of this reproduction is dependent upon the quality of the copy submitted.

In the unlikely event that the author did not send a complete manuscript
and there are missing pages, these will be noted. Also, if material had to be removed,
a note will indicate the deletion.

UMI 1567094

Published by ProQuest LLC (2014). Copyright in the Dissertation held by the Author.

Microform Edition © ProQuest LLC.
All rights reserved. This work is protected against
unauthorized copying under Title 17, United States Code

ProQuest LLC.
789 East Eisenhower Parkway
P.O. Box 1346
Ann Arbor, MI 48106 - 1346

This thesis, submitted by Aaron T. Ochsner in partial fulfillment of the requirements for the Degree of Master of Science from the University of North Dakota, has been read by the Faculty Advisory Committee under whom the work has been done and is hereby approved.

Dr. William D. Gosnold, Chairperson

Dr. Philip J. Gerla

Dr. Richard D. LeFever

This thesis is being submitted by the appointed advisory committee as having met all of the requirements of the School of Graduate Studies at the University of North Dakota and is hereby approved.

Wayne Swisher
Dean of the School of Graduate Studies

Date July 24, 2014

PERMISSION

Title Patterns and Mechanisms of Heat Transport in the Northern Denver Basin: Nebraska, South Dakota and Wyoming

Department Geology and Geological Engineering

Degree Master of Science

In presenting this thesis in partial fulfillment of the requirements for a graduate degree from the University of North Dakota, I agree that the library of this University shall make it freely available for inspection. I further agree that permission for extensive coping for scholarly purposes may be granted by the professor who supervised my thesis work or, in his absence, by the Chairperson of the department or the dean of the School of Graduate Studies. It is understood that any copying or publication or other use of this thesis or part thereof for financial gain shall not be allowed without my written permission. It is also understood that due recognition shall be given to me and to the University of North Dakota in any scholarly use which may be made of any material in my thesis.

Aaron T. Ochsner
August 1, 2014

TABLE OF CONTENTS

LIST OF FIGURES

LIST OF TABLES

ACKNOWLEDGEMENTS

I wish to express my gratitude to my advisor, Dr. William Gosnold, for his continued support and the scientific insight he provided. Much of the work for this project could not have been completed without the findings of several of Dr. Gosnold's earlier investigations. I would also like to thank my committee members, Dr. Richard LeFever and Dr. Philip Gerla, for their guidance and willingness to answer questions over the course of my studies.

Jesse Korus of the University of Nebraska's School of Natural Resources was exceptionally helpful in locating and gaining access to core samples used in laboratory analyses, and Dr. Paul Hsieh of the U.S. Geological Survey provided expert assistance in getting me acquainted with simulation software.

My appreciation also goes to my friends and fellow graduate students; Anna and James Crowell for their feedback and assistance on countless occasions, Prosper Gbolo for his encouragement and good humor, Godswill Njoku and Eric Zimny for their company in the field, and Matt Sebade for kindly providing some of the samples used for this project.

I am endlessly grateful to my parents, Steven and Rebecca Ochsner, for their unwavering love and support. I owe a great deal of my academic and personal success to them, and express my deepest gratitude to them for being such great role models. Finally, I would like to thank my girlfriend, Julia Fernandez, for her loving encouragement and enduring patience through the course of my research.

ABSTRACT

Finite difference simulations of the hydrothermal system of the northern Denver Basin are suggestive of a correlation between anomalous heat flux and the presence of faults and structural lineaments mapped in the region. Geothermal, hydrogeological, lithological, and structural data available for the northern Denver Basin were compiled and analyzed in an effort to determine the hydrothermal mechanisms responsible for observed heat flow anomalies in the study area. Measurement of thermal conductivity was conducted for 82 solid core samples and 60 unconsolidated samples from drill cuttings, yielding a harmonic mean thermal conductivity value of $1.52 \pm 0.91 W\ m^{-1}\ K^{-1}$ for the stratigraphic column of the study area. A total of 929 thermal gradient values compiled from several databases were incorporated with thermal conductivity data to produce a heat flow map of the study area, delineating prominent areas of anomalous heat flux. Data was processed using finite difference simulation software (Hydrotherm Interactive) developed by the U.S. Geological Survey for the purposes of modeling and predicting heat and fluid transport in porous media. Two-dimensional cross-sectional models were calibrated using heat flow profiles and available potentiometric surface data for the Madison and Dakota aquifers in the region. Although calibrated models resulted in accurate simulations of non-anomalous heat flow profiles, anomalous heat flow highs were not reproduced. Acknowledging the existence of several major faults and numerous structural lineaments documented in the study area, vertical pathways of fluid flow were added to simulations to recreate the effect of such structural features. Models which incorporated a

hypothetical linear fracture sufficiently accounted for previous discrepancies, and indicate probable upward advective flow through existing vertical fractures.

CHAPTER I

INTRODUCTION

Crustal heat transfer commonly occurs by means of three distinct mechanisms; convection, advection, and conduction. Although sedimentary basin settings are typically dominated by conductive heat transfer, several studies (Gosnold, 1984 & 1999; Schoon & McGregor, 1974) evaluating the geothermics of the Great Plains region have linked anomalous surface heat flow measurements to advective processes in confined aquifers. Basin-scale geothermal profiles generally exhibit (1) anomalously low heat flow in recharge zones due to the downward infiltration of relatively cold meteoric fluids, and (2) anomalously high heat flow in discharge zones or areas of up-dip flow in confined aquifers. Numerical models developed by Gosnold (1984 & 1999) are strongly suggestive of the occurrence of such mechanisms in the central Denver Basin of Colorado and Nebraska and the Kennedy Basin of central South Dakota and north-central Nebraska. Advection, the process by which thermal energy is transported due to fluid motion, is facilitated in the central Denver Basin primarily by regional flow within the Dakota aquifer (Gosnold, 1984 & 1990).

Some research is suggestive of the possibility of radiogenic heat production in the crystalline basement as the primary source of heat energy in the study area, the northern Denver Basin region, potentially providing an explanation for variations in surface heat flux. Stix (1982) reported moderate correlation between the geographic extent of Precambrian provinces and variations in surface heat flow across the state of Nebraska, but a lack of data in the northwestern

portion of the state rendered such correlations in the area inconclusive. Roy et al. (1972) attribute anomalous background heat flux (63 mW m^{-2}) in the Black Hills to radiogenic heat production, but do not provide data for the region south of the uplift.

Several authors (Cooley, 1986; Sims & Day, 1999; Blackstone, 1996; Degraw, 1969; Gott et al., 1974) delineate major faults and structural lineament features throughout the study area that may extend to the Precambrian basement or deep into the stratigraphic section. Others (Downey & Dinwiddie, 1988; Konikow, 1976; Hildebrand and Kucks, 1985) discuss evidence for fluid flow within fault and fracture systems in eastern Wyoming and southwestern South Dakota. Among these studies, Hildebrand and Kucks (1985) provide substantial geophysical and geochemical evidence for upward fluid flow within such secondary features in the southern Black Hills area.

Due to the existence in previously published literature of multiple plausible explanations for the observed variations in heat flux in the northern Denver Basin region, a comprehensive investigation of the proposed mechanisms is warranted. Utilizing finite difference simulations that incorporate geothermal, hydrogeological, structural, and stratigraphic data for the northern Denver Basin, the present study tests three primary hypotheses as possible mechanisms responsible for observed heat flow variations; (1) that heat flow anomalies along the flanks of the northern Denver Basin are attributed to advective heat transport within upward-dipping confined aquifers, (2) that upward leakage rates from the Madison aquifer in areas of subcrop are sufficient to provide significant upward heat advection, and (3) that faults and lineaments (which plausibly mark locations of high secondary permeability) mapped in the study area serve as conduits for upward fluid flow and advective heat transport at rates sufficient to produce the observed heat flow anomalies.

CHAPTER II

STUDY AREA AND GEOLOGICAL SETTING

Structural Overview

The structural setting of the study area is best understood in the context of the regional features that define the configuration of the northern Denver Basin. On a regional basis the Denver Basin is characterized as an asymmetric syncline with an axis that parallels the trend of the Colorado Front Range. The stratigraphic flanks dip sharply downward to their maximum depth of approximately 4 km at the base of the Rockies near Colorado Springs, (Curtis, 1988, Martin, 1965), and gently grade upward and eastward into Nebraska and Kansas. The Laramie Range, Hartville Uplift and Black Hills, all anticlinal products of Laramide uplift (Blackstone, 1996; Sims & Day, 1999; McCormick, 2010), form the western and northern edges of the basin. The Chadron Arch, a buried anticline that dates back to the early Pennsylvanian (Carlson, 1999), marks the boundary between the northeastern flanks of the Denver Basin and the southwestern edge of the Kennedy Basin (of central South Dakota and north-central Nebraska). Figure 1 depicts the extent of the Denver Basin, the structural features that define its northern boundaries, and the outline of the study area.

The Black Hills comprise an elongate, north-trending, doubly-plunging anticline structure with an Archean and Proterozoic core, and stratigraphic sections of Paleozoic and Mesozoic rocks on its flanks. The bulk of the anticline overtakes a large area of western South Dakota, with its western flanks dipping to the west into the Powder River Basin of Wyoming (Martin et

al., 2004; McGregor, 1972). The core of the Black Hills is composed of lower Proterozoic metasedimentary and metavolcanic rocks and upper Archean pegmatitic granites (Gosselin et al., 1988). With the exception of the presence of the Deadwood Formation (Cambrian), the stratigraphy of the flanks of the Black Hills is mostly consistent with that of the study area (discussed in the following section).

The Chadron Arch is the northern extremity of the Chadron-Cambridge arch structural trend, an anticlinal feature that extends southeastward through Nebraska and into northern

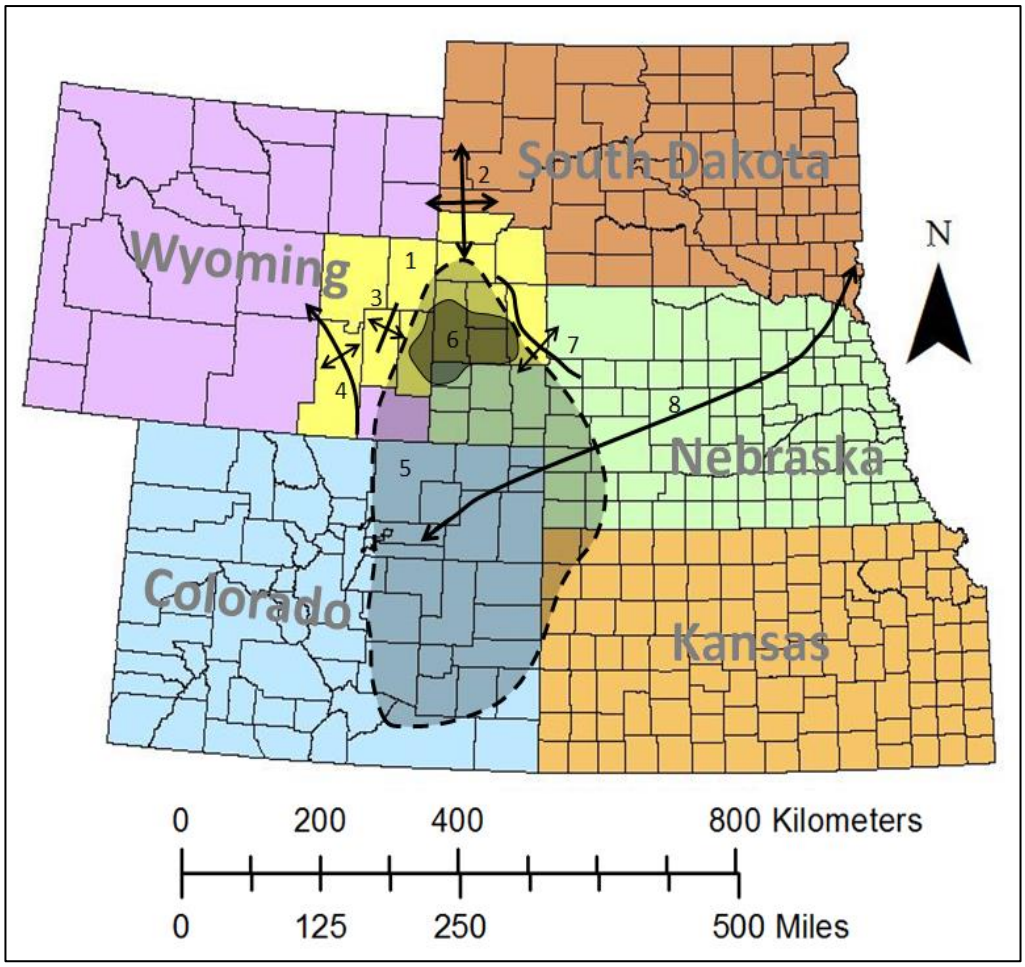

Figure 1. Study area and regional structures. (1) Study Area, shaded yellow, (2) Black Hills Uplift, (3) Hartville Uplift, (4) Laramie Range, (5) Denver Basin, (6) Alliance Basin, (7) Chadron Arch, (8) Transcontinental Arch.

Kansas. The Chadron-Cambridge arch is itself one of several northwest-trending anticlinal structures that lie along the northeast-trending Transcontinental Arch (Fig. 1), a sinuous structural trend that extends from New Mexico to Minnesota (Carlson, 1999). Near the study area, the Chadron Arch had a significant effect on Paleozoic and Mesozoic depositional patterns. Although the early Paleozoic systems (Cambrian through Mississippian) appear to have been eroded from the arch itself, sediments deposited over the arch in early Pennsylvanian through early Cretaceous time exhibit a general eastward onlapping pattern. Numerous periods of apparent nondeposition or exposure, however, are indicative of intermittent tectonic reactivation of the Chadron Arch throughout the Paleozoic (Moore & Nelson, 1974).

The Chadron Arch was also influential in the development of the Alliance Basin, which is essentially a smaller sub-basin of the Denver Basin (Fig. 2). Sequences of dolomites, shales, sandstones, and anhydrites deposited throughout the Pennsylvanian and Permian all exhibit maximum thickness in the trough of this sub-basin. Marine and evaporitic filling of the Alliance Basin is likely a result of the combined restrictive effect imposed on the area by the surrounding paleopositive elements (MachLachlan & Bieber, 1963). The nearby Lusk embayment (Fig. 2), a paleotopographic high (relative to the basins; a paleotopographic low relative to proximal uplifted areas) which separates the southeastern Powder River Basin from the northwestern Denver Basin, may have served as a marine inlet between the two basins throughout various periods of geologic time beginning in the early Pennsylvanian (Tenney, 1965).

Laramide activity in southeastern Wyoming resulted in the uplift of two prominent anticlinal structures; the Laramie Range and Hartville Uplift. The Laramie Range, which extends southward into the Front Range of the Colorado Rockies, also trends northwestward where it terminates at the Casper Mountain anticline in central Wyoming. The Precambrian core

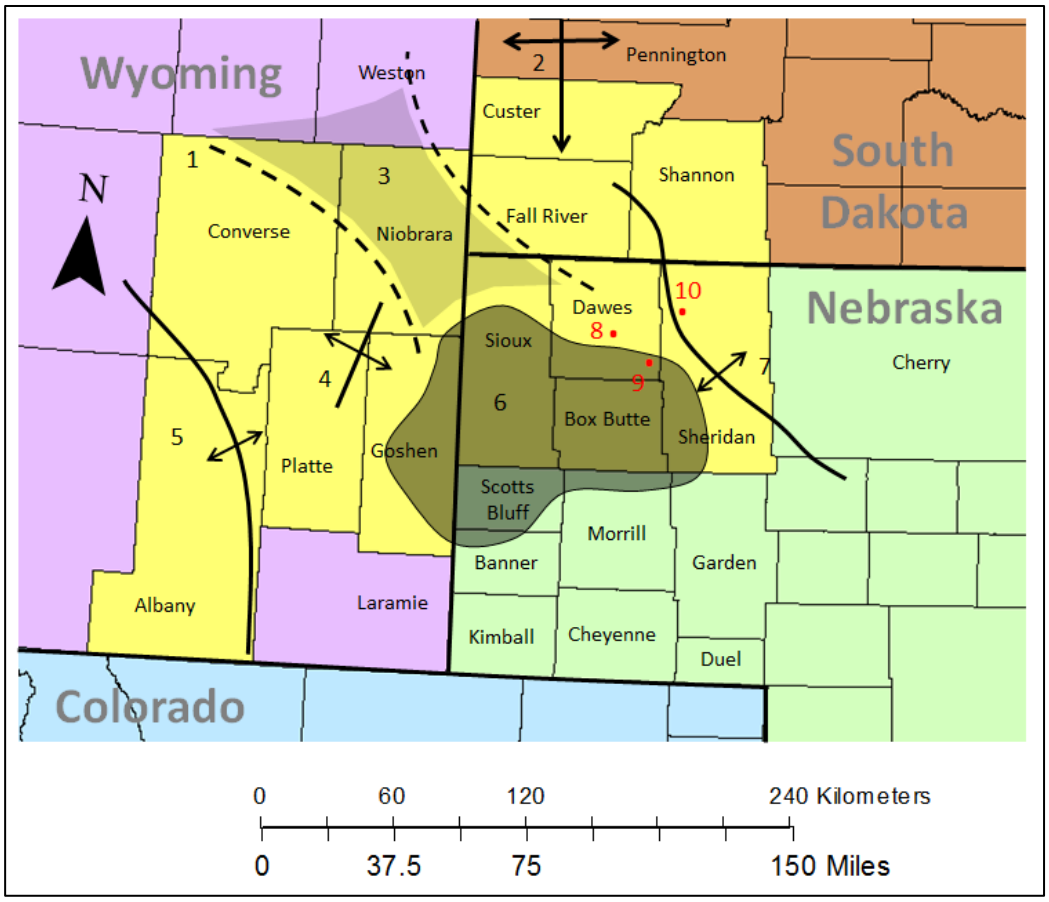

Figure 2. Study area, locations of core sample wells and regional structures. (1) Study Area, shaded yellow, (2) Black Hills Uplift, (3) Lusk Embayment, (4) Hartville Uplift, (5) Laramie Range, (6) Alliance Basin, (7) Chadron Arch, (8) Deans-1 Well, (9) Kudrna Well, (10) Murray 17-24 Well).

of the range, which consists of widely variable igneous and metamorphic terranes, contains shear zones that were likely instrumental in periods of uplift during the Laramide orogeny (Blackstone, 1996). Upturned Paleozoic and Mesozoic strata along the margins of the range exhibit progressively extreme dip angles southward toward Colorado (Condra et al., 1940). The Hartville uplift, a north-northeast-trending anticline located in Platte, Goshen and Niobrara Counties, WY, is a diverse collection of exposed Proterozoic and Archean rocks exhibiting numerous episodes of deformation and faulting (Sims & Day, 1999). Paleozoic and Mesozoic

strata flanking the uplift dip sharply downward to the west, and dip more gradually to the east into the study area (Condra et al., 1940).

Numerous faults of varying orientation, displacement, and origin are documented in the study area by several authors (Fig. 3). The Casper Mountain fault, a steeply-dipping reverse fault that intersects the northernmost Laramie Range in central Wyoming, trends east-northeast

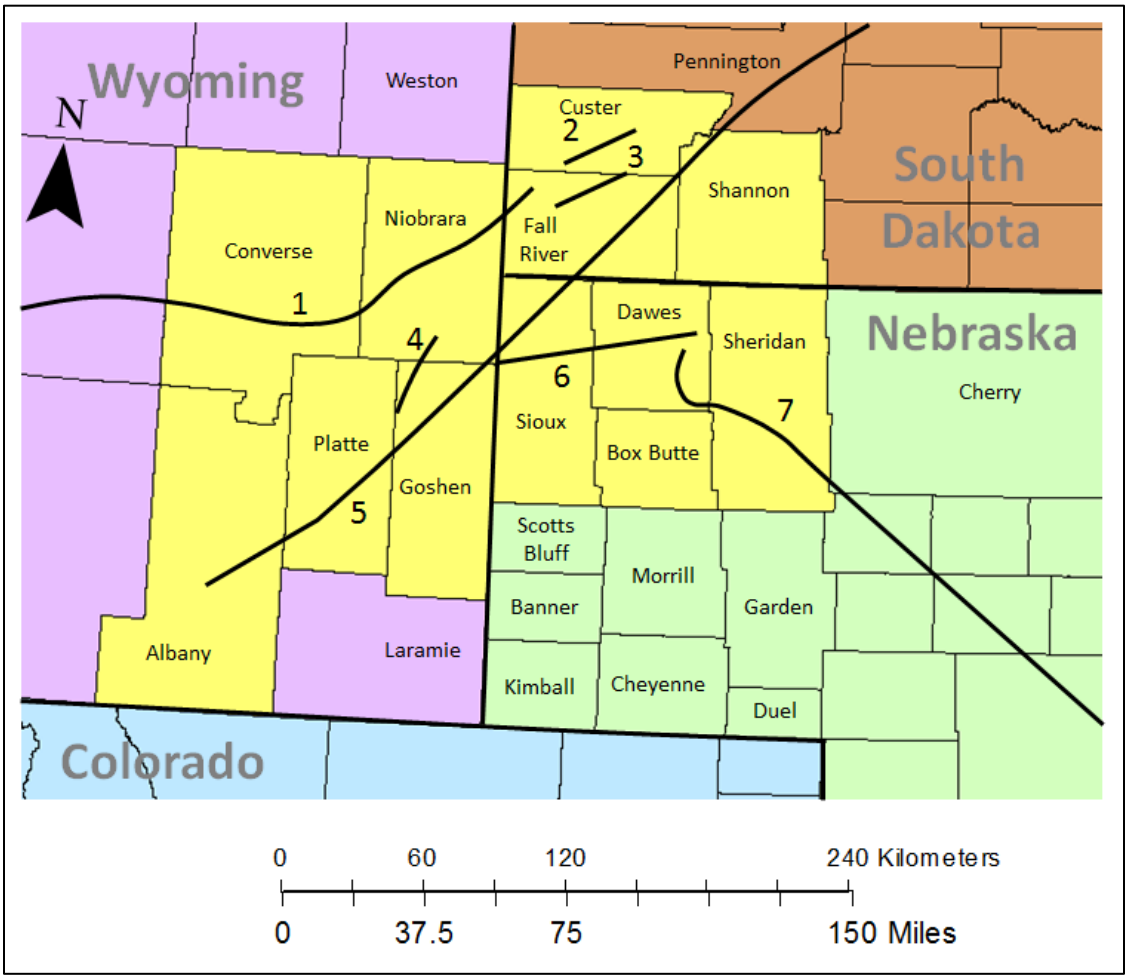

Figure 3. Locations of major faults in study area vicinity. (1) Casper Mountain Fault, (2) Dewey Structural Zone, (3) Long Mountain Structural Zone, (4) Hartville Fault, (5) Nashfork-Hartville Fault Trend (Wheatland-Whalen Fault Zone), (6) Pine Ridge Fault, (7) Hyannis-North Platte Fault. (modified from Sims & Day, 1999; Blackstone, 1996; Degraw, 1969; Gott et al., 1974)

into southwestern South Dakota. Near the Casper Mountain anticline, maximum displacement in the fault has resulted in the juxtaposition of Cretaceous strata and Precambrian basement. The Nashfork-Hartville fault trend (also referred to as the Wheatland-Whalen fault zone) is a 145 km-long extensional fault system that cross-cuts the Laramie Range and extends northeastward into Nebraska and South Dakota. In the Wyoming portion of the fault zone, the extensional fault blocks are located within the hanging wall of the Mule Creek reverse fault (Blackstone, 1996). The Pine Ridge and Hyannis-North Platte faults of northwestern Nebraska, both normal faults with offset ranging from 100 to 200 m, were discovered and interpreted on the basis of the apparent offset indicated by well-log data for Cretaceous strata (Degraw, 1969). Two faults zones in southwestern South Dakota, the Dewey and Long Mountain structural zones, host several bifurcating strike-slip faults and steep normal faults with northern footwalls (Gott et al., 1974). The Hartville Uplift vicinity is host to many steeply-dipping thrust faults, many of which are localized truncations of the Precambrian core. The most prominent of these thrust faults, the Hartville Fault, trends north-northeast along the axis of the uplift. In many areas the fault exhibits near-vertical dip, and throughout the uplift is evidential of multiple episodes of displacement (Sims & Day, 1999).

Using infrared Landsat images of the Great Plains region, Cooley (1986) mapped and categorized structural lineament features, categorizing them by their likely effect on bedrock permeability on the basis of their density and proximity to known areas of brittle deformation. Figure 4 depicts the divisions of inferred effect on permeability of observed lineament features in the study area. Lineaments in the study area may be understood by the concepts of fault block mechanisms discussed by Sonnenberg and Weimer (1981). Patterns of intersecting lineaments (such as those mapped in Figure 4 by Cooley, 1986) are presumably formed along planes of

structural weakness in the crystalline basement. The surface lineaments observed by Cooley (1986), therefore, are likely topographic manifestations of drape-folding or faulting in the substrata in response to the structural failure of the underlying basement.

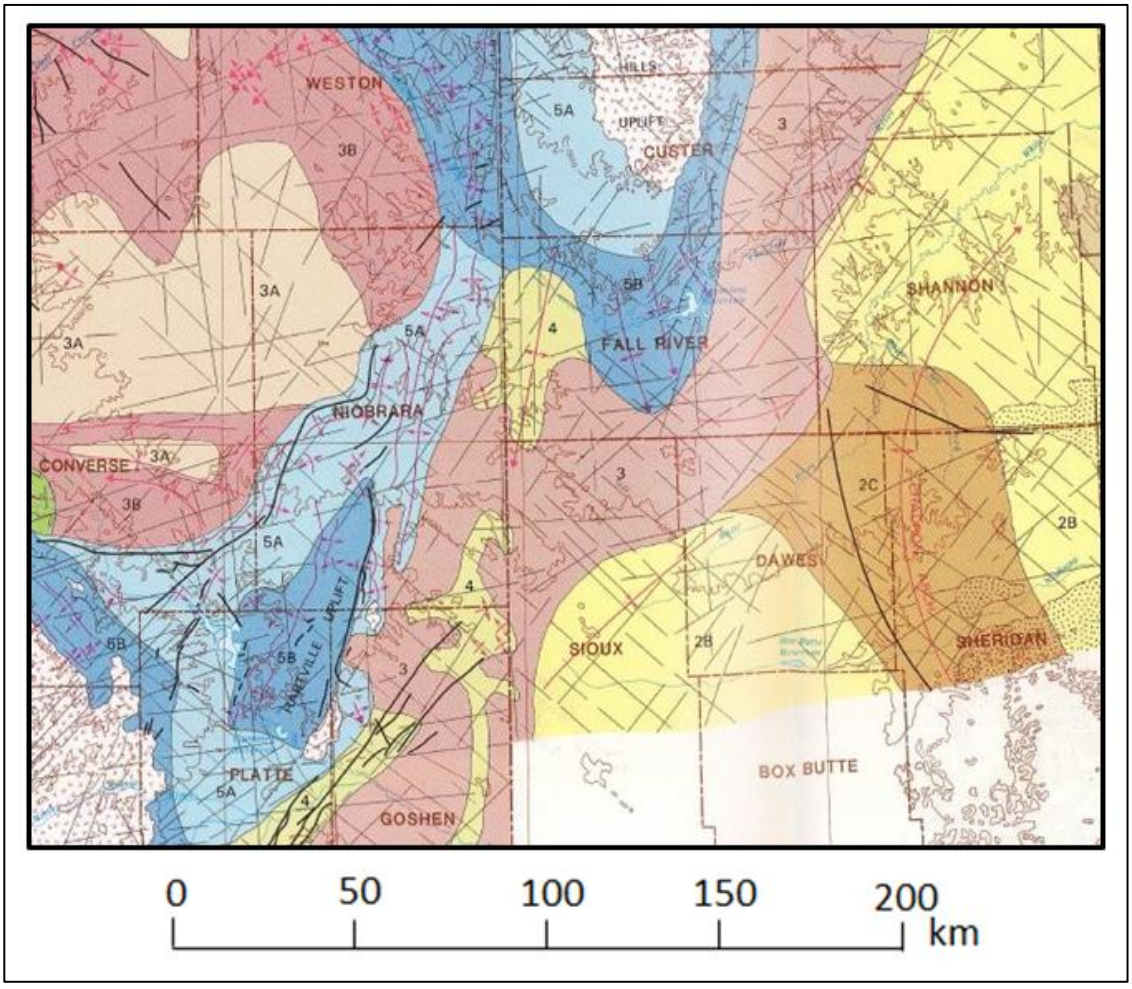

Figure 4. Distribution of structural lineaments and inferred effect on permeability. Divisions are labeled and colorized from highest to lowest inferred effect on permeability. Divisions in order from highest to lowest are as follows: 5A & 5B (blue), 4 (yellow), 3A (tan), 3 & 3B (red), 2C (orange), 2B (light yellow). (modified from Cooley, 1986)

Stratigraphic and Lithological Overview

A comprehensive characterization of any regional or localized geothermal resource requires a sufficient understanding of the distribution of principal lithological components. The geological architecture of the northern Denver Basin can be generalized as a petrologically-diverse Precambrian basement overlain by a thick section of slightly down-warped Phanerozoic strata. Along with regional structural trends, stratigraphic and lithological information is herein used to provide a context for the geothermal and hydrogeological data used to simulate the system. Relevant parameters such as thermal conductivity and transmissivity are directly dependent on several physical properties of the rock. These include, but are not limited to composition, grain morphology, sorting, fabric, and interval thickness. Because in some cases geothermal and hydrogeological data pertaining to specific intervals is not available, published descriptions may be useful for arriving at acceptable approximations.

Precambrian System

The Precambrian terrane of the Midcontinent comprises several distinct provinces of varying age, composition, and degree of deformation. The study area resides atop the converging point of three distinct Precambrian accretionary terranes; the Central Plains orogen as defined by Sims & Petermar (1986, p. 488), the Wyoming craton, and the Trans-Hudson orogen (Fig. 5). Aside from the Archean rocks of the Black Hills (Denison et al., 1984, p. 3) and Hartville Uplift (Sims et al., 2001, p. 6), the basement within the study area is composed primarily of Trans-Hudsonian rocks of Proterozoic age.

Although it has been established that rocks of the Trans-Hudsonian orogen are a direct result of the Proterozoic tectonic activity between the Wyoming and Superior cratons, some disagreement appears to exist as to whether these rocks originated in convergent (Carlson, 2007,

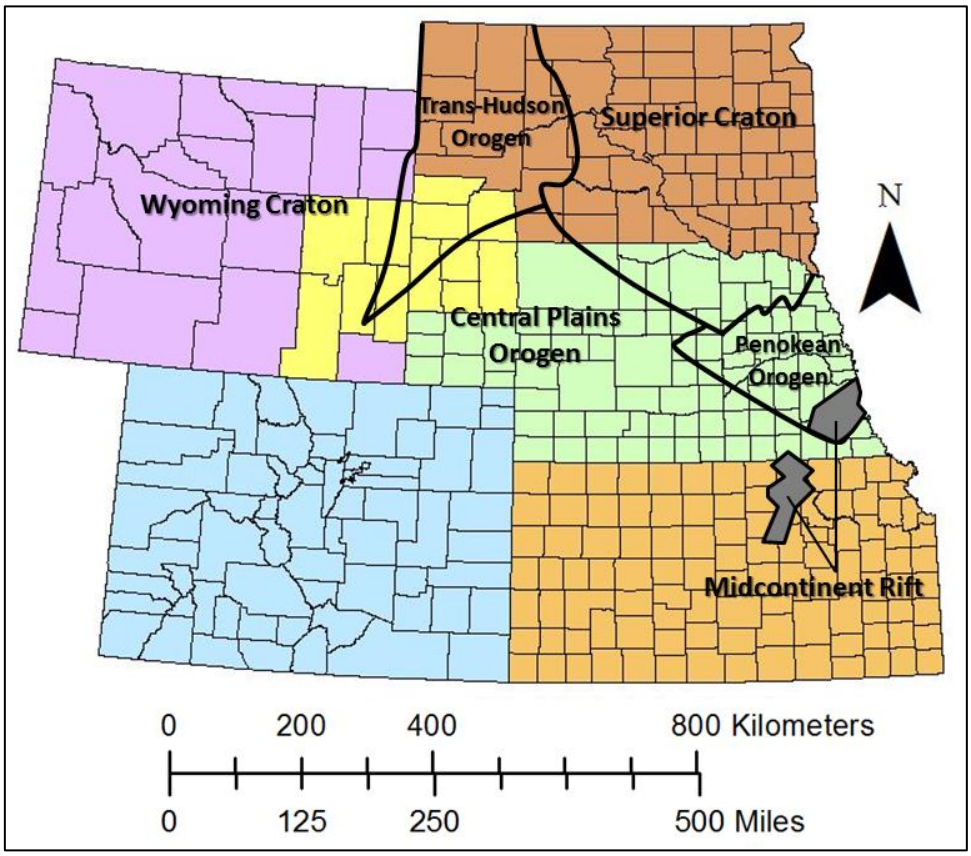

Figure 5. Major Precambrian provinces of the Nebraska region (modified from Carlson, 2007).

p. 323) or divergent (Klasner & King, 1986, p. 1083) conditions. Nonetheless, these two provinces were sutured together with the emergence of the Trans-Hudsonian orogen (ca. 1.83 Ga) (Carlson, 2007, p. 323) forming the terrane referred to as the Hudsonian protocontinent. Southwestern South Dakota and eastern Wyoming, the portion of the Trans-Hudsonian province collocated with the study area, is characterized by Proterozoic (ca. 1.7-2.1 Ga) metamorphic belts and granites that are largely undifferentiated (Denison et al., 1984, p. 4, pl. 1). This localized terrane is itself crosscut by a crustal shear zone known as the Cheyenne foldbelt (ca. 1.78-1.74 Ga) (Dahl et al., 1999, p. 1344), which intersects the study area and WY-SD-NE tri-state border trending northeasterly (Fig. 6). The foldbelt is a provincial inclusion of the Trans-

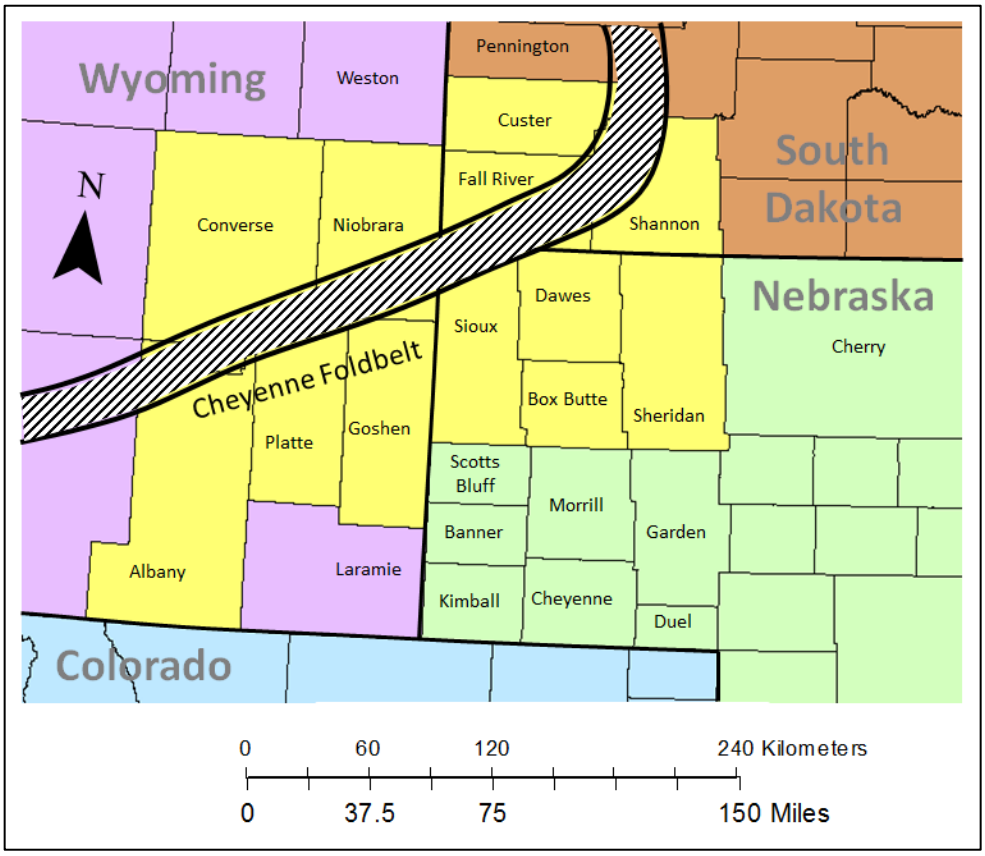

Figure 6. Map showing location of Precambrian Cheyenne foldbelt (modified from Klasner & King, 1986).

Hudsonian orogen, and is distinguished by highly deformed volcanic island-arc terrane lithologies, namely amphibolitic orthogneisses and schists (Duebendorfer & Houston, 1987, p. 554, & Klasner & King, 1986, p. 1100).

Sims and Day (1999) discuss in detail the complexity of Archean and Proterozoic geology in the southeastern Wyoming region and southern margin of the Wyoming craton. Archean rocks within the core of the Hartville Uplift anticline are heavily deformed and are intruded by granitic, dioritic and mafic dike swarms ranging in age from 2.65-1.72 Ga. Although the Archean basement is not exposed in this region, radiometric dates of drill cores have yielded ages between 3.1-2.8 Ga (Sims & Day, 1999, p. 2). Archean rocks of similar age (2.9-2.5 Ga)

are found in the Laramie Range of southern Wyoming, but are lithologically more diverse. Here, a gneissic basement is overlain by a diverse array of metasedimentary units including quartzites, metagraywacke, phyllite, and banded-iron formation (Duebendorfer & Houston, 1987, p. 556).

The Central Plains orogenic belt, which constitutes the majority of Nebraska's Precambrian terrane, is subdivided into age-distinctive provinces. Because of the southward accretionary direction of the Hudsonian protocontinent, these orogenic provinces likewise have a southward decrease in age ranging from 1.78 Ga to 1.61 Ga (Fig. 7), (Carlson, 2007, p. 324). Central Plains orogenic lithology is relatively diverse, and includes granitoids, quartz-, biotite-, and hornblende-rich muscovite schists, quartz-feldspar gneisses, amphibolite, and sillimanite-

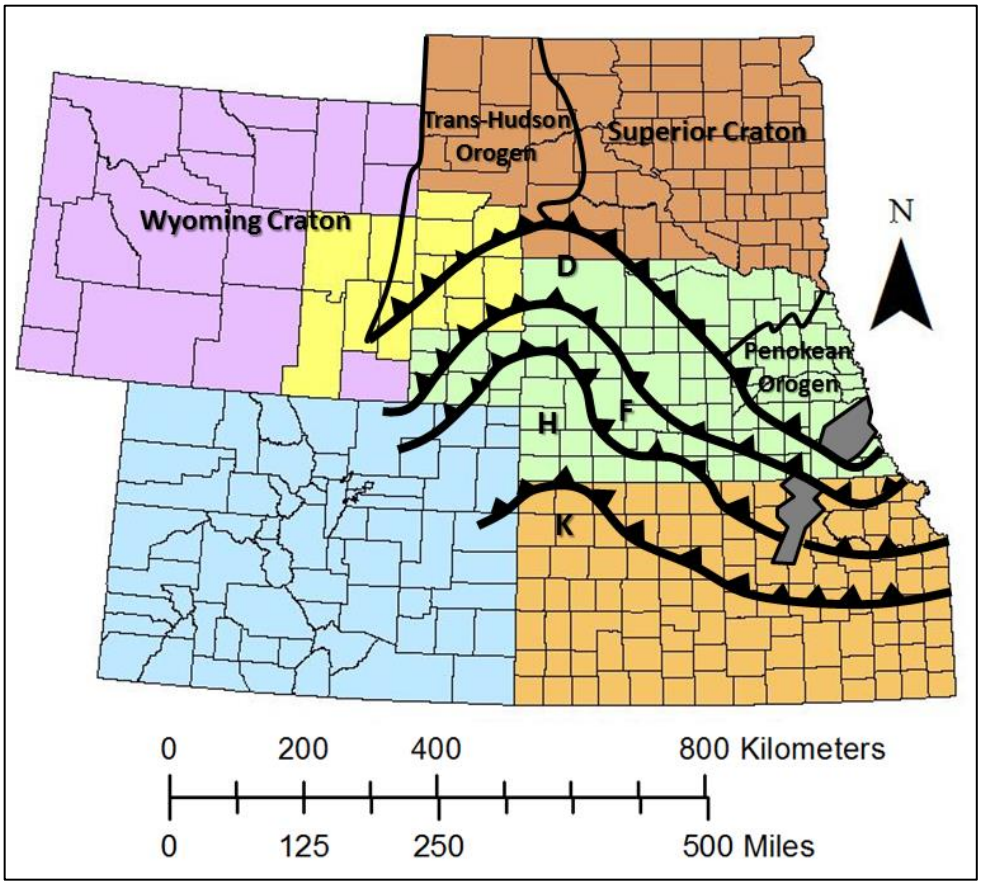

Figure 7. Precambrian accretionary terranes of the Central Plains Orogen. D- Dawes (1.78 Ga); F- Frontier (1.71 Ga); H- Hitchcock (1.67 Ga); K- Kansas (1.61 Ga) (modified from Carlson, 2007).

and muscovite-containing quartzites (Sims & Petermar, 1986, p. 489; Carlson, 1993; Condra & Reed, 1959, p. 73). More specifically, lithological emphasis is placed upon the Dawes terrane, the subdivision of the Central Plains orogen in closest proximity to the study area. This subdivision is composed of granites rich in alkali feldspar, hornblende gneisses, and chlorite schists characteristic of a continent-arc collision episode (Carlson, 2007, p.p. 322-324; Sims & Petermar, 1986, p. 490). Core samples of these lithologies from deep oil wells (Fig. 2) in northwestern Nebraska were collected from the core repository shared by the Nebraska Geological Survey (NGS) and the University of Nebraska at Lincoln (UNL) to represent the basement thermal conductivity (discussed in a later section) of the study area.

Lower Paleozoic (Cambrian through Devonian) System

Sediments situated between Precambrian and Mississippian rocks in the study area have apparently been the subject of informal debate for several decades. Maughan (1963, p. 36) describes an arkosic conglomeritic sandstone at the base of Mississippian limestones in the Laramie Range of Wyoming (Fig. 2), Condra & Reed (1959, p.72) attribute a Cambrian age to the dolomites and sandstones west of the Cambridge arch in Nebraska, and Sonnenberg & Weimer (1981, p.p.11-12) discuss the presence of coarse, dolomitic Cambrian sands in the central Denver Basin. Irrespective of lithological and stratigraphic inconsistencies, these sediments are often correlated to one another, as well as to the *Deadwood Formation*, the *Reagan Sandstone*, the *Flathead Quartzite*, and the *Sawatch Sandstone*, among others. Nonetheless, the rocks corresponding to this stratigraphic position are likely no more than 30.5 m (100 ft) in thickness within the study area, and subcrop in Sioux and Dawes counties in Nebraska (Carlson, 1970; Brown et al., 1984; & Sando & Sandberg, 1987) (Fig. 8).

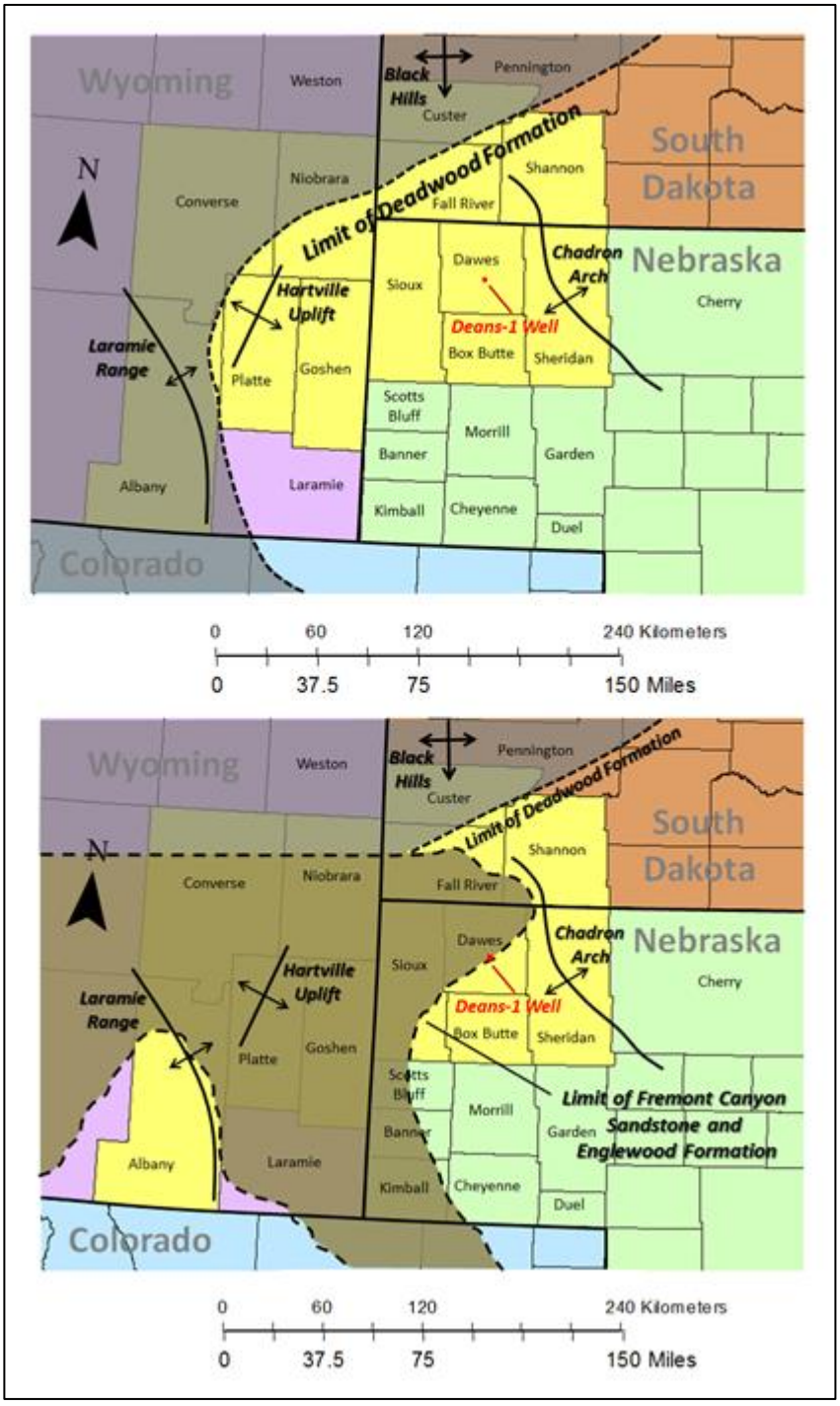

Figure 8. Limits of Deadwood, Fremont Canyon, and Englewood formations (modified from Sando & Sandberg, 1987).

Sando & Sandberg (1987) present a thorough argument for the nominal and temporal re-assignment of the sandstone unit that underlies the base of the Mississippian system in the Laramie Range and Hartville Uplift of Wyoming. The authors compare the composition, sedimentological features, geographic extent, and reported ages of several regional units often correlated to those that underlie the *Guernsey Formation* (Mississippian) of southeastern Wyoming. Among the formations evaluated in this comparison include the Deadwood Formation, *Harding Sandstone* (Colorado and Wyoming), Winnipeg Formation, and *Parting Formation* (central Colorado). The unit examined by Sando & Sandberg (1987), therein named the *Fremont Canyon Sandstone*, is a quartzite and sandstone that ranges in composition from arkose to quartz arenite. The Fremont Canyon Sandstone is present throughout the study area with the exception of the region south and southwest of the Black Hills, where pre-Mississippian sediments belong to the Deadwood Formation (Fig. 8). Sando & Sandberg (1987, p. 7) conclude that, although age-correlative with the Parting Formation, the Fremont Canyon Sandstone ought to be considered a lithologically and stratigraphically unique formation on the basis of stratigraphic, petrographic, and paleontological evidence. Contrary to the common designation of pre-Mississippian sandstones in the southeastern Wyoming region as Cambrian-aged (Carlson, 1963, p. 32; Condra & Reed, 1959, p. 72; Lugn, 1934, p. 1615; Maughan, 1963, p. 36), an age of late Devonian is assigned to the sandstones and quartzites of the Fremont Canyon Sandstone (Sando & Sandberg, 1987, p. 7).

Although no quartzite or sandstone core samples of pre-Mississippian and post-Proterozoic age were recovered from the Deans-1 well (Fig. 2) (used for the collection of Paleozoic and Mesozoic samples for thermal conductivity analysis in this study), such sediments present in the study area are herein regarded as late-Devonian on the basis of the evidence

provided by Sando & Sandberg (1987). Excluding the Deadwood Formation in the southern Black Hills region, any assignments of such sediments to the Cambrian period in previous literature are therefore disregarded.

Aside from the late Devonian sediments discussed, pre-Mississippian Paleozoic systems are apparently unrepresented in the study area and regional vicinity due to uplift-induced nondeposition or post-depositional erosion (Lugn, 1934, p. 1625 & 1628; Carlson, 1999, p. 229). A disagreement on the presence of middle and upper Ordovician rocks in the southern Black Hills exists between Peterson (1984), Carlson (1999) and Naus et al. (2001). Although Peterson (1984) and Carlson (1999) both map undifferentiated Ordovician sediments extending 20-30 km (12-18 mi) south and southwest of the flanks of the Black Hills uplift, Naus et al. (2001, p. 8) explicitly mentions an unconformity between the Deadwood (Cambrian) and Englewood (upper Devonian and lower Mississippian) formations in this region. Although it spans Late Devonian and Early Mississippian time (USGS, 2013), the Englewood Formation is herein discussed in the section that examines the Mississippian System.

Isolated pockets of lower Paleozoic rocks have been reported in restricted areas throughout the Denver Basin, particularly along its southern and eastern flanks in Colorado and Kansas (McCoy, 1953). Brief discussions of the Cambrian Reagan (Lamotte) Sandstone and the Ordovician Arbuckle Group of the southern Denver Basin are given by Carlson (1963, p. 32), Sonnenberg & Weimer (1981, p. 11), and Condra & Reed (1959, p.p. 71-72). Fossiliferous limestones of the Silurian are found in the Front Range of the Rocky Mountains along the CO-WY border according to Martin (1965), and Rothrock (1960) examines the Devonian Williams Canyon Limestone in the southern Front Range of Colorado.

Mississippian System

Mississippian-aged units within the study area are exclusively *Madison Group* sediments characterized by carbonates with varying degrees of dolomitization (Andrichuk, 1955, p. 2184). Lithological consistency in the Madison Group is relatively ambiguous both stratigraphically and geographically, which has resulted in much difficulty delineating regional Madison Group stratigraphic units. Additionally, an inter-regional inconsistency in Mississippian carbonate nomenclature exists due to a historical lack of coordination. Although the title *Madison* is often assigned indiscriminately to Midcontinent Mississippian carbonates, other names are specific to the region under investigation. For example, Mississippian carbonate sequences are given the title *Pahasapa* in the Black Hills region, while the name *Guernsey* is applied to such sequences in the Hartville Uplift area (Andrichuk, 1955, p. 2176; Petty, 2003, p. 19). Carlson (1963, p. 31), however, points out that these terms are restricted to surface outcrops in most cases. Nevertheless, because the study area is situated between three regions of differing Mississippian nomenclature (i.e. the Black Hills, Hartville Uplift, & Denver Basin), careful consideration was taken to nominally identify specimens used for this study.

The Madison group is commonly (particularly in the Williston Basin and the smaller basins of Montana and Wyoming, i.e. Powder River Basin, Big Horn Basin, etc.) divided into three principle stratigraphic formations and equivalents; the *Lodgepole*, *Mission Canyon*, and *Charles* formations (in ascending order). Carlson (1963), however, differentiates Madison equivalents in the study area by stage, namely Kinderhookian, Osagian and Meramecian (Fig. 9). In an effort to establish a standardized correlative framework for Madison and equivalent carbonates, Peterson (1984) defines 13 stratigraphic units that incorporate distinctions made by both common marker beds and conventional nomenclature (Fig. 10). The marker beds (denoted

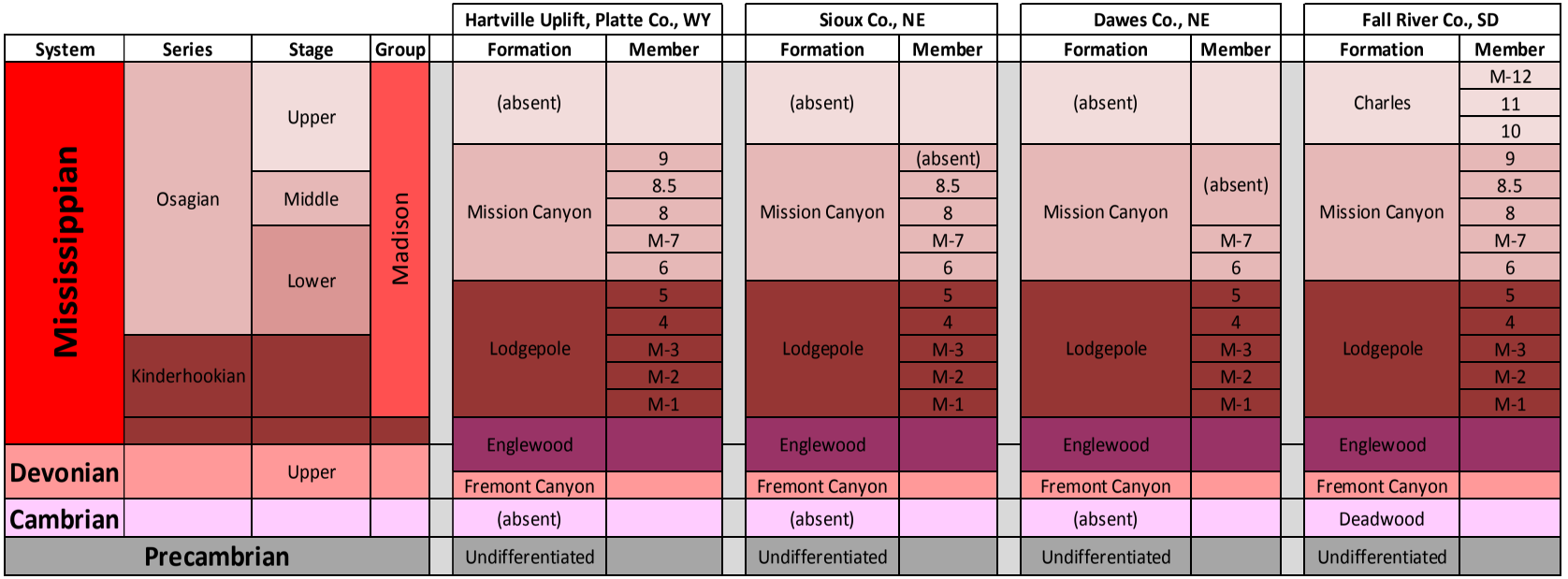

Figure 9. Stratigraphic Correlation Chart: Precambrian through Mississippian Systems.

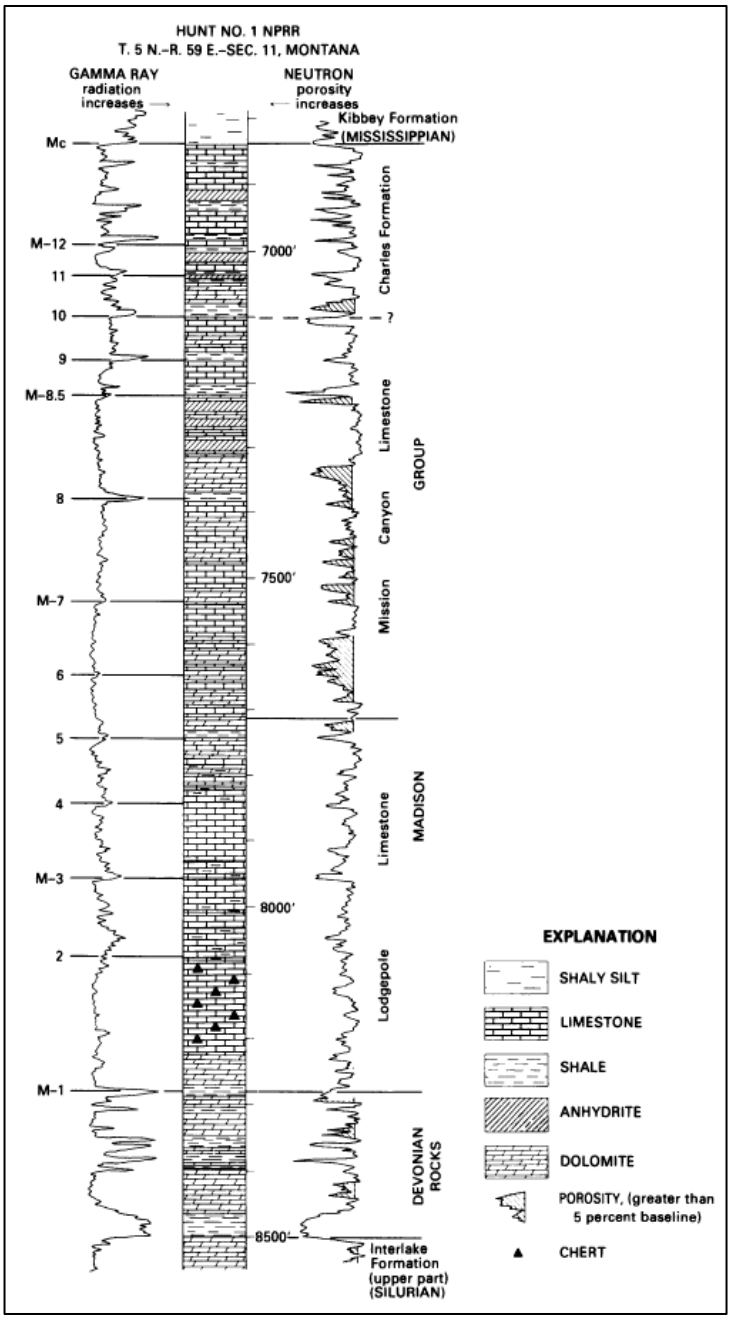

Figure 10. Well-log patterns and lithology of Madison Group marker units (from Peterson, 1984).

as M-1, M-7, etc.), characterized by their relative high-shale content, were chosen primarily on the basis of their distinctive gamma-ray signatures and widespread regional extent.

The M-1 marker denotes the Devonian-Mississippian horizon, as well as the base of the Lodgepole (earliest Kinderhookian). On a regional basis the M-1 to M-3 interval is commonly distinguishable by the presence of crinoidal carbonate mud mounds (Waulsortian mounds) (Peterson, 1984, p. 16) that, in the Williston Basin, are underlain by a gradational contact with the Bakken Formation. Brown et al. (1984, p.p. 10-11) describe this interval as a thin-bedded, highly argillaceous limestone in the northern areas of the Madison extent, and as more dolomitic toward the south where it subcrops in the study area. Peterson (1984, p. 18) and Brown et al. (1984, p. 14) describe the overlying M-3 to M-7 interval in the vicinity of the study area as oolitic limestone and dolomitic limestone beds indicative of deep marine depositional conditions. This interval represents the upper Lodgepole and lower Mission Canyon formations, as well as an early Osagian age (Fig. 9).

Middle Osagian to Meramecian intervals of the upper Mission Canyon and overlying Charles formation (M-7 to Mc, see Fig. 10) are characterized by regressive sequences of interbedded evaporites and oolitic limestones, contrasting with the deeper marine transgressive sequence of the underlying intervals (Peterson, 1984, p.p. 18-19 & Andrichuk, 1955, p. 2170). Carlson (1963) and MachLachlan & Bieber (1963) appear to disagree upon the age of the youngest Mississippian rocks present in northwestern Nebraska. While Carlson (1963, p. 32) contends that Mississippian rocks are no younger than Kinderhookian age, MachLachlan & Bieber (1963, p.p. 92-93) assert that Meramecian units are represented. Samples from the Deans-1 well (Fig. 2) used in this study for the measurement of thermal conductivity, however, are inferred to be Kinderhookian in age (and therefore likely belong to the M-1 to M-3 interval

of the lower Lodgepole) based on: (1) the described lithologic characteristics of the intervals presented by Peterson (1984) and Brown et al. (1984), (2) the evidence of erosion due to uplift of all but the lowermost Kinderhookian sediments in the study area presented by Tenney (1965, p.p. 227-228), (3) a southward disappearance of evaporites and other characteristics of regression in the Madison described by Andrichuck (1955, p. 2170), and (4) a lack of ooids and evaporites in the Mississippian core samples used for this study.

Mississippian limestone units of variable thickness are observed to be present throughout the central part of the Denver Basin (almost exclusively in Colorado), but although they are often assumed to be part of the Madison limestone, their equivalence to the formally-accepted Madison limestone type-lithology has not been verified (Curtis, 1988). The northern extremity of the Denver Basin is flanked to the west by the Laramie Range and Hartville Uplift in southeastern Wyoming. Depending on locality within these ranges, the limestone and dolomitic limestone sections of the Guernsey (Madison equivalent) unconformably overlie the Archean metasedimentary and metavolcanic rocks of the Whalen Group in places (Andrichuk, 1955, p. 2176), and overlie a basal sandstone of probable Devonian age in others (Sand & Sandberg, 1987, Plate 1). These sections, up to 66 m (215 ft) thick at the Hartville Uplift (Maughan, 1963, p. 38), likely include rocks of the M-3 to M-7 lithotype interval (Brown et al., 1984, Plate 15).

The Pahasapa (Madison equivalent) in the Black Hills of western South Dakota and eastern Wyoming is underlain by up to 18 m (59 ft) of purple-hued carbonates and shales known locally as the Englewood Formation of upper Devonian and lower Mississippian age (Andrichuk, 1955, p. 2176). Pahasapa sedimentation in this region is characterized as primarily regressive in sequence (Petty, 2003, p. 19), and has been determined to have initiated after the earliest Madison sedimentation in the Williston Basin, but prior to that on the Wyoming shelf

(Andrichuk, 1955, p. 2170). Pahasapa stratigraphy appears to be mostly correlative with marker-bed intervals M-1 through M-12 (Brown et al., 1984, Plate 19, Peterson, 1984, p. 16).

Core samples from the Deans-1 well (Fig. 2) include a purple calcareous shale that contains very-fine to fine-grained sand and other lithic fragments, as well as large green shale rip-up clasts. These rocks occur at the base of the Madison dolomitic limestones in the core section, and exhibit lithology that very closely matches the description of the *Englewood Formation* given by Sando & Sandberg (1987, p. 9). Based on: (1) the absence of Cambrian sands in the vicinity of the Deans-1 well illustrated by Carlson (1970), (2) the combined regional extent of the Fremont Canyon Sandstone (Devonian) and Englewood Formation mapped by Sando & Sandberg (1987) (Fig. 8), (3) the apparent lithological equivalency of the sample to the Englewood Formation, and (4) the presence of approximately only 0.46 m (1.5 ft) of the lithology in the core section, the Deans-1 sample is inferred to represent the southeasternmost extent of the Englewood Formation in the study area.

Although the dolomitic limestone core samples analyzed for this study are most likely Kinderhookian-aged units belonging to the M-1 to M-3 lithotype, Brown et al. (1984, plates 14-17) provide evidence of the presence of limestone and dolomitic limestone of the M-3 through M-8.5 intervals within the study area (namely the northwestern-most corner of Nebraska and along the South Dakota-Wyoming border south of the Black Hills) (Fig. 11). Carlson (1963) elaborates on the lithology, extent, and tectonic controls on sedimentation and erosion of the Madison Group in the northwestern Nebraska region. The study area exhibits a basal dolomitic section identified by Carlson (1963, p. 32) as the Chouteau-Hampton Group, and an overlying limestone unit with lithological characteristics of the Gilmore City Formation. A similar sequence is found in the southeastern corner of Nebraska, suggesting that the vast region in the

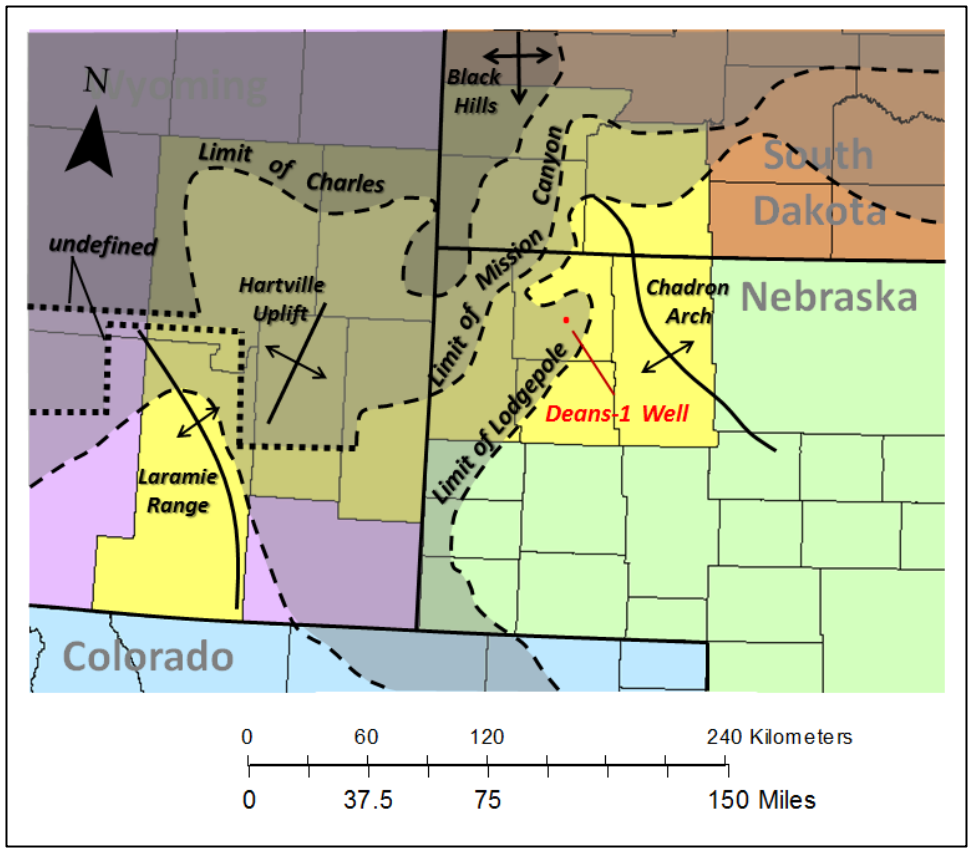

Figure 11. Limits of Madison Group formations within study area (modified from Brown et al., 1984; Downey, 1984; & Tenney, 1965).

central portion of the state now void of Mississippian sediments was once covered continuously. Mississippian sediments subcrop in Dawes and Sioux Counties, west and southwest of the Chadron Arch in Sheridan County. Several authors agree upon the likelihood that the Ouachita-aged uplift of the Chadron Arch (Fig. 2) took place concurrently with Mississippian sedimentation in the region, and resulted in the subsequent exposure and total or partial removal of those sediments (Carlson, 1993; Jorgensen et al., 1993, p. 28; Brown et al., 1984, p. 11; MacLachlan & Bieber, 1963, p.p. 92-93).

Pennsylvanian System

Stratigraphic and inter-regional patterns of Pennsylvanian sediments demonstrate a profound change in tectonic and depositional conditions with respect to those of the underlying Mississippian system. The reactivation of Precambrian fault blocks during Late Mississippian and Early Pennsylvanian time resulted in the uplift of several northwest-trending structural features that lie along the northeast-trending Transcontinental Arch (Fig. 1). Within the study area, this reactivation produced the positive elevations of the Chadron-Cambridge Arch responsible for the removal of Mississippian sediments (Carlson, 1999, p. 229). Several authors (Tenney, 1965, p.p. 228-229; Prichard, 1975, p. 115; MacLachlan and Bieber, 1963, p. 84) present evidence for uplift and exposure in the Black Hills, Hartville Uplift and Morrill County High during the transition between the Mississippian and Pennsylvanian periods. Uplift in these regions is cited not only as the primary factor responsible for thinning over the structures themselves (Sonnenberg & Weimer, 1981, p. 15), but also for the anomalously thick sequences of Pennsylvanian sediments just south of the study area. MacLachlan and Bieber (1963, p. 84) name this feature the Alliance Basin (Fig. 2), and suggest that it be considered a separate sub-basin on the basis of its periodic truncation to the south by the Morrill County High from the rest of the Denver Basin. Provenance of Pennsylvanian sediments in this region is traced to the Ancestral Rockies, Black Hills, Chadron Arch, and the Siouxana Arch (called the Cherry County paleopositive by Momper, 1963, p. 45) of central Nebraska and South Dakota (Tenney, 1965, p.p. 228-229; Prichard, 1975, p. 115).

The names *Hartville* and *Minnelusa* are often applied interchangeably in the region to the Pennsylvanian units, as well as to Permian sediments up through Leonardian age (Fig. 12). While *Minnelusa* is often reserved for the Black Hills region and *Hartville* for southeastern

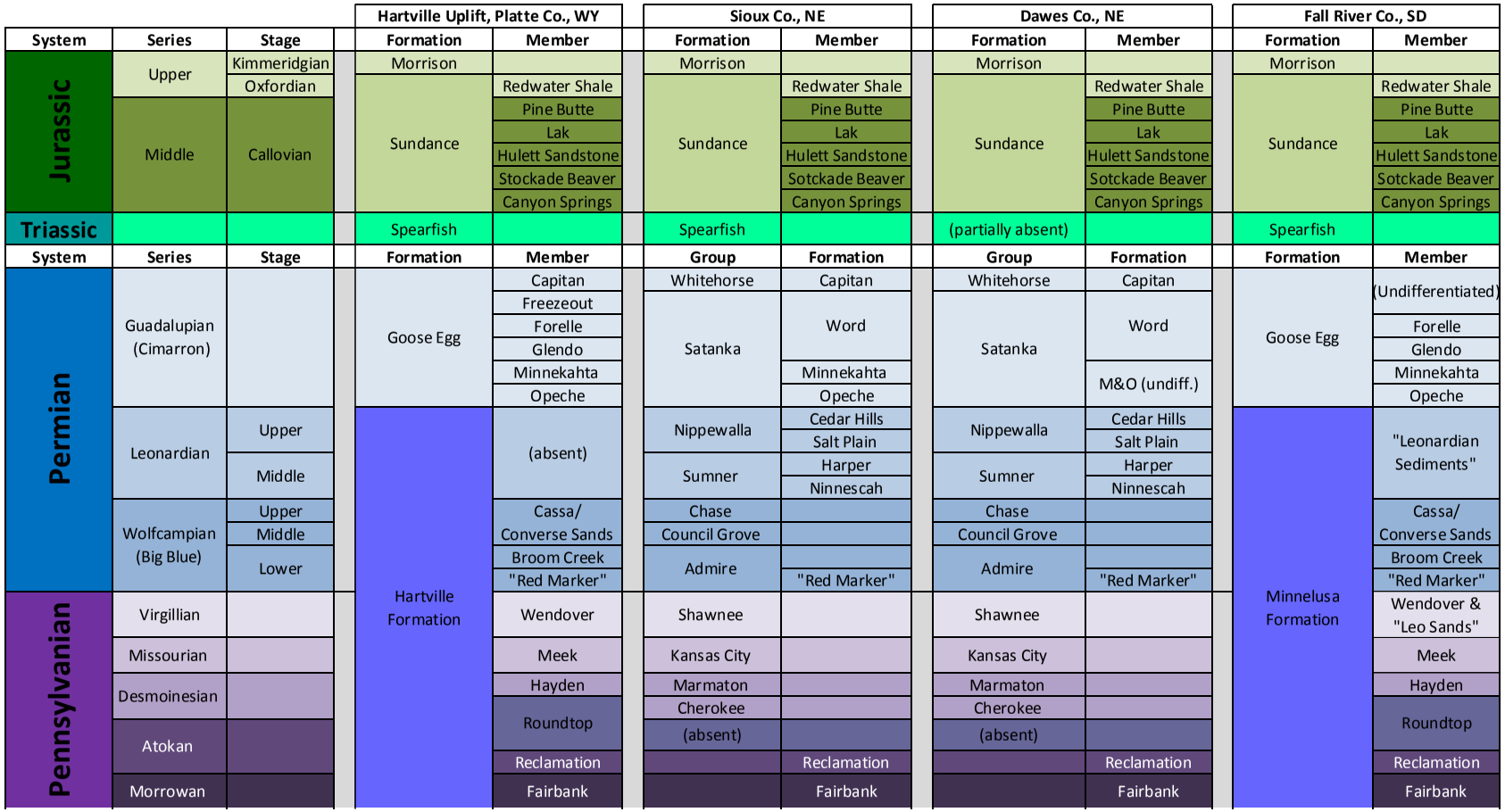

Figure 12. Stratigraphic Correlation Chart: Pennsylvanian through Jurassic Systems.

Wyoming, the two formations are more specifically differentiated from one another by the presence (Minnelusa) or absence (Hartville) of bedded evaporites (McCrae, 1956, p. 85). The presence of anhydrite and halite in the Pennsylvanian and Permian core samples of the Deans-1 well, therefore, calls for the application of the title Minnelusa in the eastern portion of the study area. This classification is in close agreement with facies maps of the Pennsylvanian and lower Permian given by MacLachlan & Bieber (1963) and Momper (1963).

During Morrowan time seas transgressed over many of the positive structures in the region, either onlapping or completely inundating them. This transgression is likely both eustatic and tectonic in origin (Momper, 1963, p. 45; Cardinal & Holmes, 1984, p. 336), and is documented by MachLachlan and Bieber (1963, p. 93) as a fining-upward clastic sequence that continued into the Atokan. Morrowan sediments in the study area are exclusively represented by the *Fairbank* member of the Hartville and Minnelusa formations (Fig. 12). The Fairbank unconformably overlies the Guernsey in the Hartville uplift region and Precambrian basement rocks on the Chadron Arch (Hoyt, 1963, p. 74; MachLachlan & Bieber, 1963, p. 86). Generally it consists of re-worked Mississippian carbonate fragments and an arkosic or lateritic matrix of Precambrian provenance (McCrae, 1956, p. 85; Prichard, 1975, p. 118). The Fairbank member transitions from a predominantly sandy facies on the Hartville uplift to a more calcareous one near the Chadron Arch (MachLachlan & Bieber, 1963, p. 86). Core samples of the Fairbank from the Deans-1 well reflect this higher carbonate-to-lithic ratio given their relatively close proximity (Dawes County, NE) to the Chadron Arch.

The basal Atokan unit, known as the *Reclamation* member of the Hartville and Minnelusa formations (Fig. 12), conformably overlies the Fairbank member. The Reclamation varies lithologically from sequences of carbonates and red shales (Tenney, 1965, p. 230), alternating

black shales and brown fossiliferous limestones (Hoyt, 1963, p. 77), and cherty carbonaceous mudstones and wackestones (Sonnenberg & Weimer, 1981, p. 16). Prichard (1975, p.p. 117-118) suggests that the boundary between the Fairbank and Reclamation members can be recognized by an upward transition from red lithics to limestone. Considering the Fairbank's predominantly calcareous lithology in the eastern part of the study area mentioned by MachLachlan & Bieber (1963, p. 86), this transition may be difficult to recognize near the Chadron Arch. According to Sonnenberg & Weimer (1981, p. 16) Atokan sediments in the vicinity of the Deans-1 well are chiefly arkosic sands, a characterization that is consistent with samples overlying sediments known to belong to the Fairbank.

Little information is provided regarding the differentiation of the Reclamation member from the *Roundtop*, the Upper Atokan unit (Fig. 12). Wilson (1978, p. 131), however, describes a series of green and pink shales interbedded with cherty carbonates in Sioux County, NE. These sediments are found in the Deans-1 core overlying sandy facies that resemble descriptions of those given for the lower Atokan by Momper (1963, p. 50). It is likely that an accurate delineation of the Lower-Upper Atoka boundary would depend heavily on paleontological evidence (Wilson, 1978, p. 131), but such research is beyond the scope of this study.

The limit of the Desmoinesian series in the study area extends further east than that of the Atokan, a consequence of the progressively-eastward onlap of Pennsylvanian seas over the Chadron Arch illustrated by Wilson (1978) (Fig. 13). Deposition of the Roundtop member continued into the Desmoinesian in southeastern Wyoming and southwestern South Dakota. Overlying the Roundtop is the *Hayden* member, the uppermost Desmoinesian unit in the study area. Tenney (1965) and Momper (1963) both correlate the Roundtop and Hayden members to the *Cherokee* and *Marmaton* groups of Nebraska. Randall (1963, p.p. 8 & 15), however lists both

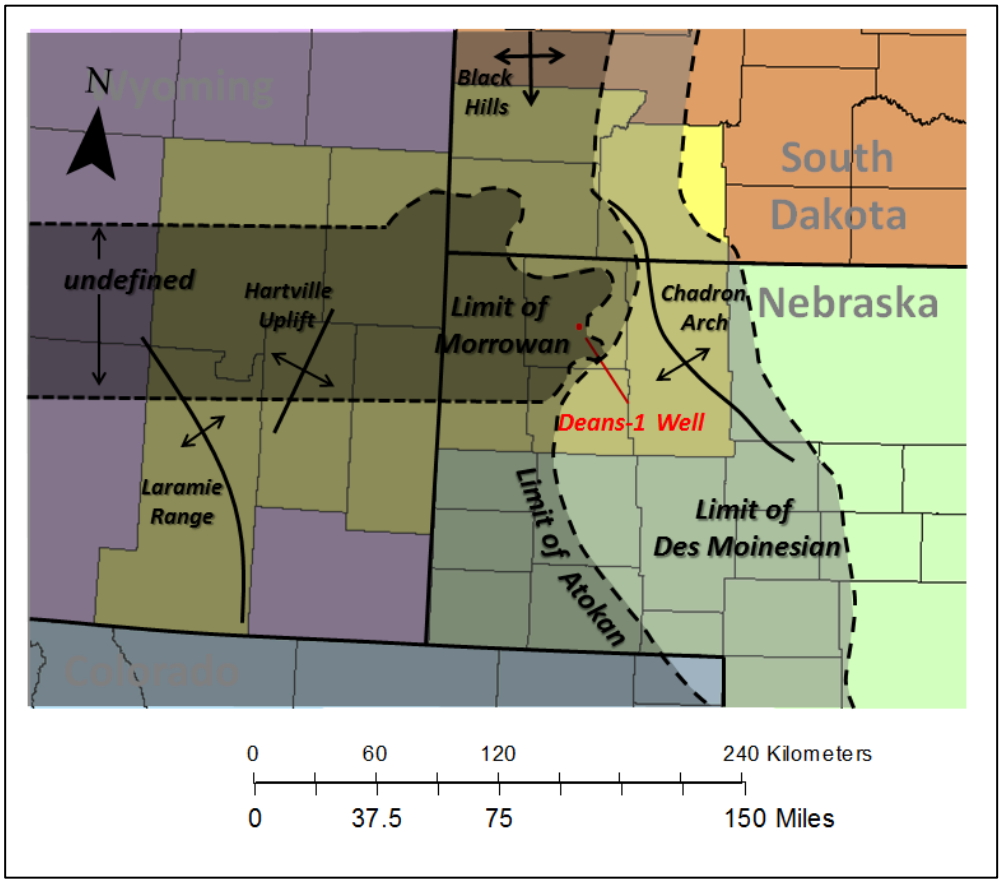

Figure 13. Limits of Morrowan, Atokan, and Des Moinesian series in study area. Missouri and Virgil are present throughout (modified from Wilson, 1978; Momper, 1963; & Machlachlan & Bieber, 1963).

the Cherokee and Marmaton as being generally restricted to the eastern Kansas region. This suggests a lack of standardized nomenclature for this interval throughout the study area. Nonetheless, the upper Roundtop and Hayden members are commonly described as a sequence of dolomite, calcareous mudstones, intermittent evaporites, and dark carbonaceous shales (Sonnenberg & Weimer, 1981, p.p. 16-17; Wilson, 1978, p. 132; Hoyt, 1963, p. 77). The Des Moines series may be differentiated from the underlying and overlying units by a basal sand horizon (MachLachlan & Bieber, 1963, p.p. 86-87) and a radioactive mudstone of dark-gray to black hue at the top of the Hayden member (Prichard, 1975, p. 120).

Missouri-aged sediments, named the *Meek* member or *Kansas City* group depending on locality (Fig. 12), are characteristically calcareous throughout the study area, but are exceptionally evaporitic in the center of the Alliance basin (MacLachlan & Bieber, 1963, p.91). These facies become more mudstone-rich near the Chadron-Cambridge arch, where positive elevations likely existed during this time (Prichard, 1975, p. 122). This pattern is consistent with the argillaceous anhydrites retrieved from the top of the Pennsylvanian section in the Deans-1 well. Limestones present near the Chadron arch are light in color and cherty, but become more dolomitic to the west (Hoyt, 1963, p. 78). Near the Hartville uplift the sequence comprises thick layers of pink limestones and dolomites punctuated by thinner gray sands and reddish shales (Wilson, 1978, p. 133). Generally the top of the Missouri can be identified with a two-foot thick bed of gray and pink chert that lies about 25 ft below the sandstone at the base of the Virgil (Prichard, 1975, p. 121).

The Virgil series is represented by the *Wendover* member in the Black Hills and Hartville uplift areas, and by the *Shawnee* in northwestern Nebraska. Although MacLachlan & Bieber (1963) map a northernmost extent of the Virgil occurring just south of the study area, Tenney (1965) and Momper (1963) both delineate the Virgil in wireline-log cross-sections that transect the study area. A northward-thinning trend likely due to pre-Permian erosion in the Virgil series is nonetheless apparent (Sonnenberg & Weimer, 1981, p. 17). Virgilian lithology is similar to that of Missouri-aged sediments, comprising thick carbonates, evaporites, red and black shales, and northeast-southwest-trending sandstone traps known as the *Leo Sands* (MacLachlan & Bieber, 1963, p. 93; Cardinal & Holmes, 1984, p. 339). A thin, red, sandy, lateritic shale unit referred to as the *Red Shale Marker* is often used to identify the top of the Pennsylvanian throughout the region (Wilson, 1978, p. 133). Montgomery (1998, p. 2178) defines the Red

Shale Marker as a dolomitic shale bed ranging in color from grayish-green to black. In considering the paleontological evidence compiled and summarized by Tromp et al. (1981, p. 14), however, it is apparent that the true Pennsylvanian-Permian boundary in this region has not been conclusively identified.

Permian System

Earliest Permian sediments, those of the Wolfcampian series (Fig. 12), consist mainly of alternating beds of dolomite, red shale and anhydrite. The lowermost sediments belong to the *Admire Group* in Nebraska and the *Broom Creek Member* of the *Hartville* and *Minnelusa* formations in Wyoming and South Dakota. The shift in lithologic prevalence from carbonate to red shale is a characteristic of the shallowing and progressive restriction of the Late Pennsylvanian and Early Permian sea within the region (MachLachlan & Bieber, 1963, p. 88). Montgomery (1998, p. 2178) divides the portion of the Admire that overlies the *Red Shale Marker* into three intervals of distinct dolomite-rich clastic rocks, each bounded by thin beds of anhydrite.

Middle Wolfcampian sediments of the *Council Grove Group* (Nebraska) and the *Cassa Member* of the Hartville and Minnelusa formations consist predominantly of massive anhydrites, dolomites, and thin sandstone beds. Mudge (1967, p. 101) notes a northward increase in the percentage of anhydrite within the Council Grove. Within the Wolfcamp as a whole, a general upward increase in the percentage of anhydrite was observed by Montgomery et al. (1998, p. 2178).

The *Chase Group* of the upper Wolfcamp can be traced throughout the study area by its basal gray shales and distinctive dolomitic sands in its lower half, and by massive anhydrites in the upper half. A major exception to this trend in the Chase Group is found in the vicinity of the

Hartville uplift, where the occurrence of salt deposits is prevalent (MachLachlan & Bieber, 1963, p. 89; Wilson, 1978, p. 134). In this region the *Cassa* (Fig. 12), which in some cases is referred to as the *Converse Sands*, is composed of crossbedded, anhydritic sandstones varying in color from white to pink (Randall, 1963, p. 9). The top of the Wolfcamp can be identified in the study area by dolomite or anhydrite beds that underlie coarse sands of the lowermost Middle Leonardian series (Mudge, 1967, p. 101).

It is unclear whether Lower Leonardian sediments are present within the study area. Although some authors divide the Leonard into upper and lower portions and discuss a conformable contact with the underlying Wolfcamp (Oldham, 1996, p. 339; MachLachlan & Bieber, 1963, p. 89), others include only the *Sumner* and *Nippewalla* groups (Fig. 12) and assign them respectively to the middle and upper Leonardian (Momper, 1963; and Tenney, 1965). Momper (1963) indicates that *Wellington* beds of the Lower Leonard are primarily restricted to western Kansas. For this reason Leonardian nomenclature is herein modeled after Tenney (1965) and Momper (1963).

The Middle Leonardian *Sumner Group* is correlative with the *Owl Canyon Formation* of the Laramie Range, Hartville Uplift, and Black Hills (Maughn, 1967, p. 134). The basal formation, the *Ninnescah Shale*, consists of red siltstones, mudstones and anhydrite. Argillaceous red sandstones of the *Harper* formation represent the upper Sumner group (Randall, 1963, p.12), but evaporites and dolomites of the *Stone Corral Formation* may lie between the Ninnescah and Harper in some areas. Momper (1963) includes the Stone Corral on stratigraphic columns for the Chadron Arch and southeastern Wyoming, but Burchett (1982) maps a northernmost extent of the Stone Corral lying just south of 42° N latitude in Nebraska.

Upper Leonardian sediments, effectively the Nippewalla Group, are divided into two formations; the lower *Salt Plain* and the upper *Cedar Hills* (Fig. 12). Salt Plain facies are predominantly composed of reddish-orange shales, fine sandstones and evaporites (Oldham, 1996, p.p. 341-342). The Cedar Hills is largely correlative with the *Lyons Sandstone* (Oldham, 1996, p. 338), a term which is often restricted to the Front Range region of the Denver Basin. These facies consist of massive, buff to yellow sandstone (Condra & Reed, 1959, p. 27) throughout most of the Denver Basin, but are rich in red shale and evaporites in most of the study area (Sonnenberg & Weimer, 1981).

In most areas the Upper Leonard has a conformable (or only slightly disconformable) relationship with the overlying *Opeche* formation of Guadalupian age. Within the region extending between the Black Hills and Hartville uplift, however, the Opeche overlies the evaporites and red shales of the Wolfcamp (Cardinal & Holmes, 1984, p.p. 333-336; Oldham, 1996, p. 337). The Upper Permian is represented in the Black Hills and Hartville uplift by the *Goose Egg* formation, which is further subdivided (from oldest to youngest) into the Opeche, *Minnekahta*, *Glendo*, *Forelle*, *Freezeout*, and *Capitan* members. Throughout the area, limestones of the Minnekahta and Forelle are described as having an interfingering relationship with the shales and siltstones of the Opeche and Glendo members Tenney (1965, p. 241). The Goose Egg correlates to the *Santanka* and *Whitehorse* groups in the Nebraska portion of the study area (Fig. 12). Santanka lithology consists primarily of red shale and gypsum (Randall, 1963, p. 19), and the Whitehorse group comprises a varied sequence of very fine-grained red sandstone, siltstone, mudstone, and dolomite (Mudge, 1967, p. 115).

Lower Mesozoic (Triassic and Jurassic) System

Martin (1965, p. 1917) identified the top of the Permian and base of the Triassic in the northern Denver Basin vicinity as a thin bed of dolomite which may correlate to the uppermost *Phosphoria Formation* of western Wyoming. Maughn (1967, p. 150) and Burk & Thomas (1956, p. 3) both discuss evaporitic redbeds that are age correlative either to the *Dinwoody* or to the uppermost Permian strata. These authors include part of the Goose Egg Formation (namely Freezeout beds) in the Triassic system, while others (Tenney, 1965; Momper, 1963) restrict the Goose Egg to the Permian. Machlachlan & Bieber (1963) trace the *Little Medicine Tongue* of the Dinwoody Formation into the study area, and although it is usually assigned an age of Lower Triassic, include it in the Goose Egg Formation. Burk & Thomas (1956) and Pipiringos & O'Sullivan (1978, pl. 1), however, both show the Dinwoody pinching out in central Wyoming and depict the *Spearfish Formation* as immediately overlying the Permian system. Some authors (Martin, 1965, p.p. 1918-1919; Sonnenberg & Weimer, p. 27) apply the names *Lykins* (Permian-Triassic) and *Jelm* (upper Triassic) to the strata immediately overlying the Permian system, but these terms are likely more appropriate for the Front Range region of the Denver Basin.

Several authors (Condra & Reed, 1959, p. 23; McCrae, 1956, p. 86; Oldham, 1996; Burk & Thomas, 1956, p. 10; Pipiringos & O'Sullivan, 1978, pl. 1) agree upon the application of the name *Spearfish* to the Triassic redbeds within the study area. Spearfish sediments in the region include red to brown shales and sandstones, as well as massive gypsum beds (Condra & Reed, 1959, p. 23; Pipiringos & O'Sullivan, 1978, p. 15). Likely due to Late Triassic exposure and erosion, the Spearfish thins northeastwardly from the Hartville uplift into the southern Black Hills, and eastwardly into Nebraska where it subcrops in Dawes County (McCrae, 1956, p.p. 86-87; Busby, 1995; Brown et al, 1984, pl. 26).

Pipiringos & O'Sullivan (1978) delineate a series of Triassic- and Jurassic-aged unconformities that can be traced throughout major basins and uplifts in Wyoming and adjacent areas. The unconformity that occurs at the base of the Jurassic system in the study area, named the J-2 unconformity, can be identified by a bed of varicolored chert pebbles presumably eroded from the *Gypsum Spring Formation* and *Glen Canyon Group* (Pipiringos & O'Sullivan, 1978, p.p. 20-21). Although the Spearfish is present throughout most of the study area, this unconformity rests on Permian strata in Box Butte and Sheridan counties, as well as parts of Dawes and Sioux counties in Nebraska (Fig. 14).

Anna (1986, pl. 2, 8 & 9) indicates the presence of only Upper Sundance and Morrison rocks within the Jurassic section of the study area. The Lower Sundance and Gypsum Spring

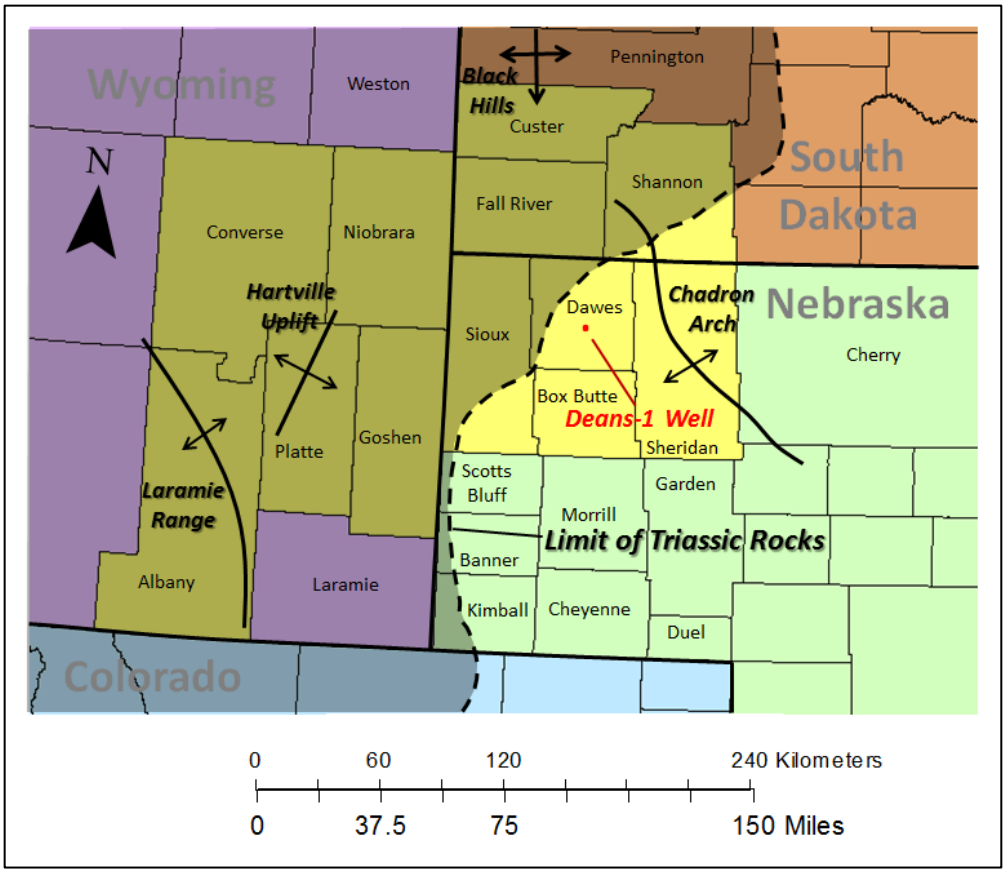

Figure 14. Limit of Triassic rocks (modified from Brown et al., 1984; & Martin, 1965).

Formations are present only in the northern part of the Black Hills. The Sundance Formation is subdivided into six members in the study area; (from the bottom upwards) the *Canyon Springs*, *Stockade Beaver*, *Hulett Sandstone*, *Lak*, *Pine Butte*, and *Redwater Shale* (Fig. 12). Sundance facies generally range from green to gray shales, calcareous sediments, and glauconitic sandstones (McCrae, 1956, p. 87). The Canyon Springs, Stockade Beaver and Hulett members of the Sundance, are primarily composed of green to gray calcareous shale and siltstone, and green to yellow cross-bedded sandstone (Anna, 1986, p. 5; Pipiringos & O'Sullivan, 1978, p. 13). These units are known collectively in the Northern Midcontinent as the *Rierdon Formation* (Schmitt, 1953, p. 366). The Lak Member, which correlates to the *Preuss Formation* to the north, is composed of red to brown sandstones and siltstones (Bartram, 1940, p. 117; Pipiringos & O'Sullivan, 1978, p. 13), and appears to be present throughout the study area with the exception of the Hartville Uplift (Schmitt, 1953, p.p. 366 & 382). Lithology of the Redwater Shale Member, the uppermost Sundance unit, comprises green to gray fossiliferous shales and sandy, calcareous coquina (Pipiringos & O'Sullivan, 1978, p. 13; Bartram, 1940, p. 117). The Redwater Shale Member correlates with the *Swift Formation* of the Northern Midcontinent (Schmitt, 1953, p. 367).

Deposition of the *Morrison Formation* occurred in a continental setting, in primarily lacustrine, fluvial and floodplain environments. Facies of the Morrison range from green to gray lacustrine shales, thin limestone beds, fluvial sands and muds, conglomerates, and varicolored clays (Bartram, 1940, p. 118; Anna, 1986, p. 6; Pipiringos & O'Sullivan, 1978, p. 13). Generally the lower part of the Morrison is richer in sandstone, and the upper part more argillaceous (McCrae, 1956, p. 87). Based on (1) the identification of the Morrison Formation by Condra & Reed (1959, p. 21) in Sioux County, NE, (2) the measurement of up to 84 m (275 ft) of Morrison

strata in the Powder River Basin by McCrae (1956, p. 87), and (3) the identification by McGregor (1972) of the Morrison in outcrops in the southern Black Hills; the Morrison is inferred to be present throughout the study area. Generally the uppermost beds of the Morrison consist of the characteristic greenish-gray shales and mudstones, but in the southern Black Hills region the base of the Jurassic-Cretaceous contact is identified by dark-gray and black carbonaceous shales (Waage, 1959, p. 46).

Cretaceous System

Lowermost Cretaceous sediments throughout the Denver Basin are described as having an interfingering (Huan, 1963, p. 120) or gradational (Waage, 1959, p.p. 11-12) relationship with the underlying Morrison Formation, making the Jurassic-Cretaceous boundary difficult to delineate in some areas. In the southern Black Hills region these sediments are known as the *Inyan Kara Group* (Fig. 15), which is separated into upper and lower sections. The lower part, known as the *Lakota Formation*, is further subdivided (from base to top) into the *Chilson*, *Minnewaste Limestone*, and *Fuson* members. These facies are predominantly fine-grained, argillaceous and carbonaceous sandstones (Dahlstrom & Fox, 1995, p.p. 3-4), and are the expression of re-worked Jurassic and older sediments derived from nearby uplifs (Martin, 1965, p. 1922). Although likely correlative throughout the study area, these units are not distinguishable westward or southward. McCrae (1956, p. 88) mentions specifically the inability to identify the Fuson Member throughout most of the Denver Basin.

Upper Inyan Kara sediments, designated the *Fall River Formation*, rest disconformably on the Lakota and are marked by a dark, thinly laminated siltstone at their base. In the study area the lithology of the Fall River varies considerably from red, yellow and purple claystones and siltstones, lignitic shale, and white, fine-grained sandstone (Waage, 1959, p.p. 12 & 61).

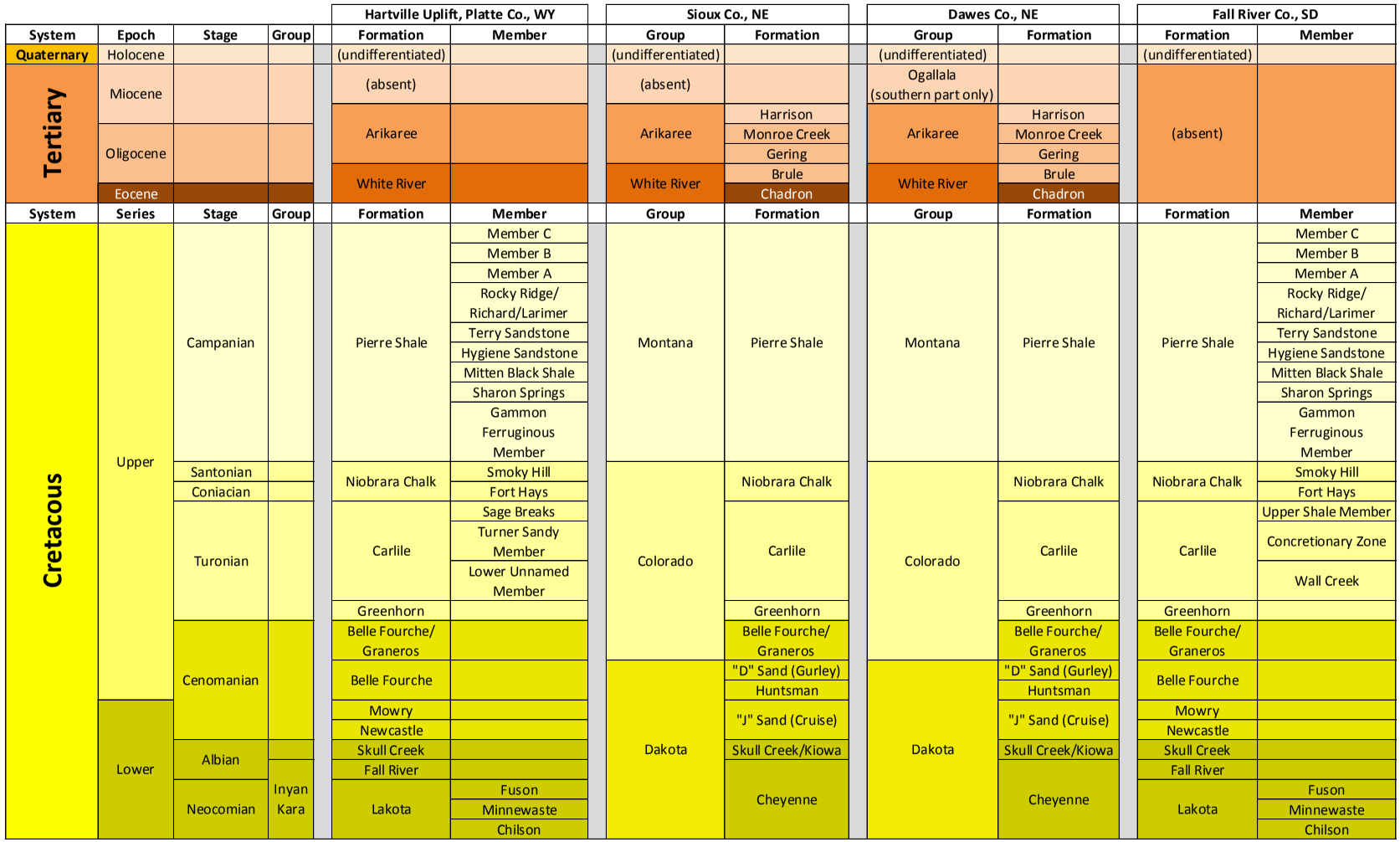

Figure 15. Stratigraphic Correlation Chart: Cretaceous through Quaternary Systems.

Generally these sediments coarsen to the south into Nebraska (Anna, 1986, p. 14). Southward into the Denver Basin the Fall River and Lakota grade into the *Cheyenne Sandstone* of the *Dakota Group* (Fig. 15). Similarly, the Inyan Kara grades westward toward central Wyoming into the Cloverly Formation (Huan & Barlow, 1962, p. 18; Huan, 1963).

The Fall River grades upward into the *Skull Creek Shale* (Waage, 1959, p. 12), a black, fissile shale and siltstone which represents a major transgression during the Early Cretaceous (McCrae, 1956, p. 88). The Skull Creek maintains a fairly uniform thickness of 46 m (150 ft) throughout the study area (Fischer et al., 2005), grades westward into the Lower *Thermopolis Shale*, and is also equivalent to the *Kiowa Shale* of the Denver Basin (Randall, 1963, p. 19; Huan, 1963).

Nomenclature for sediments overlying the Skull Creek and underlying the *Greenhorn* (Fig. 15) varies within the study area, primarily owing to the inter-tonguing and lateral-gradational character of the shaley and sandy units. In the Nebraska portion of the study area these units include (from base to top) the "*J" Sand (Cruise)*, *Huntsman Shale*, and *"D" Sand (Gurley)* (Huan, 1963, p. 121). Conventionally the *Dakota Group* in the Denver Basin includes these formations, as well as the underlying Skull Creek Shale and Cheyenne Sandstone. In the Wyoming and South Dakota portions of the study area, however, the term *Dakota* is not used. Instead the interval between the Inyan Kara and Greenhorn is filled by sediments referred to as (from base to top) the *Newcastle Sandstone*, *Mowry Shale*, and *Belle Fourche Shale*. It should be noted that some publications refer to Dakota or equivalent sediments as *Omadi*, a term introduced by Condra and Reed (1959, p. 18) for the purposes of eliminating the use of *Dakota* as both a group and formation.

"J" Sands consist of buff to tan interbedded sandstones, conglomerates and varicolored silt and claystones that are characteristic of deltaic, tidal plain, and alluvial environments (Martin, 1965, p. 1922; Curtis, 1988, p. 193; Waage, 1959, p. 16; Randall, 1963, p. 13). The "J" Sand is thicker and more extensive in the Denver Basin than is the "D" Sand, but like the "D" Sand is historically a major hydrocarbon target zone throughout the region (Bass, 1958, p. 7). The "J" Sand interval grades westward into the *Muddy Sandstone* of central Wyoming, and inter-tongues northward into the *Mowry Shale* of the Black Hills region (Martin et al., 2004; Huan, 1963). The Newcastle Sandstone is the "J" Sand equivalent in the Wyoming and South Dakota portions of the study area (Robinson, et al., p.p. 44-66). The transgressive Huntsman Shale, the dark gray and black fissile shale that separates the "D" and "J" sands, is correlative with the lower Belle Fourche Shale of Wyoming and South Dakota (Martin et al., 2004; Huan, 1963). The "D" Sand, although lithologically similar to the "J" Sand, contains more lenticular sand beds, lignite coal seams, and thin interbeds of sand and dark shale (Bass, 1958, p. 6; Huan, 1963, p. 122).

The presence of the carbonaceous, sandy gray shales of the *Graneros Formation* is questionable within the Wyoming and South Dakota parts of the study area. Although Huan (1963, figs. 1 & 2) depicts the Graneros grading northward into the Belle Fourche and *Greenhorn Formation*, and into the *Benton Shale* to the west, Rothrock (1949, pp. 11-12) and Randall (1963, p. 12) identify the Graneros in southeastern Wyoming and southwestern South Dakota. Robinson et al. (1964, Fig. 4), who provide comprehensive stratigraphic correlations throughout the Black Hills and adjacent regions, mention the presence of the Graneros only in west-central South Dakota. It is therefore apparent that the inconsistency in delineating the

Graneros throughout the study area region is a problem in nomenclature, and does not necessarily reflect the regional continuity of correlative strata.

The *Greenhorn Formation*, a sequence of thick sandstones interbedded with shale and mottled carbonates (Jorgensen et al., 1993, p. 39; Downey, 1986, p. 20), is identified in the area as lying above a regional shale-marker commonly referred to as the "X" Bentonite (Huan, 1963, p. 120). The Greenhorn Formation is one of the more extensive Cretaceous units throughout the Midcontinent (Weimer, 1978, p. 214), and is easily distinguishable as a resistant ridge- and cliff-former in the Black Hills region (Robinson et al., 1964, p. 60; Rothrock, 1949, p. 12).

Marine sediments of the *Carlile Formation* are extensive throughout the study area, ranging in thickness from 30 to 60 m (100 to 200 ft) (Weimer, 1978). Rothrock (1949, p.p. 16-20) divides the Carlile into three distinct zones in the southern Black Hills; a lower dark, sandy shale unit known as the *Wall Creek*, a middle interval containing calcareous concretions known as the *Concretionary Zone*, and an upper dark shale referred to as the *Upper Shale Member*. In southeastern Wyoming, McCrae (1956, p. 89) and Robinson et al. (1964, p. 66) identify three different nominal units that appear to correlate lithologically with those named by Rothrock (1949) (Fig. 15). Southward into the Denver Basin the Carlile is represented primarily by the *Codell Sandstone* (Curtis, 1988, p. 188).

The *Niobrara Chalk Formation* consists of calcareous muds, massive limestones, and gray shales (Condra & Reed, 1959, p. 17; Downey, 1986, p. 20) that exhibit up to 150 m (500 ft) thickness in the study area (Weimer, 1978). The Niobrara is divided into two members; the lower *Fort Hays Member* and the upper *Smoky Hill Member*, both of which are predominantly calcareous muds. The lower unit, however, is characterized by higher kaolinite and illite content, and the upper by smectite and bentonite, (Stach, 1976, p. 1).

The *Pierre Shale Formation*, the thickest single formation in the Denver Basin, exhibits perhaps the greatest variation in thickness within the study area. The Pierre Shale ranges in thickness from about 1500 m (5000 ft) near the Hartville Uplift to being completely absent over the Chadron Arch in the eastern part of the study area (McCoy, 1953). The delineation of the base of the Pierre is fairly conspicuous; it is marked by an upward sharp decrease in the amount of calcareous sediments relative to the underlying Niobrara (Curtis, 1988, p. 188). Generally the Pierre Shale is composed of dark-gray to blue-ish fissile shales and clays. Kitely (1977) and Schultz et al. (1980) present thorough assessments and explanations of Pierre Shale composition and distribution, and outline the members included in Figure 15.

Cenozoic System

The Pierre shale comprises the uppermost geologic unit throughout the northern part of the study area. The Cenozoic System in the remaining portion of the study area—namely southern Niobrara County and northern Goshen County in Wyoming, as well as southern Sioux and Dawes counties in Nebraska (Fig. 2)—is represented only by *White River Group* and *Arikaree Group* sediments (Love & Christiansen, 1985; Burchett, 1969) (Fig. 15).

In northwestern Nebraska the *Chadron Formation*, the lowermost formation of the White River Group, is composed of varicolored (yellow, orange, purple) paleosols and shales with intermittent sands and volcanic ash (Terry, 1998, p.p. 21-22). The overlying *Brule Formation* contains brown volcaniclastic siltstones, laminated silty clays of variable color, gypsum, and channel sandstones. (LaGarry, 1998, p.p. 75-83)

The Arikaree Group is subdivided into three members; the *Gering*, *Monroe Creek* and *Harrison*. The Gering, the basal member, is composed primarily of interbedded fluvial gravels and eolian sands. Additional eolian sands of the middle Monroe Creek grade upward into the

Harrison, which includes buff sands and siliceous paleosols (MacFadden & Hunt, 1998, 144-146).

Ogallala sediments, mainly granitic sands and gravels (Breyer, 1975), are primarily restricted to southern Dawes and Sheridan counties in Nebraska (Burchett, 1969). Aside from dispersed and localized Quaternary terrace, eolian and alluvium deposits, the South Dakota portion of the study area is void of Cenozoic sediments (Martin et al., 2004).

Hydrogeological Overview

The hydrogeological system of the study area is part of a much broader system of aquifers that extend throughout the Great Plains region of the United States. The U.S. Geological Survey defines three primary regional aquifer systems that encompass those of the study area; the Western Interior Plains (WIP), Great Plains, and High Plains aquifer systems (Jorgensen et al, 1993; Helgesen et al, 1993; Signor et al., 1996). The two confined systems, the WIP and Great Plains aquifers, receive recharge from precipitation, runoff, and stream flow along outcrops in uplifted areas throughout the Central Plains (Naus et al., 2001, Carter et al., 2001). Although the two most prominent structural highs—the Black Hills uplift and Laramie Range—supply the majority of this recharge on a regional basis, outcrops along the Hartville Uplift are believed to contribute a significant portion of recharge to the confined aquifers within the study area (Downey, 1984, p. 2).

The presence of several major faults and zones of high lineament density (Figures 3 & 4) may have a significant effect on groundwater flow patterns in the study area. In many cases vertical fault and lineament planes impede flow in the horizontal direction and simultaneously facilitate it vertically. Downey and Dinwiddie (1988), however, discuss the unpredictability of the effect of subsurface faults and lineaments on confined aquifer flow. Although the primary

permeability and porosity of aquifer rocks may be supplemented by secondary permeability in the form of fractures, the primary properties may conversely be decreased by mineralization catalyzed by the initial state of increased fluid flow. Additionally, Anna (1986) acknowledges evidence that suggests that compressional and tensile tectonic features are respectively associated with lower and higher permeability conditions, but emphasizes the need for further investigation into the matter.

Western Interior Plains Aquifer System

On a regional basis, the Western Interior Plains (WIP) aquifer system comprises Cambrian through Mississippian geologic units that extend from western Iowa and Missouri to the Front Range of Colorado, and from northern Nebraska to Oklahoma and northern Texas (Jorgensen et al., 1993). However, because of the near absence of pre-Mississippian Paleozoic units in the study area, the WIP aquifer system includes only the limestones and dolomites of the lower Madison Group. The subsurface limits of the Madison Group are depicted in Figure 11.

Recharge rates to the Madison aquifer in the Black Hills and Laramie Range have been calculated at approximately 4.248×10^{-1} m^3 s^{-1} and 2.831×10^{-2} m^3 s^{-1}, respectively (Downey, 1984). Downey (1984) also calculated Madison Group flow rates of approximately 0.6 m/year in the region between the Hartville uplift and southern Black Hills.

Cooley et al. (1986) cite secondary permeability as the primary catalyst of flow in the Madison due to its low intergranular porosity. Groundwater flow in the Madison is therefore predominantly controlled by structural joints, dissolution cavities and bedding planes. A significant portion of recharge to the Madison on the western flanks of the Black Hills flows southwestward into the southern Powder River Basin, and then southeastward into the northern

Denver Basin (Konikow, 1976). The potentiometric surface of the Madison in the study area vicinity is shown in Figure 16.

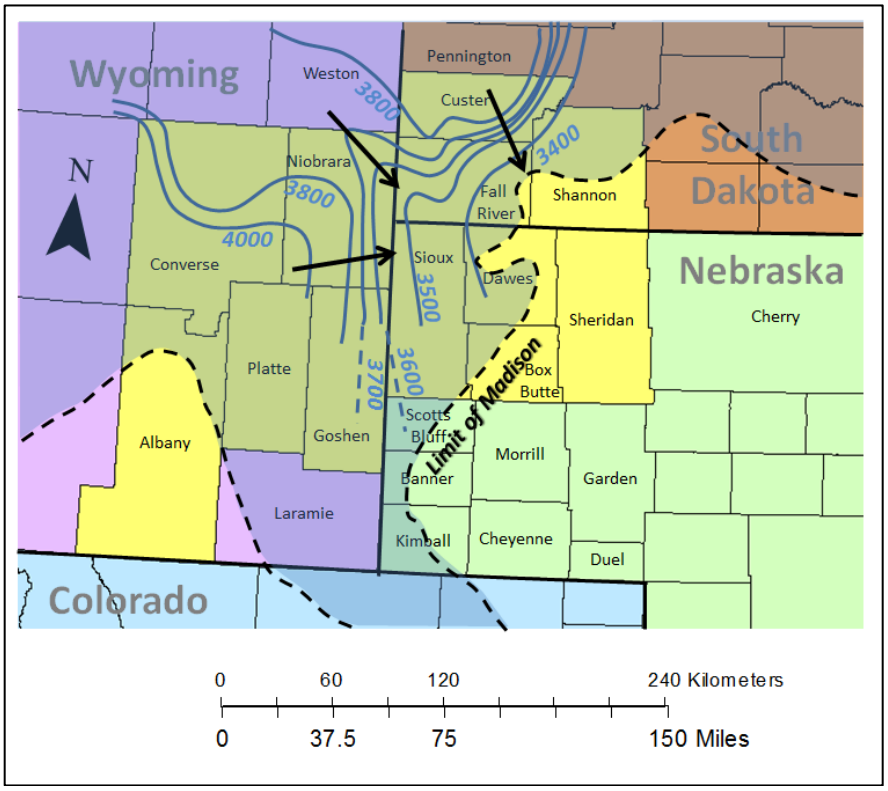

Figure 16. Potentiometric surface of Madison aquifer. Contours are in feet. Arrows indicate flow directions (modified from Konikow, 1976; Downey, 1984; & McKaskey, 2013).

Although some USGS publications regard the overlying dolomites, shales, and anhydrites of the Pennsylvanian and Permian systems as the confining layer of the WIP aquifer system (Jorgensen et al, 1993, p. 48), the lower Minnelusa Formation in the study area vicinity is characterized by others as an aquifer system. McKaskey (2013) calculates vertical hydraulic gradients between the Madison and Minnelusa throughout the study area. This data indicates higher hydraulic heads in the Minnelusa in the western margin of the study area, and higher hydraulic head in the Madison to the east. Hydraulic heads between the two aquifers are approximately equivalent in the tri-state border area, the structural bridge between the Powder

River and Denver basins known as the Lusk Embayment (Fig. 2). The hydraulic gradient data provided by McKaskey (2013) effectively reflects a trend of downward leakage from the Minnelusa in the Hartville Uplift and Laramie Range vicinity, and that of upward leakage from the Madison in the southern Black Hills. Naus et al. (2001) attribute much of this interaction to secondary porosity and paleo-karst features in the upper Madison.

Great Plains Aquifer System

The hydrostratigraphy of the Great Plains aquifer systems includes the sandstones and shales of the lower Cretaceous, namely those of the Dakota Group (or Inyan Kara plus the sands of the Newcastle). Rocks of the Great Plains are further subdivided by the USGS into two separate aquifers separated by a confining layer. The lower Apishapa aquifer includes the sands and silts of the Cheyenne formation (or Lakota and Fall River formations, see Fig. 15), and the upper Maha aquifer comprises the upper portion of the Dakota Group (Newcastle or Huntsman and "D" and "J" sands). Both units extend throughout a particularly vast region of the Central Plains, covering parts of South Dakota, Nebraska, Wyoming, Colorado, and Kansas. In the study area the Apishapa consists of a much larger percentage of sandstone (up to 75%) than the strata of the Maha (as little as 25%), resulting in a fairly significant difference in permeability and effective porosity (Helgesen et al., 1993).

Much of the recharge to the study area portion of the Great Plains aquifer system is attributed to the Black Hills and Hartville Uplift. Helgesen et al. (1993) estimate the recharge rates in these areas at approximately 0.11 $m^3 s^{-1}$. Flow occurs in an easterly to southeasterly direction through the study area (Figure 17), but follows a more eastward path across Nebraska and South Dakota (Signor et al., 1996; Bredehoeft et al., 1983). Flow vectors determined by Downey (1986, pl. 3) for the lower Cretaceous aquifer in the study area vicinity indicate the

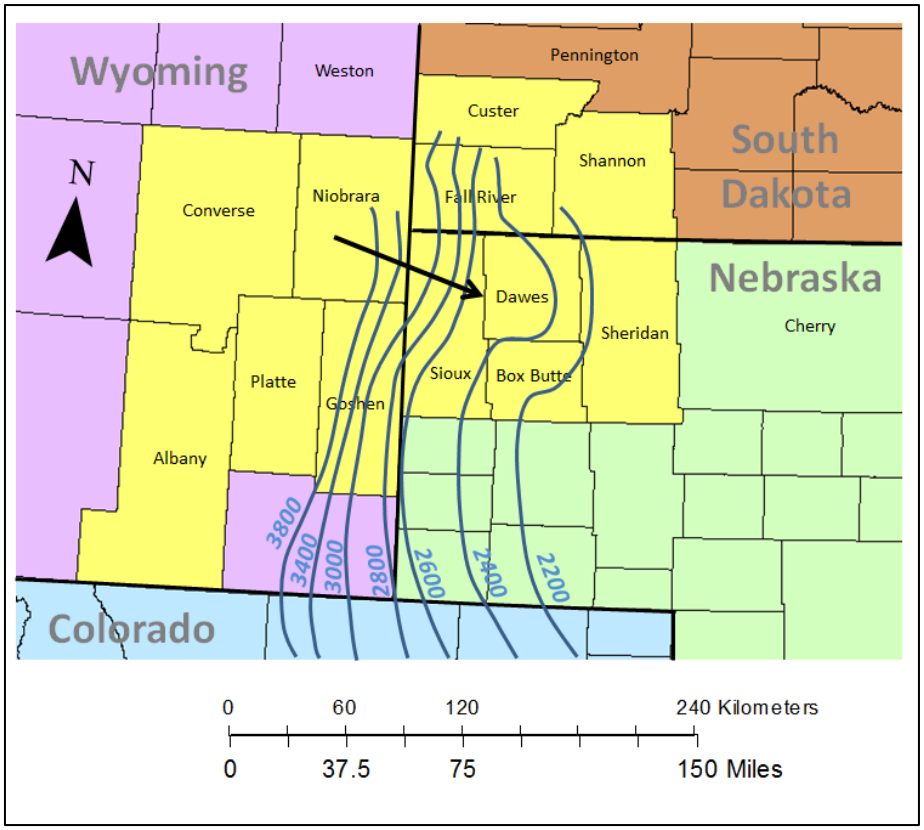

Figure 17. Potentiometric surface of Dakota aquifer. Contours are in feet. Arrows indicate flow directions (modified from Signor et al., 1996; & Bredehoeft et al., 1983).

possibility of a northeasterly flowpath from the Laramie Range and Hartville Uplift into the southern Black Hills.

The overlying shales of the upper Cretaceous comprise the Great Plains confining system. Although the relatively permeable Niobrara Chalk is included in this section, the adjacent shales and mudstones of the Belle Fourche, Greenhorn, Carlile, and Pierre Shale formations exhibit much lower permeabilities (Bredehoeft et al., 1983) and are collectively much thicker in comparison. Vertical flow between the overlying High Plains aquifer and the underlying Great Plains aquifer is locally determined by the vertical hydraulic gradients between

the two units. Nevertheless, the Great Plains confining system generally serves as a flow barrier between the two aquifers in most areas (Signor et al., 1996, p. 35).

High Plains Aquifer System

Due to the vast regional extent of its principal host unit, the Ogallala Formation, the High Plains aquifer is commonly referred to as the Ogallala Aquifer. Although Nebraska hosts the largest portion of the aquifer's total area (approximately 41 million of the total 112 million acres) and largest saturated thickness (over 180 m) (Stanton et al., 2011), the High Plains aquifer extends into southeastern Wyoming, south-central South Dakota, eastern Colorado, western Kansas, and the panhandles of both Oklahoma and Texas. Stratigraphically the High Plains aquifer includes geological units dating back to Tertiary time, and extends upward into loosely-consolidated Quaternary deposits of varying depositional origin. In most areas the base of the High Plains aquifer occurs at the top of the massive siltstones of the White River Group (see Fig. 15). The aquifer's primary zones of saturation include the fine sands of the Arikarree Group; the unsorted sands, silts and gravels of the Ogallala Formation; and regionally-differentiated assortments of Quaternary loess, alluvial and valley-fill deposits (Gutentag et al., 1984). In the study area the High Plains aquifer is restricted to the Arikaree Group in eastern Wyoming and parts of northwestern Nebraska, and is absent in southwestern South Dakota. Although much of the recharge to the unconfined High Plains aquifer is attributed to precipitation and runoff, countless areas of hydrologic connection to surface water bodies are well documented (Stanton et al., 2011).

Regional Geothermics and Previous Investigations

The study area is part of the Great Plains region, a tectonically stable physiographic province for which geothermal heat flow is transferred primarily by means of conduction.

Morgan and Gosnold (1989) calculated the mean heat flow values for the major conterminous U.S. physiographic provinces, and reported an average 66 ± 26 mW m^{-2} for the Great Plains. Areas in the Rocky Mountains and further west exhibit heat flow values upwards of 100 mW m^{-2}. Because high heat flow is often associated with radiogenic heat production and flux variability of the upper mantle, which are characteristic of regions that have undergone geologically-recent tectonism (Blackwell, 1971), anomalous heat flow values measured in regions of tectonic stability are often attributed to different processes. Many such anomalies (both low and high) are correlated with zones of recharge and discharge of confined bedrock aquifers. In the Great Plains regional advective heat transport generally occurs from west to east, following the gentle eastward slope across the region (Gosnold, 1990).

Roy et al. (1972) correlate the major physiographic provinces of the conterminous United States to heat flow provinces by determining the values of reduced heat flow for numerous localities. Reduced heat flow q_0 is the intercept value for the linear relation $q = q_0 + Ab$ in which surface heat flow q is calculated given the amount of radiogenic heat production A (μW m^{-3}). The variable b is the slope (m) that relates heat production to surface heat flow. Variation in reduced heat flow is attributed by the authors to regional fluctuations in upper mantle heat flow, and generally increases westward across the U.S. Surface heat flow measurements in the Black Hills as low as 20 mW m^{-2} (Sass et al., 1971b) are characteristic of the meteoric recharge to upturned aquifer outcrops along the flanks of the uplift (Gosnold, 1999). Reduced heat flow determinations for the Black Hills provided by Roy et al. (1972), however, indicate a background (or reduced) heat flux of at least 63 mW m^{-2} in the vicinity.

In 1979 the Department of Energy (DOE) sponsored a geothermal resource assessment program for the state of Nebraska. Researchers were tasked with gathering temperature gradient

data in 30 shallow (approximately 150 m depth) wells, analyzing available bottom-hole temperature (BHT) data for the state, and producing a map to outline major geothermal resource areas in Nebraska (Gosnold et al., 1982). Although most values in the state fall within the range of 38 to 67 mW m^{-2}, two areas of anomalously high heat flow were delineated in the study. Gosnold et al. (1981) reported values as high as 145 mW m^{-2} in north-central Nebraska, a manifestation of discharge from four major aquifers in which regional flow drives advective heat transport (Gosnold, 1999). Five heat flow measurements collected in northwestern Nebraska (one in Dawes County and four in Sheridan County) range from 65 to 112 mW m^{-2} (Fig. 18), and are all within close proximity of the Chadron Arch (Fig. 2).

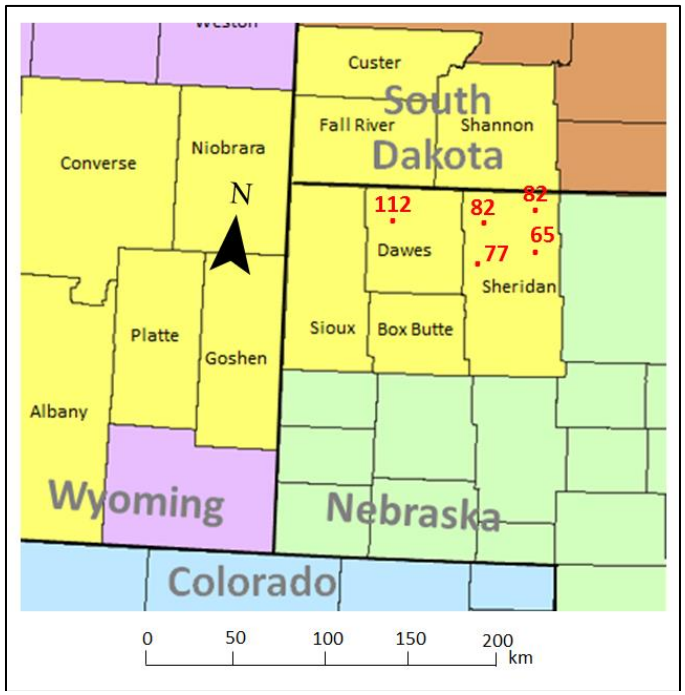

Figure 18. Locations of equilibrium temperature gradient measurements and observed heat flow values. Heat flow values (mW m^{-2}) are colored red (modified from Gosnold et al., 1981)

Stix (1982) compiled satellite imagery for central Nebraska in an effort to correlate surface manifestations of the regional structural framework to observed geothermal anomalies.

The study also aimed to relate variations in the Precambrian basement (in lithology and age) to regional trends in heat flow throughout the state. Mapped delineations of Precambrian lithologic provinces and locations of measured heat flow values (from Gosnold et al., 1981) suggest a possible attribution of the local heat flow anomaly in northwestern Nebraska to radiogenic heat production in the granitic basement.

Hildebrand and Kucks (1985) dismiss radiogenic heat production as a significant contribution to the heat flux anomalies measured in southwestern South Dakota. The anomalies are instead credited to the upward migration of recharged fluids through vertical faults and lineament features in the area (figs. 3 & 4). According to the authors, although much of these geothermal waters likely disperse in highly permeable aquifers encountered along their upward descent (most probably Cretaceous and Cenozoic aquifers), some breach the surface in the form of thermal springs, such as those located near Hot Springs, SD (northern Fall River county).

Gosnold (1984) provides an explanation for high heat flow measured in shallow holes in western Nebraska. Models constructed to simulate regional flow in the Dakota (Great Plains) aquifer suggest that high heat flow values are likely attributed to groundwater flow rates of approximately 1.2 m yr^{-1}. These simulations are indicative of upward and eastward heat advection within Cretaceous aquifers from the central trough of the Denver Basin to its eastern flanks in western Nebraska. Flow patterns of the Madison and Dakota aquifers for the northern, shallower portion of the Denver Basin may, however, attest to the presence of heat transport mechanisms different than those operating in deeper parts of the basin. Potentiometric data presented by several authors (figs. 16 & 17) (Konikow, 1976; Downey, 1984 & 1986; McKaskey, 2013; Signor et al., 1996; Bredehoeft et al., 1983) suggests that recharge to the aquifers in the study area occurs much closer in proximity, and that southeastward flow from the

southern Powder River Basin via the Lusk Embayment (Fig. 2) is substantial. These factors, in addition to the shallow structure of the northern trough and local presence of faults and lineaments (Figures 3 &4), are grounds for further study of the mechanisms controlling observed surface heat flow anomalies.

CHAPTER III

METHODOLOGY

Data

Heat Flow

Crustal conductive heat transfer is calculated using Fourier's Law of thermal conduction, which is expressed as

$$q = -\lambda(\partial T/\partial z) \quad (Eq. 1)$$

where q is the rate of thermal energy flux per unit area (mW m^{-2}), λ is the thermal conductivity (W m^{-1} K^{-1}) of the heat transfer medium, and $\partial T/\partial z$ is the vertical temperature gradient (°C/km). Because heat transfer occurs in the direction of decreasing temperature, the negative sign in the equation is conventionally included to account for the negative change in elevation with increasing temperature (Beardsmore & Cull, 2001, p.p. 12-13). The relationship between the Celsius and Kelvin temperature scales (an offset of 273.15 degrees) results in an equivalence between changes in temperature on either scale.

Thermal Conductivity.

Background & Theory.

Calculation and Measurement of Thermal Conductivity. The heat transfer medium in a sedimentary basin setting is the complete stratigraphic section of the region of interest within the basin. With regards to calculating heat flow and modeling two- or three-dimensional heat transfer within this stratigraphic medium, the measurement of as many unique lithologies as

possible is essential for accuracy. A representative thermal conductivity of the stratigraphic section of interest is calculated using the harmonic mean;

$$\frac{1}{\lambda_H} = \frac{1}{Z}\sum_{i=1}^{n}\frac{z_i}{\lambda_i} \qquad (Eq.2)$$

where λ_H is the harmonic mean thermal conductivity of the stratigraphic section (W m^{-1} K^{-1}), λ_i is the thermal conductivity of the *i*th bed (W m^{-1} K^{-1}), z_i is the thickness of the *i*th bed (m), and Z is the total thickness of the complete stratigraphic section (m). Parameters used in Equation 2 are conceptually depicted in Figure 19.

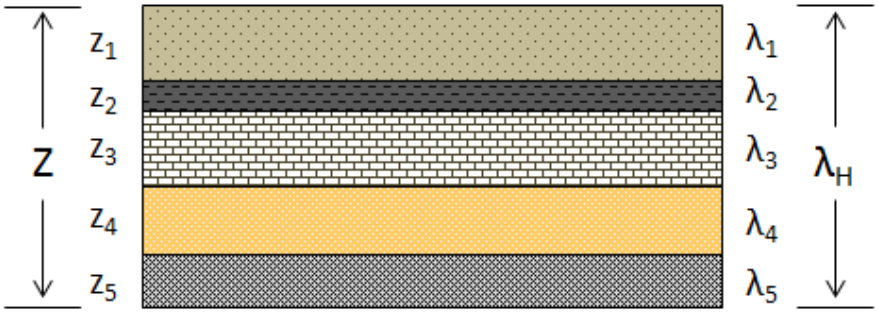

Figure 19. Conceptual depiction of variables used in the calculation of harmonic mean thermal conductivity of a stratigraphic section.

In situ measurements of thermal conductivity involve the use of a line-source needle probe instrument. This technique is designated as the transient method of thermal conductivity measurement, and requires the application of heat to and subsequent temperature measurements of in situ rocks (Beardsmore & Cull, 2001, p. 116). Laboratory techniques of thermal conductivity measurement, however, involve the use of an electronic divided bar apparatus. This procedure is known as the steady-state method of thermal conductivity measurement (Beardsmore & Cull, 2001, p. 108). The electronic divided bar utilizes Fourier's Law (Eq. 1) by

applying a known temperature gradient over the entire thermal stack (depicted in Figure 20) of the apparatus and monitoring the change in temperature gradient ΔT across the sample over time.

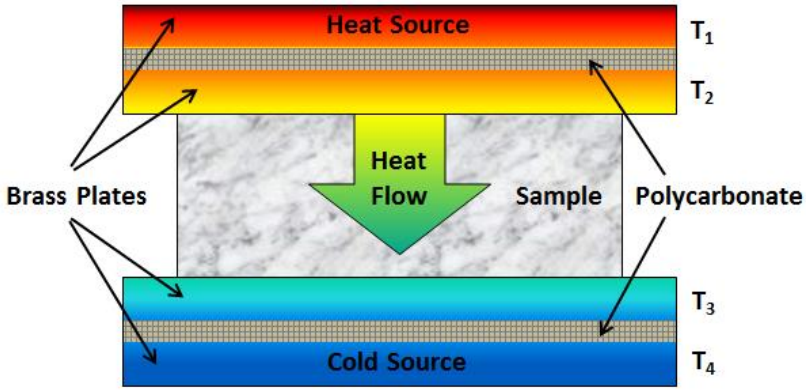

Figure 20. Configuration of electronic divided bar apparatus and conceptual depiction of measurement process (modified from Antriasian, 2010).

Once ΔT reaches equilibrium, the thermal conductivity of the sample is calculated using the following equations:

$$\lambda = d/R \quad (Eq.3)$$

$$R = A\frac{\Delta T - c}{a(D+b)} \quad (Eq.4)$$

$$\Delta T = \frac{T_2 - T_3}{(T_1 - T_2) + (T_3 - T_4)} \quad (Eq.5)$$

where λ is the thermal conductivity (W m^{-1} K^{-1}) of the sample, d is the thickness of the sample in mm, D is the diameter of the sample in mm, A is the surface area of the sample (mm^2), a, b, and c are coefficients of a polynomial determined during the calibration process, and *T1, T2, T3,* and *T4* are the temperatures of the brass plates of the thermal stack (Fig. 20) (Antriasian, 2010).

Prior to analysis with the divided-bar apparatus, samples must be saturated in water to (1) minimize the thermal effects of air convection within the sample pore space during measurement, and (2) to simulate the subsurface saturation conditions of the in situ rock unit.

Prior to saturation the samples are placed in a vacuum chamber to remove the air within the pore space, allowing for complete saturation of the connected pore space to occur more quickly and efficiently. (Beardsmore & Cull, 2001).

Unconsolidated Sample Thermal Conductivity Correction Theory. Ideally thermal conductivity is measured using solid rock samples collected from cores or outcrops. However, in some cases only drill cuttings are available for measurement, and in other cases the rock samples themselves cannot be kept in consolidated form during the drilling, cutting, saturation, or measurement process. Friable sandstones and fissile shales, for example, are often not suitable for laboratory thermal conductivity measurement.

Such unconsolidated sediments, however can be packed into a hollow cylindrical cell (Fig. 21) and saturated for divided-bar analysis. The cell walls typically consist of clear plastic or PVC, and the ends are fitted with circular copper or brass plates. The measured conductivity of the cell itself and the aggregate contents of the cell (rock fragments and water) can be corrected to represent the actual thermal conductivity of the corresponding consolidated lithology.

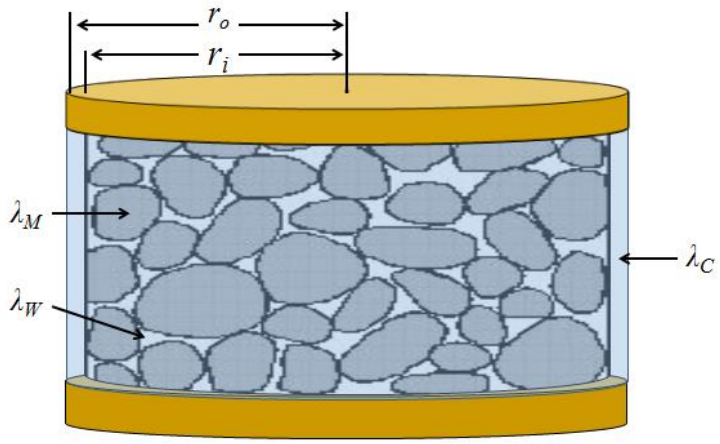

Figure 21. Example illustration of hollow cell used for unconsolidated sample thermal conductivity measurement and parameters used in calculations.

Several authors discuss the relationships between consolidated and unconsolidated thermal conductivity measurements, and present viable corrections applicable to drill cuttings and friable samples. Sass et al. (1971a) describe the relationship between the saturated sample conductivity and its constituent conductivities as

$$\lambda_A = \lambda_M^{1-\emptyset} \lambda_W^{\emptyset} \qquad (Eq. 6)$$

and the calculation of the unconsolidated sample matrix conductivity as

$$\lambda_M = \lambda_W \left(\frac{D^2}{d^2} \frac{\lambda_T}{\lambda_W} - \frac{D^2 - d^2}{d^2} \frac{\lambda_C}{\lambda_W} \right)^{1/(1-\emptyset)} \qquad (Eq. 7)$$

in which λ_A is the conductivity of the aggregate rock fragment and water mixture, λ_M is the conductivity of the sample rock matrix, λ_W is the conductivity of water, taken to be 0.615 W m^{-1} K^{-1} after Beardsmore & Cull (2001, p. 112), λ_C is the conductivity of the plastic wall of the hollow cell (depicted in Figure 21), taken to be 0.42 W m^{-1} K^{-1} after Beardsmore & Cull (2001, p. 112), and λ_T is the total conductivity of the cell and aggregate contents. This value is synonymous with the raw, uncorrected thermal conductivity value calculated in Equation 3 during divided-bar analysis. All thermal conductivity values are expressed in W m^{-1} K^{-1}. D and d are the outer and inner diameters (m) of the hollow cell, respectively, and ϕ is the porosity of the contents contained in the hollow cell (expressed as a decimal).

Beardsmore and Cull (2001) describe a similar series of relationships;

$$\lambda_A = (\lambda_T - \lambda_C) \left(\frac{r_o}{r_i} \right) + \lambda_C \qquad (Eq. 8)$$

$$\lambda_M = \left(\frac{\sqrt{\lambda_A} - \emptyset \sqrt{\lambda_W}}{1 - \emptyset} \right)^2 \qquad (Eq. 9)$$

in which the variables r_o and r_i are the outer and inner radii (m) of the hollow cell (depicted in Figure 21), respectively.

Estimated values of consolidated rock conductivity can be obtained by first calculating the matrix conductivity λ_M of the rock fragments within the hollow cell. If porosity values of the corresponding consolidated, in situ rocks can be easily obtained (most likely from well log records or core analysis) or accurately estimated, an aggregate conductivity estimation of the solid, saturated rock can be calculated by re-writing Equation 6 (after Sass et al., 1971a) as

$$\lambda_{SA} = \lambda_M^{1-\emptyset_0} \lambda_W^{\emptyset_0} \quad (Eq. 10)$$

where λ_{SA} is the thermal conductivity (W m^{-1} K^{-1}) of the solid aggregate saturated rock, and ϕ_0 is the porosity (expressed as a decimal) of the in situ rock.

For isotropic rocks such as limestone or pure, well-sorted sandstone, the aforementioned relationships (Equations 6 through 10) are relatively straightforward. Significant problems in correcting hollow-cell thermal conductivity values arise, however, with samples of particularly high clay-mineral content. Because the thermal conductivity of clay minerals is higher in the horizontal direction than in the vertical direction, significant discrepancies between solid-sample and hollow-cell conductivities of shales and siltstones are most probable. Deming (1994) documents this problem by demonstrating a clear inverse relationship between thermal conductivity anisotropy and thermal conductivity perpendicular to bedding planes. The following equation presented by Deming (1994) is intended for correcting the conductivity values of unconsolidated shale-rich samples for the vertical direction:

$$\lambda_Z = exp\left\{\frac{\ln(\lambda_A) - 0.5406}{0.61}\right\} \quad (Eq. 11)$$

Beardsmore and Cull (2001) also present a modification of the relationship introduced by Deming (1994), which is written as

$$\lambda_Z = exp\left\{\frac{\ln(\lambda_A) - 0.6267}{0.548}\right\} \quad (Eq. 12)$$

Procedures

Sample Collection and Laboratory Measurement. Solid samples were collected from three wells in northwestern Nebraska and several outcrop locations in the Black Hills, SD (Appendix A). Although one Precambrian gneiss sample from the Murray 17-24 well was used in thermal conductivity analysis, the Precambrian schist sample from the Kudrna well was too weathered and brittle to be analyzed. Samples used to represent the stratigraphic column of the study area originated primarily from the Deans-1 well, but the upper Permian (Goose Egg) section was represented by outcrop samples (labeled BHAO1, 3 & 5) taken from the Black Hills in order to fill stratigraphic gaps in the core inventory of the Deans-1 well (see Appendix B). Two additional samples (labeled MS1 and MS2), which are representative of the Sundance and Morrison formations, were collected by fellow graduate student Matt Sebade from outcrops at the Derby Dome anticline, which flanks the eastern side of the Wind River range near Lander, WY.

Thermal conductivity samples from the Deans-1 well were selected on the basis of both lithologic uniqueness and stratigraphic nomenclature in order to produce a complete and representative conductivity profile of the section. The identification of stratigraphic tops, a step necessary for sample interval delineation, was completed by comparing the well's gamma ray and neutron logs to those of the type-section given by Momper (1963). The depth intervals determined with these logs were matched with the appropriate stratigraphic unit and corresponding conductivity samples. This information, as well as lithologic descriptions of each sample, is given in Appendix B.

The solid samples from both cores and outcrops were cut into cylindrical configurations; the thicknesses and diameters of which were measured to a precision of 0.01 mm using a digital caliper. Solid sample dimensions are given in Appendix C. Sample preparation also included 24 hours of vacuum chamber de-pressurization and a subsequent 24-hour period of water saturation. Sample mass was measured with a precision of 0.01 g both before and after saturation in order to calculate connected porosity values. Measured porosity and density values for solid samples are reported in Appendix D.

A total of 82 solid samples and 38 unconsolidated samples were measured using both stationary electronic divided bar (SEDB) and portable electronic divided bar (PEDB) instruments. A temperature range of 15 to 35 °C was utilized for each of the four instruments (2 SEDBs and 2 PEDBs). Thermal conductivity measurements for solid samples are included in Appendix D, and those for unconsolidated samples are listed in Appendix E.

Correction of Unconsolidated Sample Thermal Conductivity. Unconsolidated samples, which are representative of the Tertiary and upper Cretaceous portions of the stratigraphic section, were retained from shallow test holes drilled in the 1970s and 1980s by the Nebraska Conservation and Survey Division and University of Nebraska-Lincoln School of Natural Resources. Specifications for these wells are given in Appendix A. Appendix F lists sample IDs with corresponding lithologic descriptions and stratigraphic nomenclature, and detailed lithologic logs for each of the wells used are provided by Gosnold and Eversoll (1983).

Twenty of the solid samples were subsequently crushed and re-measured for the purposes of testing corrections (Equations 6 through 12) for the unconsolidated samples. These samples were selected for the purpose of testing corrections intended for both isotropic and anisotropic lithologies. Lithologic content therefore ranges from homogeneous carbonates (limestones and

dolomites) and sandstones to siltstones and calcareous shales. Crushed-sample and solid-sample conductivities are plotted against one another for all samples (Fig. 22), only isotropic samples (Fig. 23), and only anisotropic (shale-rich) samples (Fig. 24).

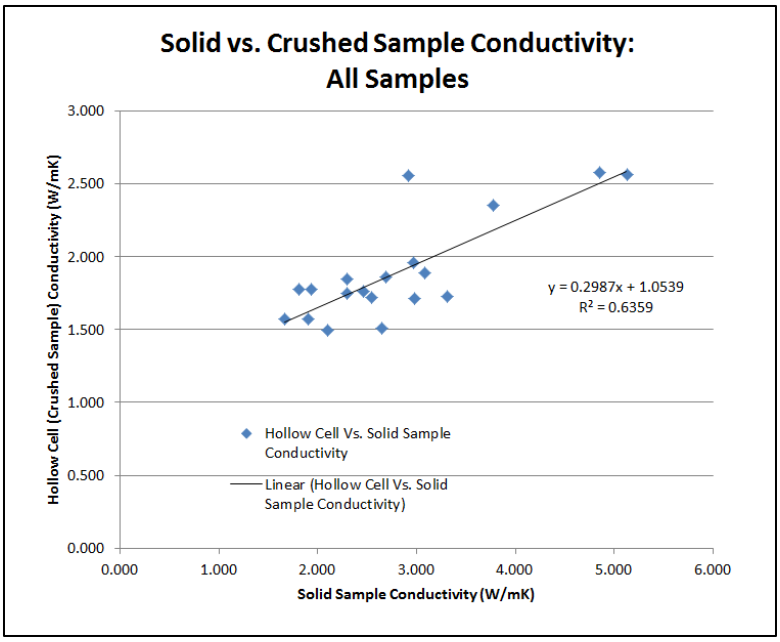

Figure 22. Thermal conductivity of samples measured in solid and crushed form.

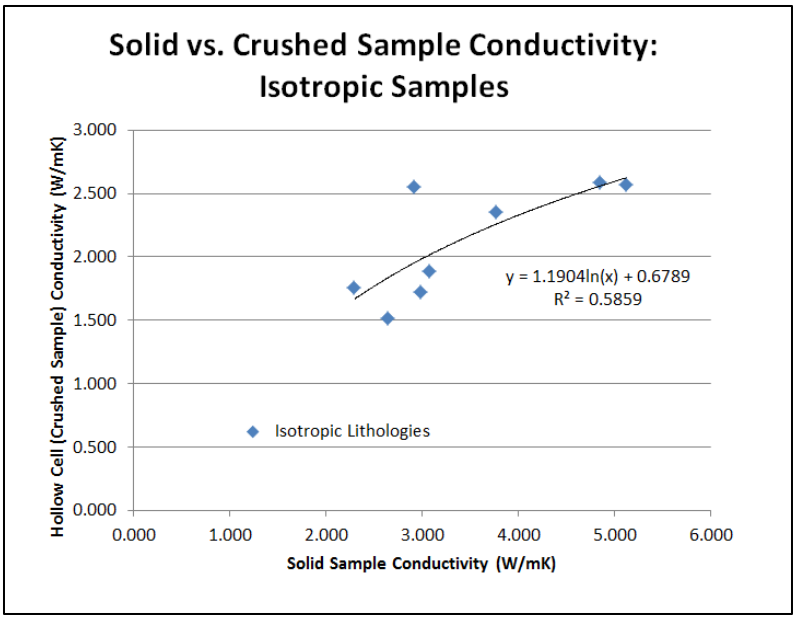

Figure 23. Thermal conductivity of isotropic samples measured in solid and crushed form.

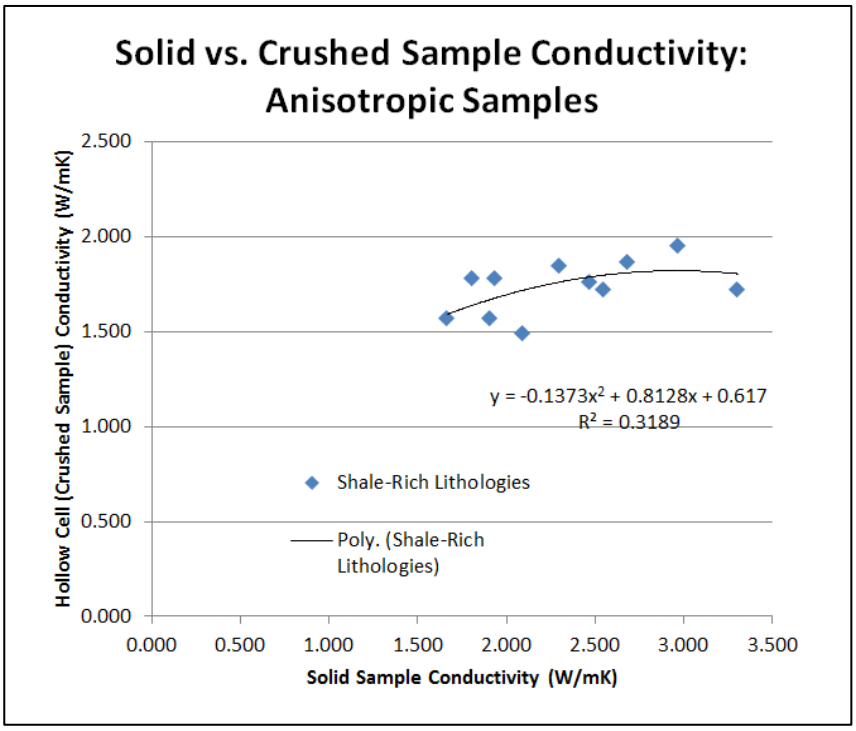

Figure 24. Thermal conductivity of anisotropic samples measured in solid and crushed form.

Samples were separated into two categories on the basis of hand-specimen descriptions. Clean sandstones and homogeneous carbonates were designated as isotropic, and samples that included a significant amount of shale content were classified as anisotropic. Although Equations 6 through 12 were all utilized, the corrections themselves are effectively represented by (1) a combination of Equations 7 and 10, hereafter referred to as Eq. 7-10, (2) a combination between Equations 9 and 10, hereafter referred to as Eq. 9-10, and (3) Equations 11 and 12 applied separately. The results of these corrections are presented in Tables 1 and 2. Based on the discussions of these formulas provided by Sass et al. (1971), Beardsmore & Cull (2001), and Deming (1994), Equations 7-10 and 9-10 were expected to be most applicable to isotropic, and Equations 11 and 12 were expected to be most applicable to anisotropic (shale-rich) samples.

Table 1. Results of corrections applied to thermal conductivity values measured of crushed isotropic samples.

Sample ID (Isotropic Samples)	Crushed Sample Avg. λ ($W m^{-1} K^{-1}$)	Solid Sample Avg. λ ($W m^{-1} K^{-1}$)	Simple Lithology	Eq. 7-10 Avg. λ ($W m^{-1} K^{-1}$)	Eq. 9-10 Avg. λ ($W m^{-1} K^{-1}$)	Eq. 11 Avg. λ ($W m^{-1} K^{-1}$)	Eq. 12 Avg. λ ($W m^{-1} K^{-1}$)	Crushed Sample % Disc.	Eq. 7-10 % Disc.	Eq. 9-10 % Disc.	Eq. 11 % Disc.	Eq. 12 % Disc.
4-10 (1-1)cr	2.351	3.781	s.s.	4.507	3.435	4.871	3.035	-37.8	19.2	-9.1	28.8	-19.7
5-10 (2-3)&(3-3)cr	2.554	2.921	s.s.	4.731	3.664	5.275	3.413	-12.6	62.0	25.4	80.6	16.9
10-4 (2-2)cr	2.562	5.127	dolo. s.s.	3.495	3.345	3.207	2.887	-50.0	-31.8	-34.7	-37.5	-43.7
13-14(1-2)cr	2.581	4.853	s.s. & anhy.	6.095	4.277	7.995	4.527	-46.8	25.6	-11.9	64.8	-6.7
18-15 (1-1)cr	1.746	2.298	l.s. & dolo.	2.992	2.628	2.485	1.858	-24.0	30.2	14.4	8.1	-19.1
19-18 (3-4)cr	1.885	3.078	dolo.	3.292	2.802	2.907	2.089	-38.8	7.0	-9.0	-5.6	-32.1
27-4 (1-2)cr	1.713	2.981	dolo.	2.111	2.222	1.404	1.369	-42.5	-29.2	-25.5	-52.9	-54.1
27-14(2-2)cr	1.513	2.648	l.s. & dolo.	2.691	2.363	2.108	1.541	-42.9	1.6	-10.8	-20.4	-41.8
							Avg. % Disc.	**-36.9**	**10.6**	**-7.6**	**8.2**	**-25.1**
							Avg. Abs. % Disc.	**36.9**	**25.8**	**17.6**	**37.3**	**29.3**

Table 2. Results of corrections applied to thermal conductivity values measured of crushed anisotropic samples.

Sample ID (Anisotropic Samples)	Crushed Sample Avg. λ ($W m^{-1} K^{-1}$)	Solid Sample Avg. λ ($W m^{-1} K^{-1}$)	Simple Lithology	Eq. 7-10 Avg. λ ($W m^{-1} K^{-1}$)	Eq. 9-10 Avg. λ ($W m^{-1} K^{-1}$)	Eq. 11 Avg. λ ($W m^{-1} K^{-1}$)	Eq. 12 Avg. λ ($W m^{-1} K^{-1}$)	Crushed Sample % Disc.	Eq. 7-10 % Disc.	Eq. 9-10 % Disc.	Eq. 11 % Disc.	Eq. 12 % Disc.
4-11 (1-1)cr	1.955	2.969	siltstone	2.555	2.585	1.918	1.803	-34.1	-13.9	-12.9	-35.4	-39.3
6-7 (2-3)cr	1.866	2.687	shale	2.642	2.536	2.030	1.745	-30.6	-1.7	-5.6	-24.5	-35.1
8-19 (1-1)cr	1.721	2.554	calcareous shale	2.665	2.464	2.057	1.653	-32.6	4.4	-3.5	-19.5	-35.3
9-2 (2-4)&(3-4)cr	1.569	1.788	calcareous shale	4.016	2.414	4.040	1.598	-12.2	124.6	35.0	126.0	-10.7
9-5 (3-4)cr	1.489	2.098	calcareous shale	2.047	1.982	1.334	1.110	-29.0	-2.4	-5.5	-36.4	-47.1
14-2 (2-3)cr	1.848	2.304	calcareous shale	6.047	3.255	7.890	2.751	-19.8	162.5	41.3	242.5	19.4
14-15(2-2)cr	1.762	2.469	calcareous shale	4.088	2.965	4.145	2.316	-28.6	65.5	20.1	67.9	-6.2
16-18 (2-3)cr	1.725	3.305	l.s. & shale	3.247	2.701	2.844	1.954	-47.8	-1.7	-18.3	-13.9	-40.9
18-19 (2-4)&(3-4)cr	1.780	1.872	l.s. & shale	4.428	2.737	4.741	2.007	-4.9	136.6	46.2	153.2	7.2
							Avg. % Disc.	**-26.6**	**52.6**	**10.8**	**51.1**	**-20.9**
							Avg. Abs. % Disc.	**26.6**	**57.0**	**20.9**	**79.9**	**26.8**

Tables 1 and 2 are separated by isotropic and anisotropic samples (respectively) in order to (1) compare the effects of each correction method on samples of similar lithology, and (2) test the reliability of the correction methods against isotropic properties. Tables 1 and 2 list the crushed- and solid-sample conductivities, conductivity values calculated with each correction method, and the percent discrepancies between each correction method conductivity value and the solid-sample conductivity. Percent discrepancies were calculated as

$$\%\ Disc\ = \left(\frac{\lambda_{Corr.} - \lambda_{Solid}}{\lambda_{Solid}}\right) 100 \qquad (Eq. 13)$$

Percent discrepancies for each correction method are averaged at the bottom of both tables. The average absolute values of the percent discrepancies are also given, and are calculated as

$$\%\ Disc\ _{AAV} = \frac{1}{n}\sum_{i=1}^{n} |\%\ Disc_i| \qquad (Eq. 14)$$

These averages provide a sufficient measure of the accuracy of each correction method. The percent discrepancies for each correction method are also plotted for each sample in Figures 25 and 26. With respect to the isotropic samples, these results indicate a wide margin of error for all correction methods employed. Although Equations 11 and 12 are not considered applicable to isotropic samples, in some cases they yield more accurate results than those intended for isotropic samples. From Figure 26, corrections applied to anisotropic samples appear to yield more accurate results. However, none of the corrections produce an average percent discrepancy of less than |±10%|, and likewise none produce an average absolute value percent discrepancy of less than 20%.

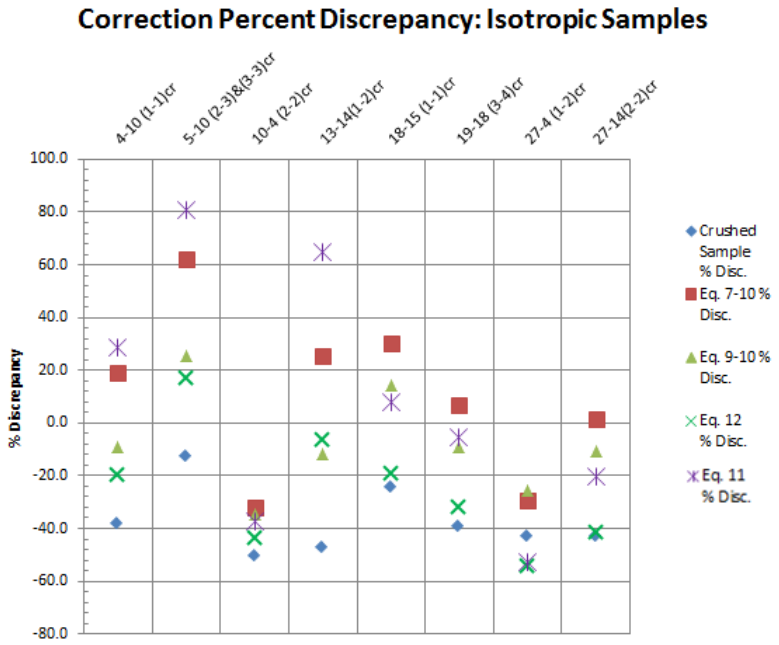

Figure 25. Percent discrepancy from solid conductivity values of corrections applied to isotropic samples.

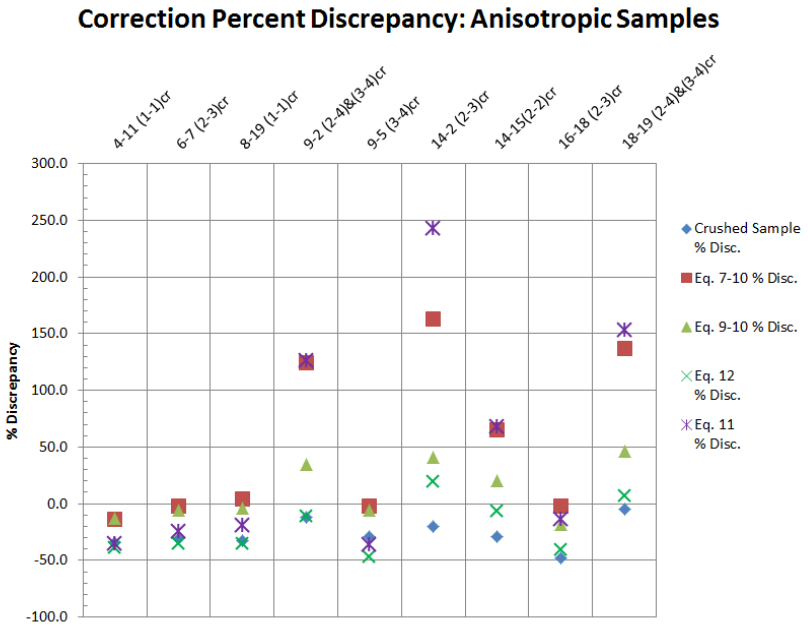

Figure 26. Percent discrepancy from solid conductivity values of corrections applied to anisotropic samples.

It should be noted that the characterization of each sample as isotropic or anisotropic was based explicitly upon hand-sample observations. It is for this reason that lithologic descriptions in Tables 1 and 2 are specified as "simple" lithologies. Lithologic characterizations based upon thin-section analysis or other detailed lithologic analyses would likely results in an isotropy scale, and would therefore lead to more accurate predictions of correction reliability and applicability.

Percent discrepancies of corrected conductivity values from Eq. 7-10, Eq. 9-10, Eq. 11, and Eq. 12 were then plotted against the solid sample conductivities themselves (Figures 27-30). These graphs were constructed to determine the acceptable solid conductivity ranges of confidence for each correction method. Although an apparent inverse relationship between conductivity and percent discrepancy exists for Equations 7-10, 9-10, and 11, the correlation for Equation 9-10 is strongest, and is shown in Figure 28. No such correlation is observed for Equation 12 (Fig. 30).

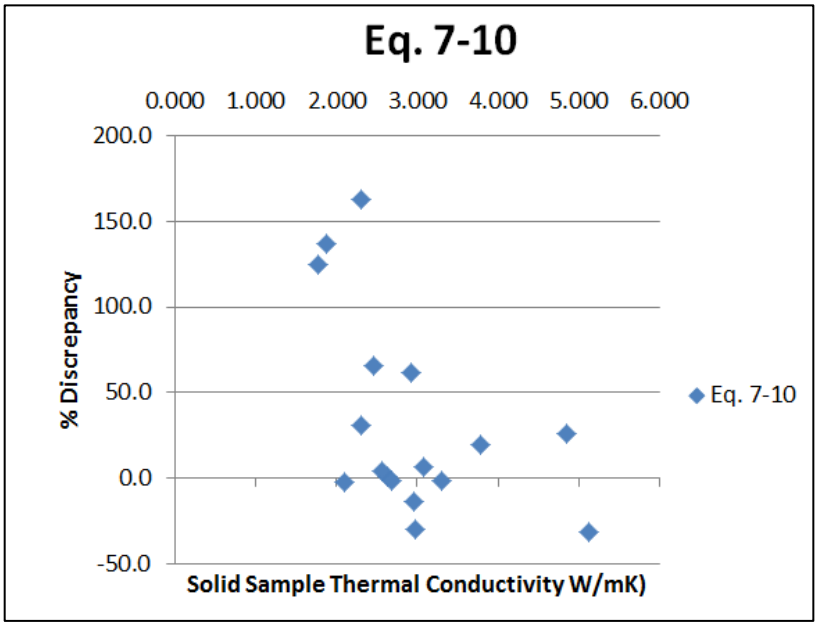

Figure 27. Percent discrepancy of Eq. 7-10 vs. solid sample thermal conductivity.

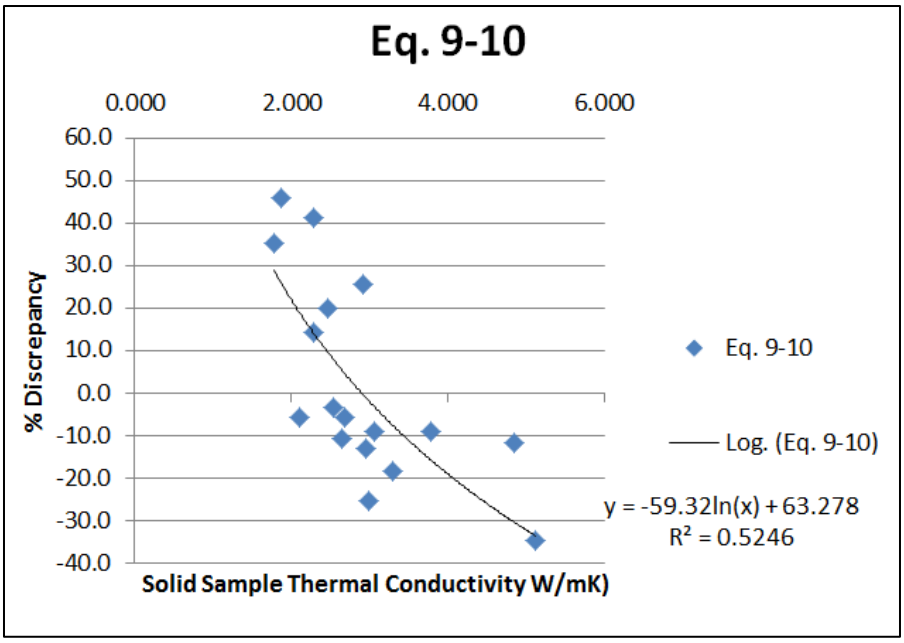

Figure 28. Percent discrepancy of Eq. 9-10 vs. solid sample thermal conductivity.

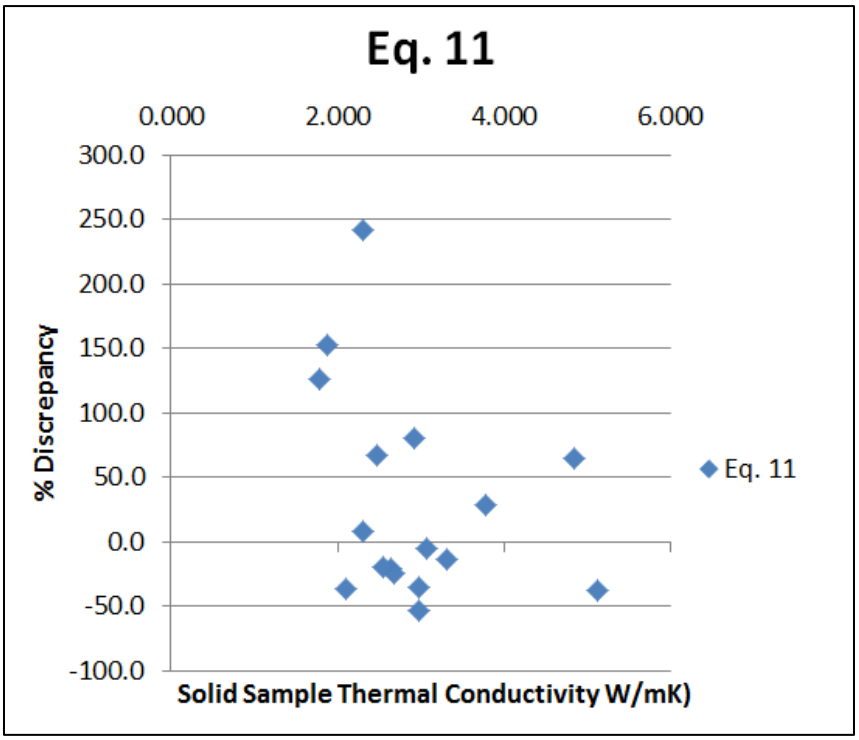

Figure 29. Percent discrepancy of Eq. 11 vs. solid sample thermal conductivity.

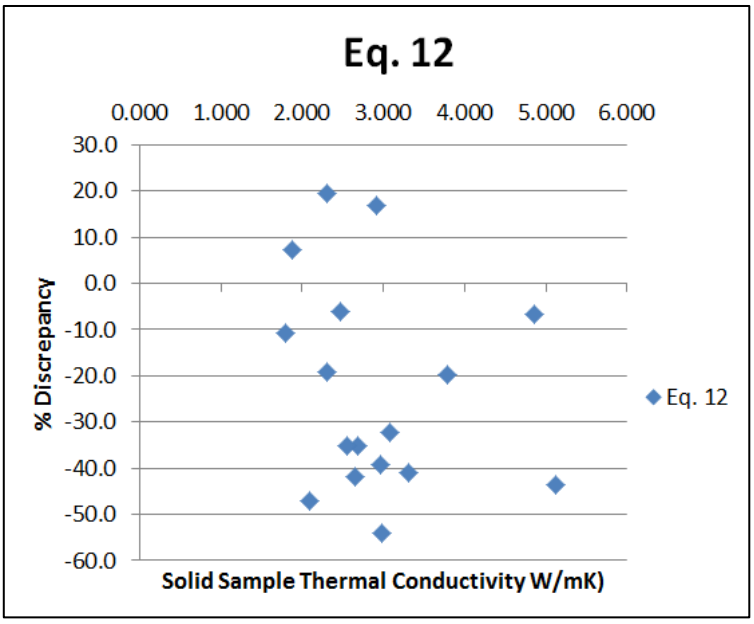

Figure 30. Percent discrepancy of Eq. 12 vs. solid sample thermal conductivity.

Based on its comparatively low discrepancies in conductivity (shown in Tables 1 and 2 and Figures 25 & 26), Equation 9-10 was determined to produce the most reliable corrections for both isotropic and anisotropic samples. A conductivity range of applicability exists, however, outside of which the correction is not considered to be accurate. Figure 31 shows the evident relationship between the percent discrepancy of the uncorrected crushed sample conductivity and its corresponding solid sample conductivity. A logarithmic best-fit was found for the data, and is expressed as

$$\%Disc = -35.72 \ln(\lambda_{Solid}) + 5.3651 \quad (Eq. 15)$$

By calculating the values of λ_{Solid} for *%Disc* values of 0 and -10, the relationship suggests that solid-sample conductivities within the range of 1.162 to 1.537 W m^{-1} K^{-1} are within 10% of their crushed-sample conductivity counterparts. Combined with the acknowledgement of the

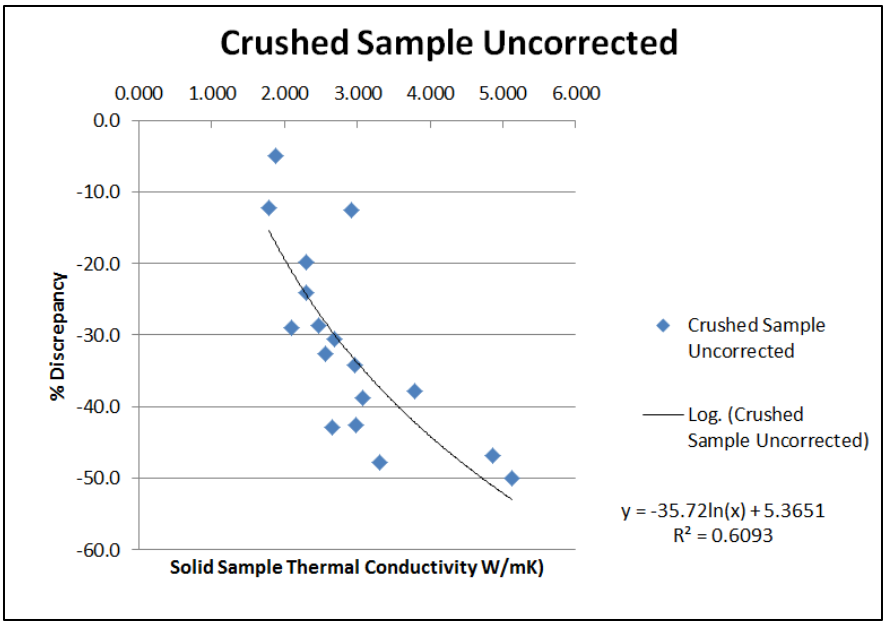

Figure 31. Percent discrepancy of uncorrected crushed sample thermal conductivity from solid sample thermal conductivity.

proportional relationships between crushed- and solid-sample conductivity shown in Figures 22-24, it is reasonable to say that if

$$\lambda_{Crushed} + \lambda_{Crushed}(0.10) > 1.537\ W\ m^{-1}\ K^{-1} \quad (Eq.16)$$

then the percent discrepancy between λ_{Solid} and $\lambda_{Crushed}$ is likely to increase considerably. By adding 10% of the crushed sample conductivity value, samples for which Equation 9-10 should be applied can be chosen. It should be noted that Equation 15 is not itself an acceptable correction. It is used here to determine an estimated limit of probable applicability of Equation 9-10. The lack of correlation between the Equation 9-10 percent discrepancy and the uncorrected crushed-sample conductivity (Fig. 32) suggests that no range of applicability of Equation 9-10 can be definitively determined. Equation 9-10 is applied simply on the inference that if

$$\lambda_{Crushed} + \lambda_{Crushed}(0.10) \leq 1.537\ W\ m^{-1}\ K^{-1} \quad (Eq.17)$$

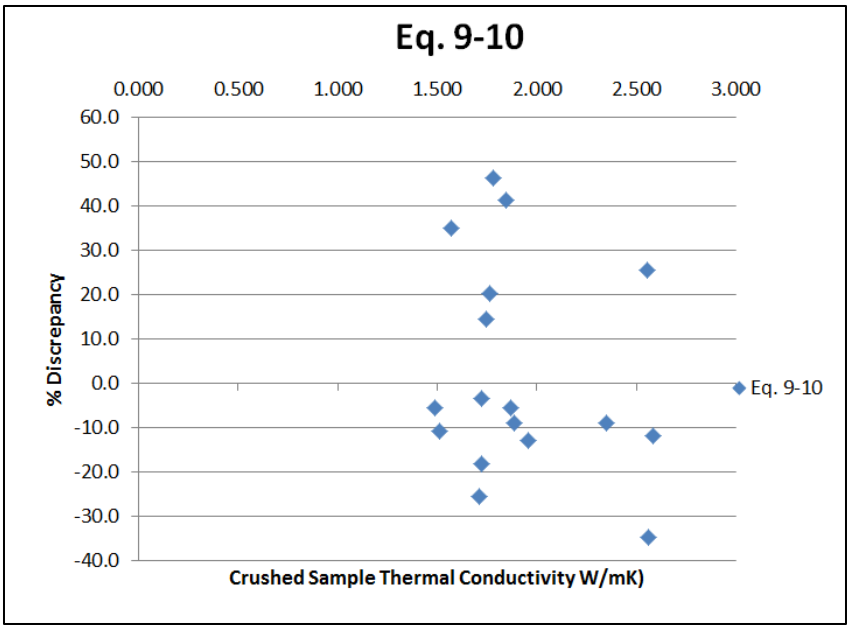

Figure 32. Percent discrepancy of Eq. 9-10 from solid sample thermal conductivity compared to uncorrected crushed sample conductivity.

then the following relationship is most likely:

$$\lambda_{Crushed} \cong \lambda_{Solid} \pm 10\% \quad (Eq. 18)$$

For these reasons, in addition to the relationship shown in Figure 28, the application of Equation 9-10 to $\lambda_{Crushed}$ values defined by Equation 17 is apparently not appropriate. Based on this reasoning, no corrections were applied to Tertiary or upper Cretaceous (Montana and Colorado groups) samples. Their average hollow-cell ($\lambda_{Crushed}$) conductivities are shown in Table 3. Such reasoning is further validated by the comparison of three separate conductivity values of the Pierre Shale. The $\lambda_{Crushed}$ values and corrected conductivity values from Equation 9-10 found for the Pierre Shale in this study are 1.077 ± 0.117 W m^{-1} K^{-1} and 1.766 ± 0.292 W m^{-1} K^{-1}, respectively. The accepted range of Pierre Shale conductivity of 1.0 to 1.2 W m^{-1} K^{-1} (reported by Gosnold et al., 1997) substantiates the lack of applicability of Equation 9-10 to lower conductivity shale-rich samples inferred here.

Table 3. Uncorrected crushed sample thermal conductivity data for unconsolidated Tertiary and Cretaceous samples.

Unit	Average λ ($W\ m^{-1}\ K^{-1}$)	St. Dev.	RSD (%)	N
Harrison	1.145	0.005	0.432	2
Monroe Creek	1.178	0.027	2.281	2
Gering	1.155	0.120	10.426	2
Brule	1.130	0.142	12.594	3
Chadron	1.136	0.169	14.850	3
Pierre	1.077	0.117	10.838	5
Niobrara	1.095	0.120	10.957	3
Carlile	1.176	0.093	7.932	5
Greenhorn	1.253	-	-	1
Graneros	1.237	0.065	5.254	5

Samples included in Table 4 are representative of Dakota Group and Morrison formation lithologies. The applicability of Equation 9-10 on each crushed-sample conductivity value was determined on the basis of the value's response to the criteria defined by Equations 16 through 18. All but one sample (sample 2-12cr) meet the criterion of having a $\lambda_{Crushed} + \lambda_{Crushed}(0.1)$ greater than 1.537 $W\ m^{-1}\ K^{-1}$, and are therefore corrected using Equation 9-10. Porosity values used in Equation 10 for the samples corrected were obtained from core analysis data for the Deans-1 well.

Compilation and Application of Thermal Conductivity Data. All solid-sample and unconsolidated sample (both corrected and uncorrected) thermal conductivity data were compiled for the purposes of producing harmonic mean thermal conductivity values for major stratigraphic units and for the entire stratigraphic column. Because it is not possible to provide representative samples of every layer within the section, the section was simplified into the series of lithologic units shown in Table 5. For most units, conductivity values were calculated using a

Table 4. Thermal conductivity data for unconsolidated core samples and calculated corrected conductivity.

Sample	Lithology	Unit	Uncorrected Avg. λ (W/mK)	λ St. Dev.	λ RSD (%)	N	$\lambda_{Crushed}$ + (0.1)$\lambda_{Crushed}$	Corrected λ (W/mK)
1-3cr	bituminous black shale	D Sand	1.504	0.009	0.580	3	1.654	1.856
2-12cr	shale, black, fissile	Huntsman	1.335	0.087	6.549	3	1.469	-
3-11u-cr	v.f. sandstone & mudstone, gray to brown	J Sand	1.799	0.018	1.009	3	1.979	2.351
5-3cr	gray shale	Cheyenne/Lakota	1.485	0.071	4.750	3	1.634	2.134
MS2cr	sandy red, yellow & gray-white paleosol	Morrison	1.477	0.096	6.515	3	1.624	2.141

simple arithmetic mean of either crushed- or solid-sample measurements. Three units, including the Spearfish formation and both Atokan formations, were assigned conductivity estimates on the basis of lithologic similarity to units for which representative measurements exist.

Table 5. Thermal conductivity data compiled for study area stratigraphic column.

System	Unit	Top (m)	Thickness (m)	Avg. λ (W m^{-1} K^{-1})	N
Tertiary	Harrison	12.50	28.35	1.145	2
	Monroe Creek	40.84	27.74	1.178	2
	Gering	68.58	22.86	1.155	2
	Brule	91.44	152.40	1.130	3
	Chadron	243.84	89.92	1.136	3
Cretaceous	Pierre	333.76	241.10	1.077	5
	Niobrara	574.85	90.83	1.095	3
	Carlile	665.68	79.86	1.176	5
	Greenhorn	745.54	10.36	1.253	1
	Belle Fourche/Graneros	755.90	72.85	1.237	5
	D Sand	828.75	18.59	1.424	3
	Huntsman	847.34	27.43	1.323	2
	J Sand	874.78	30.48	1.610	3
	Skull Creek	905.26	55.47	1.193	2
	Cheyenne/Lakota	960.73	85.04	2.951	4
Jurassic	Morrison	1045.77	35.36	2.141	1
	Sundance	1081.13	25.30	2.853	1
Triassic	Spearfish	1106.42	7.32	2.700	0
Permian	Goose Egg	1113.74	84.12	3.013	2
	Minnekahta (Goose)	1197.86	7.62	3.123	1
	Nippewalla (Uppper Leo)	1205.48	41.15	4.041	1
	Sumner (Middle Leo)	1246.63	67.06	2.687	1
	Chase (Upper Wolf)	1313.69	36.58	3.283	5
	Council Grove (Mid Wolf)	1350.26	60.96	3.551	8
	Broom/Admire (Lower Wolf)	1411.22	33.53	3.716	5
Pennsylvanian	Shawnee/Wendover (Virgil)	1444.75	28.04	2.897	7
	KC/Meek (Missouri)	1472.79	32.92	2.657	9
	Marmaton/Hayden (Upper DesMoines)	1505.71	21.03	2.888	7
	Cherokee/Upper Rountop (Lower DesMoines)	1526.74	9.45	2.870	3
	Lower Roundtop (Upper Atoka)	1536.19	18.29	2.870	0
	Reclamation (Lower Akota)	1554.48	8.53	2.350	0
	Morrow/Fairbank	1563.01	12.80	2.346	4
Mississippian	Madison	1575.82	10.06	2.920	4
Devonian	Englewood	1585.87	1.52	2.442	1
PreC	Precambrian	1587.40	-	2.546	2

Crushed Sample (Uncorrected)
Crushed Sample(Corrected)
Solid Sample
Estimation
Solid Sample & Corrected Crushed

The units in Table 5 were further simplified into eight system-based (Tertiary, Cretaceous, etc.) units to be used in simulations. Conductivity values and thicknesses for each unit in Table 5 were used to calculate the harmonic mean conductivity values of each of the model units shown in Table 6. Additionally, a harmonic mean conductivity value of 1.522 W m^{-1} K^{-1} was calculated for the entire 1575 m stratigraphic column.

Table 6. Harmonic mean conductivity values calculated for simulation stratigraphic units.

Top (m)	Thickness (m)	Model Unit	λ_H (W m^{-1} K^{-1})
12.50	321.26	Tertiary	1.139
333.76	495.00	Upper Cretaceous	1.120
574.85	217.02	Lower Cretaceous	1.695
1045.77	67.97	J/Tr	2.420
1113.74	91.74	Goose Egg	3.022
1205.48	370.33	Minnelusa	3.071
1575.82	11.58	Madison	2.847
1587.40	-	PreC	2.546

Thermal Gradient.

Background & Theory. The vertical crustal temperature gradient is defined as the difference between surface temperature and the temperature measured at a specified depth, and is expressed as

$$\frac{\partial T}{\partial z} = \frac{T_z - T_s}{z} \qquad (Eq. 19)$$

where *Tz* is the temperature (°C) at depth *z* (m) and *Ts* is the surface temperature (°C). Although this relationship is theoretically straightforward, precision borehole temperature profiles measured under equilibrium conditions indicate the influence of both natural and anthropogenic events on subsurface temperature recordings.

Roy et al. (1972) cite several natural factors as possible sources of error in vertical thermal gradient measurement. Variations in surface topography, vegetation cover, and natural groundwater flow in the shallow subsurface can result in erroneous temperature gradient measurements in shallow boreholes. Gosnold et al. (1997 and 2011) discuss the effects of diurnal, seasonal and century-scale changes in average air and ground-surface temperatures, and their relationships to thermal gradient measurements. From these studies a direct relationship is found between the magnitude of climatic warming and latitude, a trend that indicates a corresponding perturbation of temperature profiles in the shallow subsurface.

Temperature gradients calculated with bottom-hole temperature (BHT) data from oil and gas drilling logs can also be significantly flawed. Many BHT values, including those used in this study for the calculation of temperature gradient, are the maximum temperature recorded during the circulation of drilling fluid within the borehole. Because this fluid is, in most cases, cooler than the in situ formation fluids, the use of BHT data in temperature gradient and heat flow calculations results in a systematic underestimation. Several authors attempt to solve this problem by providing linear or polynomial correction equations derived from the differences between BHT data and equilibrium temperature profiles.

Harrison et al. (1982) compare BHT data to temperature measurements in air-drilled boreholes and bottom-hole pressure tests. The two latter measurements are assumed more accurate than BHT measurements, and are the basis of the correction

$$T_{cf} = -16.512 + 0.018268z - (2.3449 \times 10^{-6})z^2 \quad (Eq. 20)$$

where T_{cf} is the change in temperature (°C) applied to the BHT value and z is the depth (m) of measurement. Förster and Merriam (1995) developed a correction for southeastern Kansas using drillstem test (DST) recordings on the basis that DST temperature readings are

more representative of formation fluids than are BHT values. The temperature correction factor is expressed as

$$T_{cf} = 0.012z - 3.68 \quad (Eq. 21)$$

in which T_{cf} is the change in temperature (°C) applied to the BHT value and z is the depth (m) of measurement.

Crowell et al. (2012) utilize integration methods to quantify the accuracy of these correction methods with respect to equilibrium data. Results of this study suggested that the Förster correction was best suited for the Denver Basin, and equilibrium data yielded a linear correction equation tailored specifically for Denver Basin BHT data. Crowell and Gosnold (2013), however, discuss a re-evaluation of these methods. Because linear BHT corrections do not account for the effect of thermal conductivity on the change in temperature gradient with depth, it was appropriate to replace the linear correction of Crowell et al. (2012) with a polynomial. The reversion to a polynomial-based correction equation effectively results in an expression similar to that developed by Harrison et al. (1982) (Crowell, 2014).

Procedures. Temperature data used in thermal gradient calculations was compiled from several distinct sources, and includes bottom-hole temperature (BHT) measurements from oil and gas exploration records, equilibrium measurements collected by Gosnold (1981), and temperature measurements from test wells collected by the USGS as part of the Central Midwest Regional Aquifer System Analysis (CMRASA) program (Helgesen and Hansen, 1989). BHT data for Wyoming was compiled by the Southern Methodist University Geothermal Laboratory, Nebraska BHT data was collected from the Nebraska Oil and Gas Conservation Commission, and South Dakota BHT data was downloaded from the National Geothermal Data System.

A total of 929 temperature gradient values were compiled, corrected (where applicable) and mapped in Figures 33-35 using ordinary Kriging interpolation methods in order to delineate areas of anomalous temperature gradient highs. Because the Harrison et al. (1982) correction is undefined in depths shallower than 600 m, the correction was only applied to BHT values measured at depths greater than 600 m. The same restriction was applied to the Förster correction for the sake of comparison. Specific care was also taken to acknowledge the effect of post-glacial warming on temperature profiles measured in the shallow subsurface (Gosnold et al., 1997 & 2011). To minimize this uncertainty, only temperature gradients measured in wells of depths greater than 150 m were included in the dataset (after Roy et al., 1972).

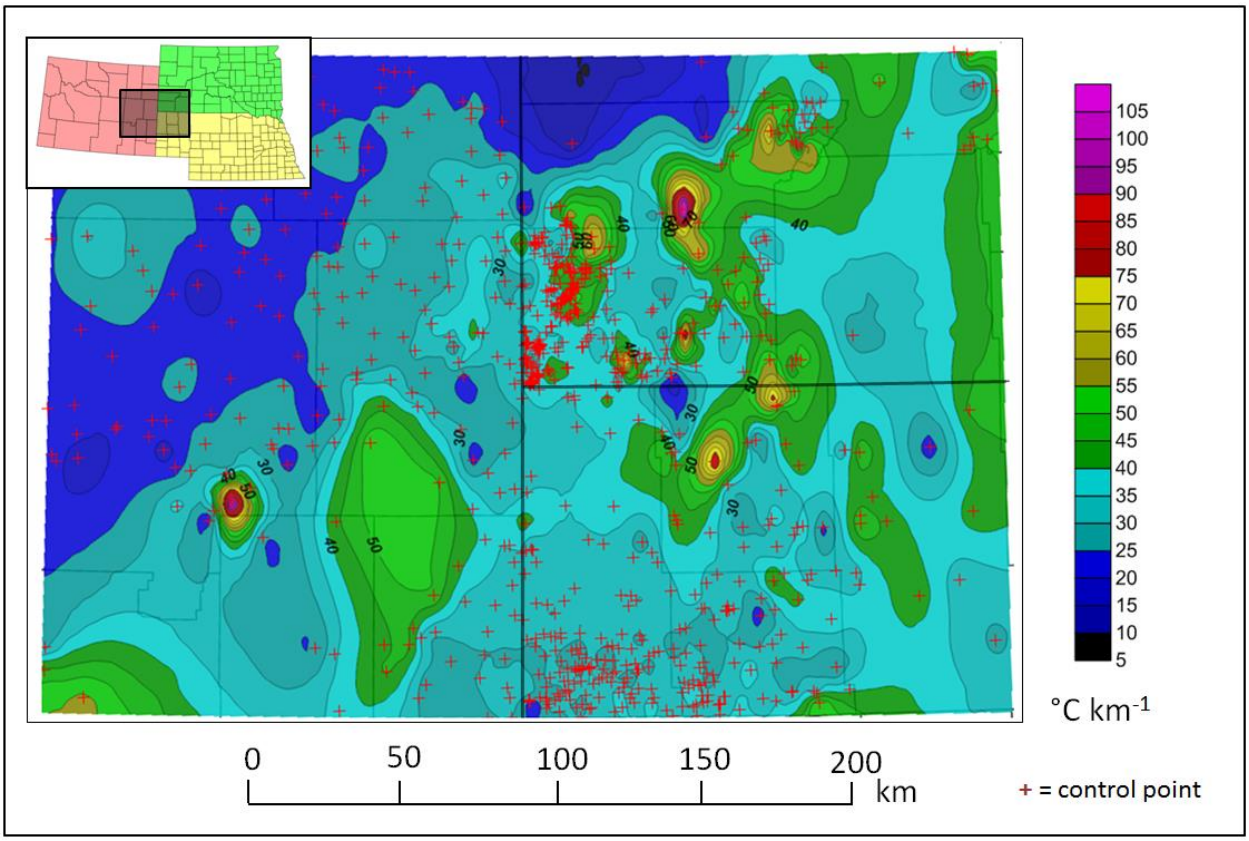

Figure 33. Kriging interpolation of uncorrected thermal gradient.

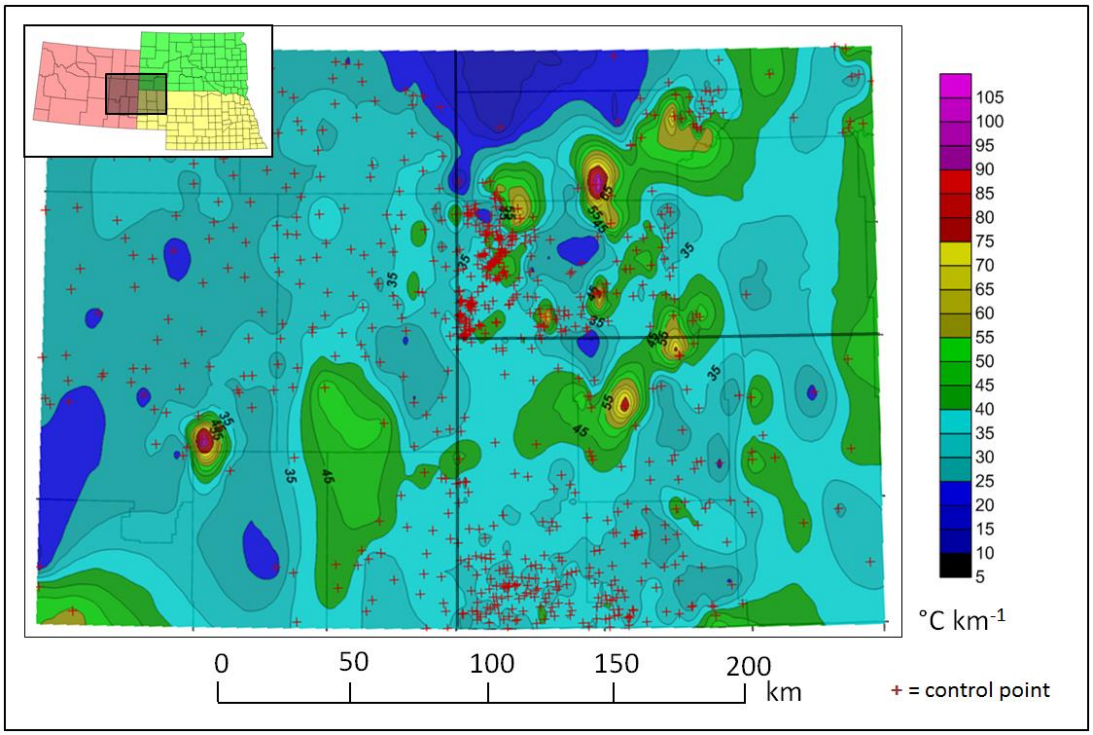

Figure 34. Kriging interpolation of Harrison (1982) corrected thermal gradient.

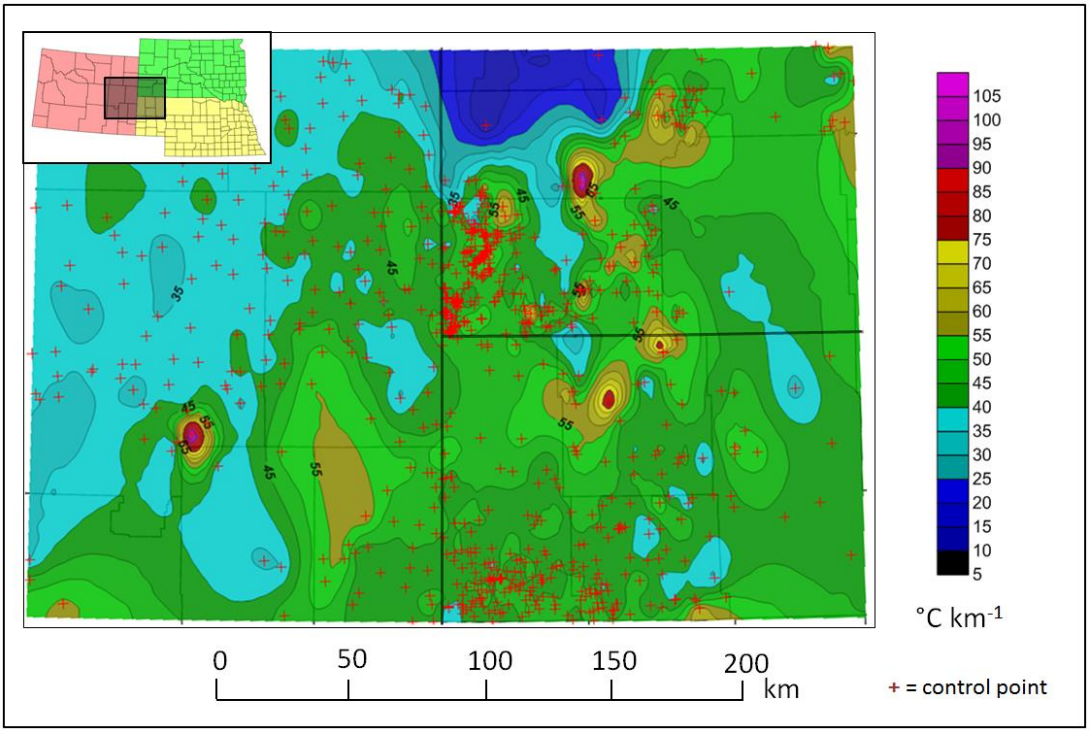

Figure 35. Kriging interpolation of Forster corrected thermal gradient.

Mapped geographic variations in temperature gradients are expected to correlate to the variations in elevation of subsurface aquifers. More specifically, high temperature gradients were predicted to result from advective upwelling of heated fluids within up-turned permeable hydrostratigraphic units along the margins of the northern Denver Basin. Thermal gradient lows within the study area are conversely expected to be attributed either to (1) areas of confined-aquifer recharge along outcrop zones, or (2) conduction-dominated geothermal settings in which the harmonic mean thermal conductivity of the local stratigraphic section is high relative to that of other stratigraphic configurations (namely variations in thickness) nearby.

Hydrogeological Parameters

Groundwater flow in confined aquifers is defined by Darcy's Law:

$$q = -KA\left(\frac{\partial h}{\partial l}\right) \quad (Eq. 22)$$

where q is discharge ($m^3\ s^{-1}$), A is the cross-sectional area (m^2) of the flow medium, K is the hydraulic conductivity ($m\ s^{-1}$) of the flow medium, and $\partial h/dl$ is the lateral change in hydraulic head (dimensionless) measured in the flow medium. The negative sign in the equation accounts for the occurrence of discharge in the direction of negative change in hydraulic head.

Hydrostratigraphic Framework. A west-east stratigraphic cross-section was constructed for use as a transect in two-dimensional simulations. Stratigraphic tops data were compiled for the transect and simplified into eight major stratigraphic units. Along with surface elevation data for each well, elevations of stratigraphic units calculated from tops were plotted and converted into the profile shown in Figure 36. The orientation of the transect is marked in Figure 37, and identification information for all wells used in cross-section construction is listed in Appendix G.

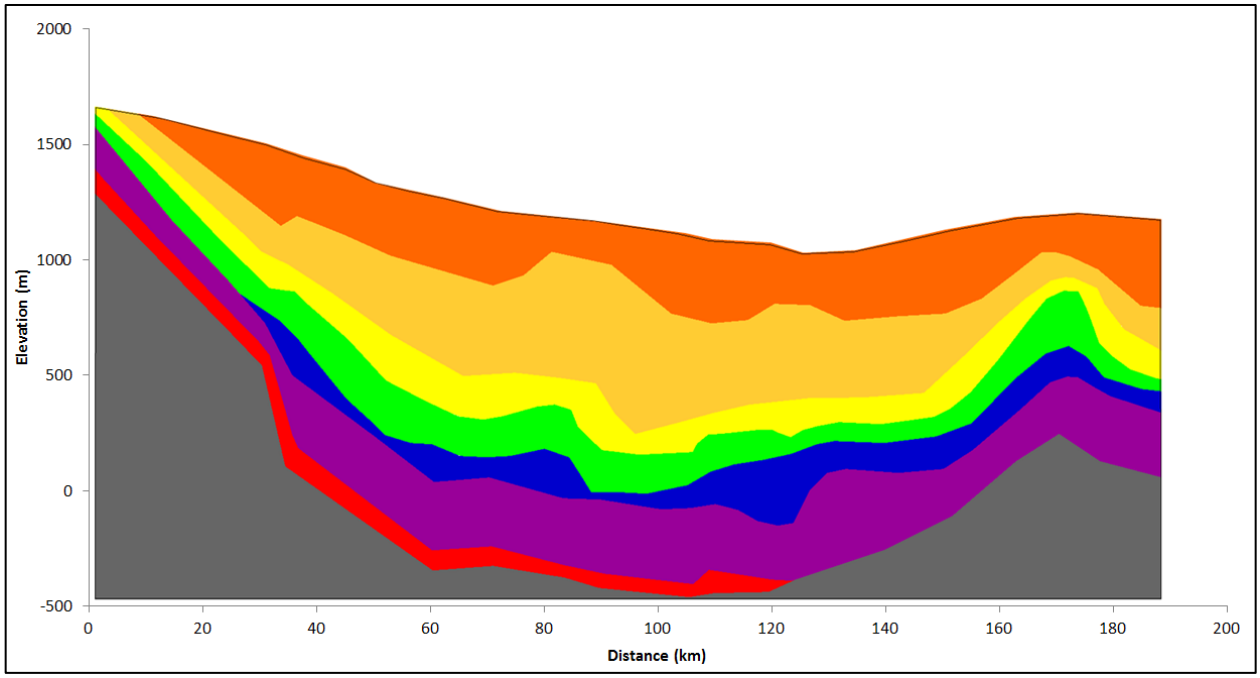

Figure 36. Stratigraphic cross-section produced for two-dimensional simulations.

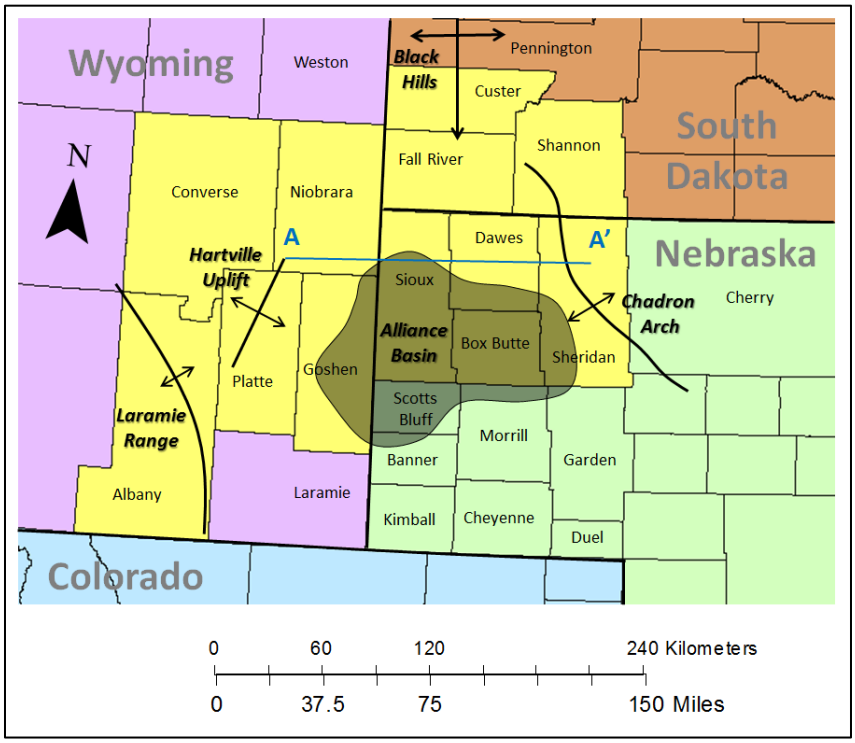

Figure 37. Location of simulation transect (A-A').

The stratigraphic profile depicted in Figure 36 is a vertically-exaggerated representation of a transect along which groundwater flow in the WIP and Great Plains aquifers is likely (discussed in the hydrogeological overview section, Chapter II). Because discharge occurs in the direction of decreasing hydraulic head, and hence the direction perpendicular to the contours of a potentiometric surface map, the orientation of the transect was optimized with respect to one flow direction indicated by the potentiometric surfaces presented in Figures 16 and 17.

Permeability and Porosity. Porosity, permeability, and density values assigned to stratigraphic units for simulation purposes are listed in Table 7. Many of the permeability and porosity data for the lower Cretaceous through Precambrian units (with the exception of the upper Permian through Jurassic sections) were obtained from records of core analysis performed on core samples from the Deans-1 well.

Estimations of permeability, porosity and density for the Tertiary and upper Cretaceous geohydrologic units were obtained from published values for corresponding units or similar lithologies. Permeability values for the Tertiary section were estimated based on those of similar lithologies within the High Plains (Tertiary and Quaternary) aquifer reported by Gutentag et al. (1984, p. 26). Porosity values for the Tertiary section were estimated from those of similar lithologies provided by Fetter (2001, p. 75), and density values were estimated using values measured of sandy and silty sediments in eastern Nebraska by Nolan et al. (2007).

Permeability data for upper Cretaceous units (Belle Fourche/Graneros through Pierre) were obtained from Bredehoeft et al. (1983, p. 20) or estimated from values of similar lithology, and porosity and density values for the Pierre shale were obtained from Schultz et al. (1980, p. 72). Densities for the Skull Creek through D Sand units were estimated from samples of similar

Table 7. Permeability, porosity and density data assigned to study area stratigraphic units.

Unit	Top (m)	Thickness (m)	Avg Horizontal Perm (mD)	Horizontal Perm. St. Dev. (mD)	Avg Vertical Perm (mD)	Vertical Perm. St. Dev. (mD)	Average Porosity (%)	Porosity St. Dev. (%)	N	Avg. Density (g/cm^3)	N
Harrison	12.50	28.35	18219	-	18219	-	35	-	0	1.60	0
Monroe Creek	40.84	27.74	18219	-	18219	-	35	-	0	1.60	0
Gering	68.58	22.86	36438	-	36438	-	35	-	0	1.60	0
Brule	91.44	152.40	1822	-	1822	-	35	-	0	1.60	0
Chadron	243.84	89.92	3644	-	3644	-	35	-	0	1.60	0
Pierre	333.76	241.10	1.0	-	0.1889	-	20.8	-	0	2.06	0
Niobrara	574.85	90.83	15741	-	10000	-	20	-	0	2.1	0
Carlile	665.68	79.86	0.1	-	0.007871	-	20	-	0	2.1	0
Greenhorn	745.54	10.36	31.48	-	10	-	20	-	0	2.1	0
Belle Fourche/Graneros	755.90	72.85	0.1	-	0.0006296	-	20	-	0	2.1	0
D Sand	828.75	18.59	1333.6	845.0	1014.0	832.8	22.8	3.7	13	2.1	0
Huntsman	847.34	27.43	47.4	62.8	23.0	37.9	19.5	4.6	8	2.1	0
J Sand	874.78	30.48	191.9	321.0	112.6	273.6	20.7	5.7	21	2.1	0
Skull Creek	905.26	55.47	40	-	20	-	20	-	0	2.1	0
Cheyenne/Lakota	960.73	85.04	281.7	795.1	68.9	110.8	18.1	6.3	18	2.05	4
Morrison	1045.77	35.36	1.0	-	1.0	-	10	-	0	2.3	0
Sundance	1081.13	25.30	1.0	-	1.0	-	1.90	-	1	2.64	1
Spearfish	1106.42	7.32	1.0	-	1.0	-	1.0	-	0	2.5	0
Goose Egg	1113.74	84.12	0.1	-	0.1	-	0.57	-	2	2.68	2
Minnekahta (Goose)	1197.86	7.62	0.1	-	0.1	-	0.16	-	1	2.70	1
Nippewalla (Uppper Leo)	1205.48	41.15	0.1	-	0.1	-	4.18	-	1	2.54	1
Sumner (Middle Leo)	1246.63	67.06	391.2	397.3	185.0	326.3	22.1	8.9	9	2.10	1
Chase (Upper Wolf)	1313.69	36.58	23.5	95.4	24.1	90.7	11.6	6.9	44	2.66	5
Council Grove (Mid Wolf)	1350.26	60.96	83.8	187.8	50.3	190.0	13.6	8.3	53	2.53	8
Broom/Admire (Lower Wolf)	1411.22	33.53	0.3	1.1	0.1	0.3	8.0	3.5	31	2.69	5
Shawnee/Wendover (Virgil	1444.75	28.04	3.5	16.3	1.5	8.8	6.2	5.2	76	2.54	7
KC/Meek (Missouri)	1472.79	32.92	23.5	82.7	14.6	60.4	9.4	6.7	58	2.59	9
Marmaton/Hayden (Upper DesMoines)	1505.71	21.03	0.02	0.1	0.02	0.1	6.2	5.4	37	2.60	7
Cherokee/Rountop (Lower DesMoines)	1526.74	9.45	5.0	16.2	0.5	1.6	9.9	4.6	14	2.54	3
Lower Roundtop (Upper Atoka)	1536.19	18.29	1.91	4.5	0.14	0.2	5.3	2.9	13	2.63	1
Reclamation (Lower Akota)	1554.48	8.53	0.9	0.6	0.4	0.4	12.6	1.9	7	2.50	0
Morrow/Fairbank	1563.01	12.80	0.43	0.6	0.60	1.2	10.1	3.6	19	2.48	4
Madison	1575.82	10.06	22.1	27.2	16.4	26.0	20.7	9.2	32	2.25	4
Englewood	1585.87	1.52	0.66	0.7	0.01	0.0	11.0	1.6	5	2.51	1
Precambrian	1587.40	-	0.01	0.00	0.01	0.00	0.45	0.0	2	2.74	2

Estimation: Publication
Estimation: Similar Lithology
Citation
Core Analysis Measurement
Laboratory Measurement

lithology. Permeability for the Skull Creek was estimated based upon that for similar lithologies. Permeability values for Jurassic, Triassic and upper Permian units were estimated from the median values of the respective units reported by Signor et al. (1996, p. 19), and porosity and density values for the Morrison and Spearfish formations were estimated based upon those of

similar lithologies. Density for the Reclamation (Lower Atokan) was estimated using values of similar lithologies.

Harmonic mean values for horizontal and vertical permeability, porosity, and density were calculated for each hydrostratigraphic unit used in simulations. This was done by replacing λ with the appropriate variable in Equation 2. Based on the difference in permeability values between those of core analysis measurements and those of estimations and publication citations, however, harmonic mean permeability values calculated for the lower Cretaceous were not sufficient for the simulation of realistic flow within the aquifer. Although the thickness of the Englewood Formation was included in the simulated representation of the Madison, permeability values for the Madison were rounded from core analysis data in order to avoid applying the effects of the Englewood across the entire simulated hydrostratigraphic unit. Table 8 displays the values of permeability, porosity and density calculated or estimated for each stratigraphic unit. Values in parentheses are those eventually used in calibrated simulations.

Table 8. Permeability, porosity and density data calculated or estimated for simulation stratigraphic units. Values in parentheses are those eventually used in calibrated models.

Top (m)	Thickness (m)	Model Unit	K_H(horz.) (mD)	K_H (vert.) (mD)	Porosity$_H$ (%)	ρ_H (g cm^{-3})
12.50	321.26	Tertiary	2868	1434	35	1.600
333.76	495.00	Upper Cretaceous	0.2799	0.003894	20.38	2.080
574.85	217.02	Lower Cretaceous	89 (1000)	40 (500)	19.43	2.082
1045.77	67.97	J/Tr	1.00	1.00	2.812	2.438
1113.74	91.74	Goose Egg	0.1000	0.1000	0.4686	2.680
1205.48	370.33	Minnelusa	0.2497	0.2032	8.722	2.475
1575.82	11.58	Madison	4.210 (22)	0.07570 (16)	18.54	2.279
1587.40	-	PreC	0.01	0.01	0.45	2.736

Principles of Advective Heat Flow

Among the earliest attempts to develop numerical solutions for thermal energy transport by fluid flow in porous media are those given by Stallman (1963). A synthesis of formulas obtained from Fourier's Law (Eq. 1) and Darcy's Law (Eq. 22) yields an analytical solution relating aquifer properties and flow rates to three-dimensional temperature distributions. In discussing the utilization of subsurface temperature variation as a tool for reverse engineering solutions to groundwater flow problems, Anderson (2005) presents a version of the heat transport equation developed earlier by Stallman (1963), written as

$$\frac{\kappa_a}{\rho_a c_a}\nabla^2 T - \frac{\rho_w c_w}{\rho_a c_a}\nabla \cdot (Tq) = \frac{\partial T}{\partial t} \qquad (Eq.\,23)$$

where κ_a is the effective thermal diffusivity of the aggregate saturated porous medium ($m^2\ s^{-1}$), $(\rho c)_a$ and $(\rho c)_w$ are the volumetric heat capacities ($J\ m^{-3}\ K^{-1}$) for the aggregate saturated porous medium and liquid water, respectively, q is the Darcy velocity ($m\ s^{-1}$), T is temperature (°C), and t is time (s). The first term in the equation represents the two-dimensional temperature changes due to heat transfer by conduction, and the second term describes those attributed to fluid flow. It should be noted that several assumptions, which were also incorporated into the simulations discussed herein, are inherent in Eq. 23. These assumptions are detailed by Saar (2011), but two are particularly worthy acknowledgement for this study; (1) the assumption of thermal conductivity constancy and isotropy across the two-dimensional domains of each simulated rock unit (only vertical thermal conductivity), and (2) that the volumetric heat capacity remains constant in time. Equation 23 nonetheless describes the solutions for temperature changes calculated for simulation domain grid cells for each time step.

In order to understand the distinct roles of heat transfer by conduction and advection, it is helpful to separate the components and express the two as a ratio. Such a ratio can be calculated using the analytical methods (outlined above) applied in finite difference approximations for the simulation domain, and is useful in this study for identifying two-dimensional areas in which thermal transport by advection is more prevalent than that by conduction. The Peclet number aids in this objective, and is written as

$$Pe = \frac{L|q|}{\kappa_a} \quad (Eq. 24)$$

and

$$\kappa_a = \frac{\lambda_a}{(\rho c)_a} \quad (Eq. 25)$$

where *Pe* is the thermal Peclet number (dimensionless), *L* is the length parameter (m), λ_a is the aggregate conductivity (W m^{-1} K^{-1}) of the saturated mass, and all other variables are as above.

Model

Software Overview

Hydrotherm Interactive (HTI) is a finite difference simulation program developed by the USGS for the purposes of modeling fluid and thermal energy transport in porous media. HTI – Version 3 includes a graphical user interface (GUI) that can be utilized for the input of hydrothermal and geological parameters, and for displaying graphical animations of output results (Kipp et al., 2008). The preprocessor is used to define the simulation domain, rock units, initial temperature and pressure conditions, spatial and temporal discretization schemes, boundary conditions, and solver settings. The spatial discretization, a cell-block grid composed

of 89 columns and 92 rows, is depicted in Figure 38. Using the postprocessor, solutions to finite difference approximations can then displayed for each time step in animated form.

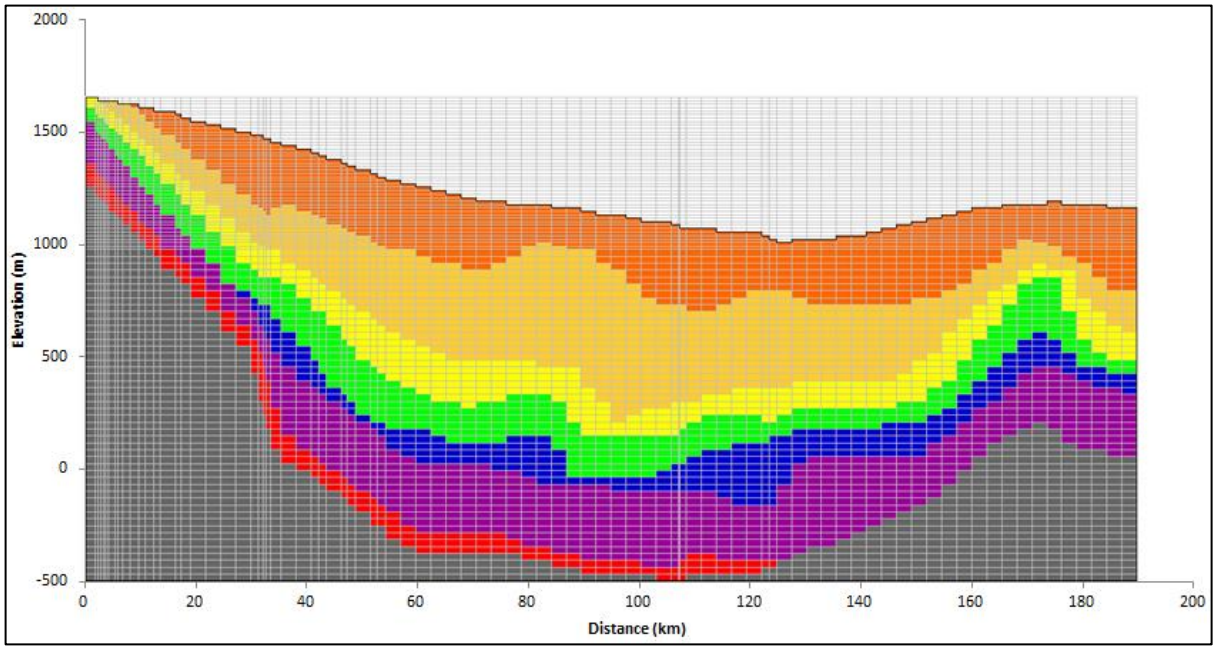

Figure 38. Spatial discretization scheme used in simulations. Grid is composed of 89 columns and 92 rows.

Input of Geothermal and Hydrogeological Parameters

HTI provides the option to manually specify pressure conditions within the simulation domain, or to apply hydrostatic pressure conditions based upon the atmospheric pressure specified at the upper (surface) boundary. Pressures within the Madison and Minnelusa formations were calculated using hydraulic head distributions given by Konikow (1976) and Signor et al. (1996) and the relationships

$$P = \rho g h_p \quad (Eq. 26)$$

and

$$h_p = h - z \quad (Eq. 27)$$

in which P is the pressure at a given point in the water column (kg m^{-1} s^{-2} or Pa), or that of the hydrostratigraphic zone of interest; ρ is the fluid density (taken here as 1000 kg m^{-3}); g is the acceleration due to gravity (9.81 m s^{-2}); h_p is the height of the water column (m) that provides pressure head to the hydrostratigraphic zone of interest; h is the total hydraulic head (m), or the height of the water column above a reference datum; and z is the height (m) of the hydrostratigraphic zone of interest above the reference datum. The calculated pressure values for the Madison and Minnelusa were compared to those applied by HTI under assumed hydrostatic pressure conditions given an atmospheric pressure of 1.01325×10^5 Pa. Because the two were acceptably consistent with one another (no abnormal pressures were calculated from hydraulic head data), hydrostatic pressure gradients were applied to the simulation domain.

Although the Devonian Fremont Canyon and Englewood formations are present within the study area, their thicknesses were regarded as negligible for modeling purposes. The thermal conductivity value measured for the Englewood Formation was included in the calculation for the simulated rock unit representative of the Madison. Specific heat values of rock types used in simulations (granite, sandstone, shale, limestone, etc.) are listed by Robertson (1988), and generally fall within the range of 0.77 to 1.13 kJ kg^{-1} K^{-1}. For this reason the specific heat value of all rock units used in simulations is assumed to be 1.00 kJ kg^{-1} K^{-1}.

Model Calibration

Simulation results using the original permeability, porosity, thermal conductivity, and density values calculated or estimated for each rock unit (Tables 6 and 8) were tested against heat flow profiles (calculated from thermal conductivity data and thermal gradient data shown in Figure 33), and against published flow patterns and rates for the Dakota and Madison aquifers in the study area. Although many values were left unchanged, permeability values were adjusted

(adjustments are given in parentheses in Table 8) to yield hydrothermal conditions representative of those observed. Adjustments were made with careful consideration of the respective lithologies.

CHAPTER IV

RESULTS

Summary of Results

Heat Flow Results

The harmonic mean conductivity for the complete stratigraphic section (1.522 W m^{-1} K^{-1}) was calculated using the values listed in Table 5, and applied to Fourier's Law (Eq. 1) with temperature gradient datasets to produce the map of uncorrected heat flow shown in Figure 39. Heat flow maps produced using the Harrison (Eq. 20) and Förster (Eq. 21) corrections were not included on the basis of the following interpretations of Figures 33-35: (1) corrected gradients

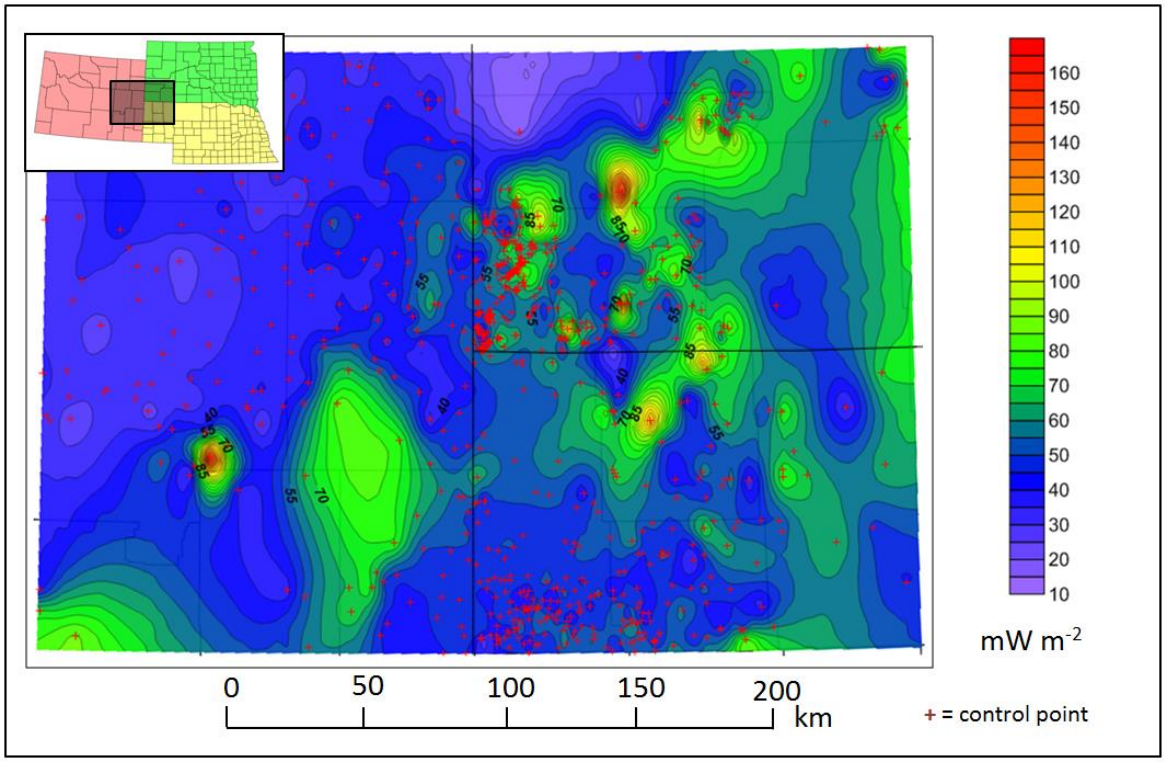

Figure 39. Kriging interpolated heat flow of study area.

produced by the Harrison equation appear to produce no significant difference with respect to the gradient values that lie along simulation transects, making the correction unnecessarily speculative; and (2) corrected gradients produced by the Förster equation are likely overestimations of the thermal regime within the study area. For the same reasons, the uncorrected heat flow map (Fig. 39) is herein presented as a representative illustration of heat flow patterns in the study area. The exclusion of the Förster correction heat flow map is based upon the expected heat flow ranges (40-60 mW m^{-2}) for tectonically-stable provinces (specifically, regions within such provinces that do not exhibit anomalous heat flow due to advection or radiogenic heat production) reported by Gosnold (1990). Heat flow results from simulations were therefore compared to the uncorrected heat flow map (Fig. 39) for the purposes of calibration.

Simulation Results

In order to calibrate models to the observed hydrologic and geothermal regimes of the study area, several simulations were run using various ranges of rock parameters. Combined with a background heat flux of 60 mW m^{-2} (the boundary condition specified for the basal boundary of the simulation domain), the rock parameter values provided in Tables 6 and 8 yielded the temperature field depicted in Figure 40. In order to produce a simulation heat flow profile, simulated temperature gradient data along the model profile was exported and combined (using Fourier's Law, Eq. 1) with thermal conductivity values adjusted for localized stratigraphy. The heat flow profile taken from the study transect in Figure 41 is compared in Figure 42 to the modeled heat flow profile produced from the calibrated simulation. Referring to Figure 42 just west of the 112 mW m^{-2} anomaly, the comparison of observed and simulated heat flow profiles

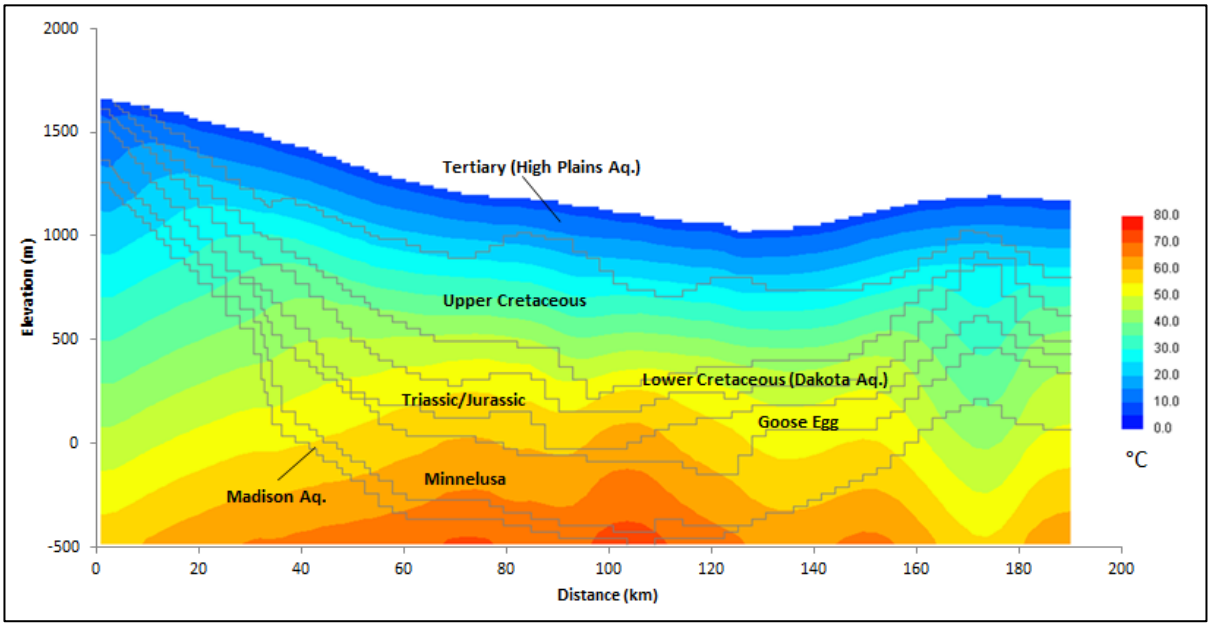

Figure 40. Simulated temperature distribution of study transect after 900,000 years.

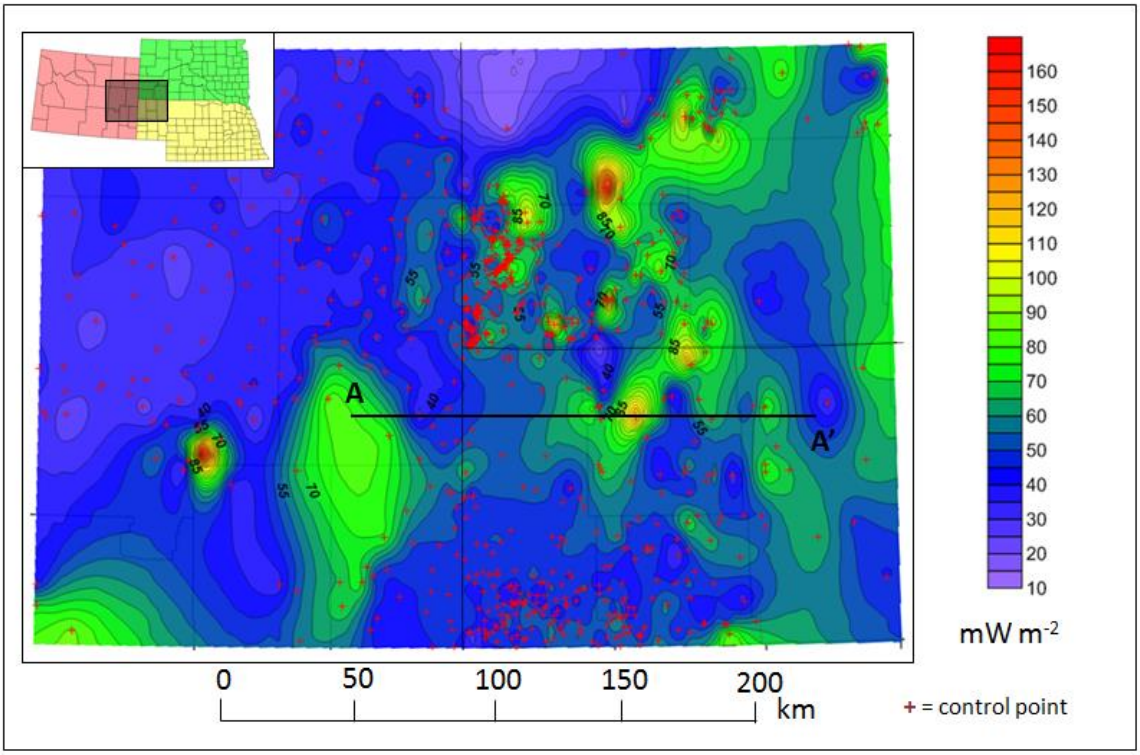

Figure 41. Location of simulation transect in relation to observed heat flow patterns.

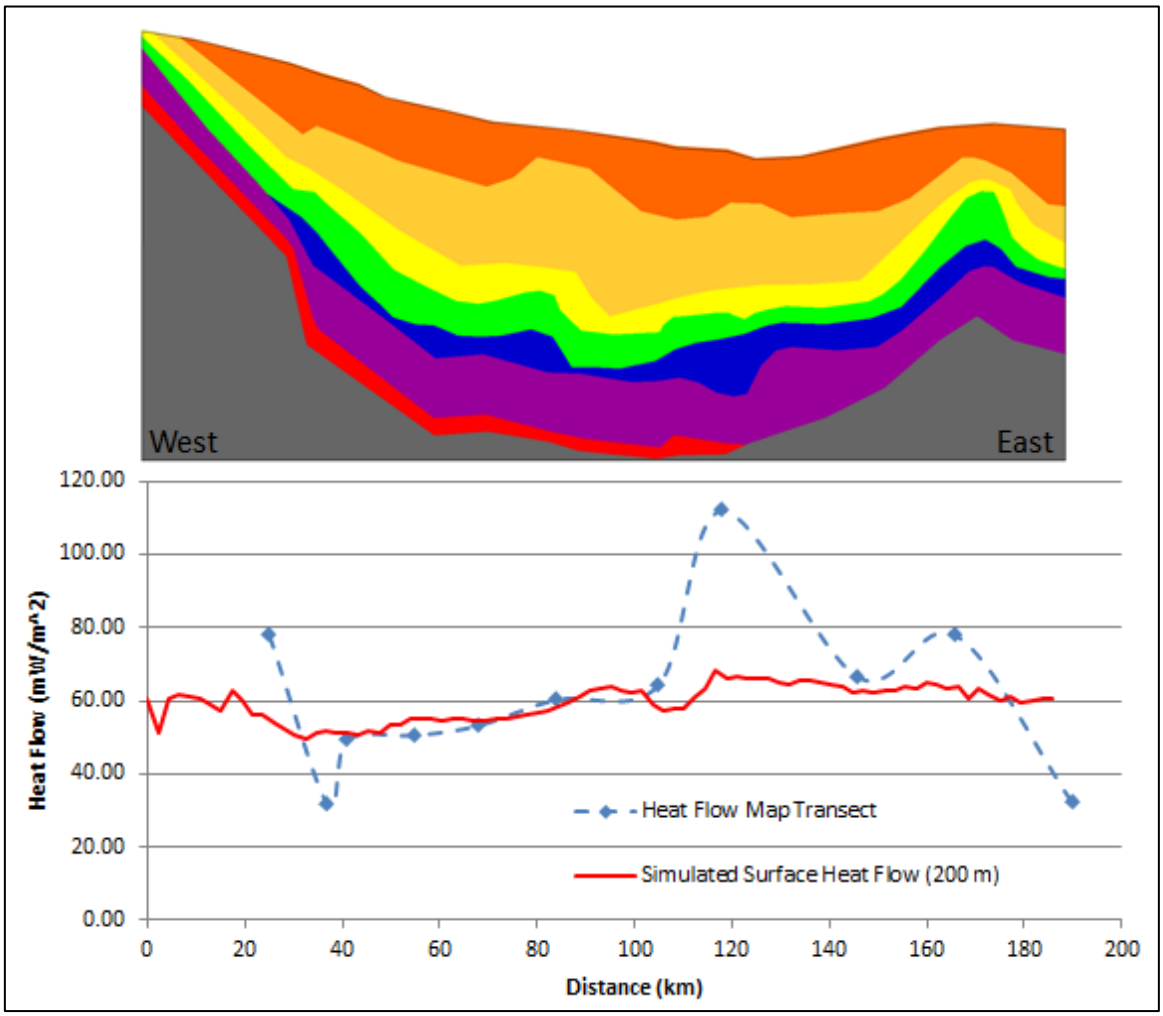

Figure 42. Comparison of observed heat flow profile to calibrated heat flow simulations. Simulated heat flow is calculated for the upper 200 meters of the model cross-section.

across the transect suggests that the calibrated model yields an accurate simulation of heat flow outside of anomalous zones. Additionally, the use of a background (reduced) heat flow value of 60 mW m^{-2} for the simulation transect is consistent with the reduced heat flux of 63 mW m^{-2} calculated for the Black Hills by Roy et al. (1972). It is noteworthy that the temperatures calculated for the Madison Formation (shown in Fig. 40) were compared to those given by Gries (1977), Konikow (1976) and Cooley et al. (1986). Although only temperatures for the western

margin of the simulation transect could be validated with these sources, the lateral changes in simulated temperature are consistent with those published. All simulations converged to steady-state conditions after approximately 900,000 years.

Two test simulations were run for the purposes of isolating and identifying the magnitude of the separate components of heat transfer within the simulation domain. Figure 43 shows the difference in the lateral heat flow profile under realistic conditions, thermal conduction

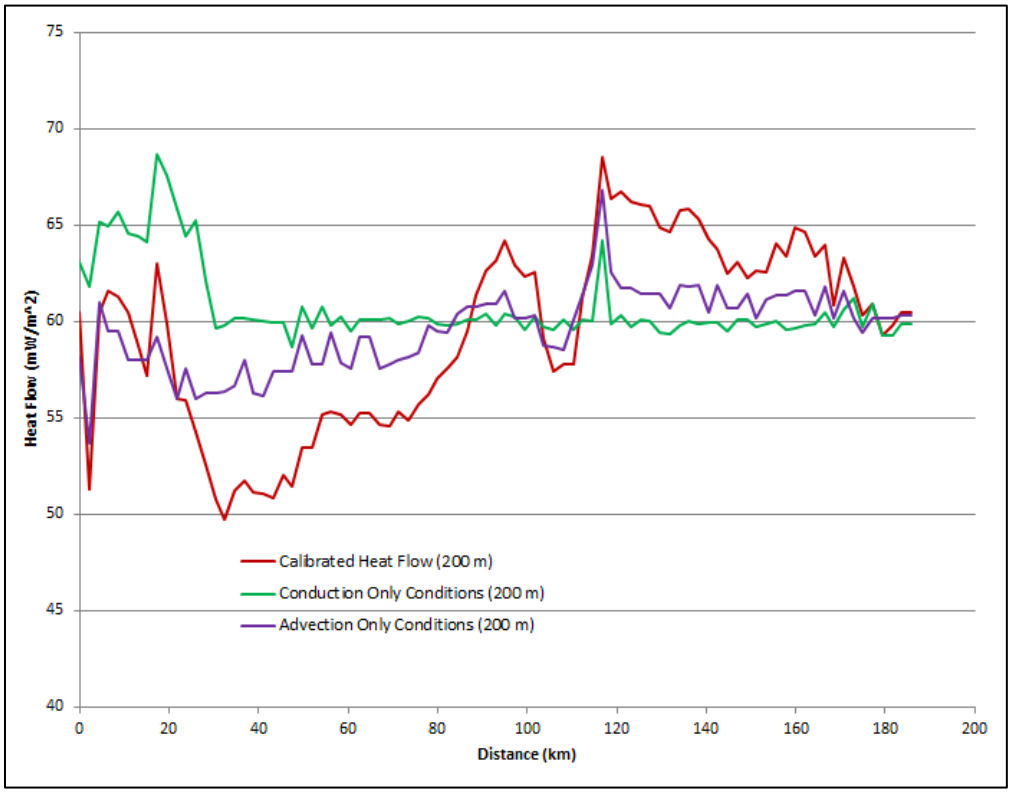

Figure 43. Heat flow profile under calibrated conditions, isolated conduction conditions, and isolated advection conditions. Simulated heat flow is calculated for the upper 200 meters of the model cross-section.

only (no advective heat transfer) conditions, and advection only conditions (no temporal temperature changes due to conduction). To isolate the component of heat conduction, all horizontal and vertical permeability values for all simulated rock units were reduced effectively to zero millidarcys. This results in the removal of all heat transfer effects due to groundwater

motion, so that heat energy is transferred purely by conduction through the simulation domain. In this method, modeled heat flow values are increased across the western margin of the transect and reduced across the eastern margin, indicating respective net cooling and warming effects of the primary aquifers. It should be noted, however, that this is not indicative of the advective properties of individual permeable units, or of the effects of advection in all portions of the basin (discussed later).

Figure 43 also includes the results of removing the temporal effects of heat conduction across the domain. With a basal heat flux of 60 mW m^{-2} and an initial temperature gradient of 20 °C km^{-1}, all rock thermal conductivity values were set to 3.0 W m^{-1} K^{-1} such that a constant conductive heat flux of 60 mW m^{-2} (see Fourier's Law, Equation 1) was maintained throughout the domain for all time steps. Using realistic permeability values, any temporal changes in temperature and heat flux across the domain are thereby attributed explicitly to fluid flow. As expected (given the initial conditions and the results of isolating the conduction component), the resultant heat flow across the profile is similar to 60 mW m^{-2}, but reflects minor variations due to advection.

Figure 44 illustrates the values of mass fluid flux (g s^{-1} cm^{-2}) over three orders of magnitude for aquifer units in the simulation domain. Results indicate mass fluid flux ranges of 3.0×10^{-6} to 5×10^{-5} g s^{-1} cm^{-2} in the High Plains Aquifer, 1×10^{-8} to 3×10^{-6} g s^{-1} cm^{-2} in the Dakota Aquifer, and 1×10^{-8} to 1×10^{-7} g s^{-1} cm^{-2} in the Madison Aquifer. Calculations of average Darcy velocities yield 13.6 m yr^{-1} for the High Plains Aquifer, 2.37 6 m yr^{-1} for the Dakota Aquifer (compared to the range of 3.05×10^{-3} to 3.05 m yr^{-1} given by Helgeson et al., 1993), and 9.7×10^{-2} m yr^{-1} for the Madison Aquifer (compared to a value of $\leq$ 0.61 m yr^{-1} given by Downey, 1984). Arrows in Figure 44 indicate general directions of flow. It is noteworthy

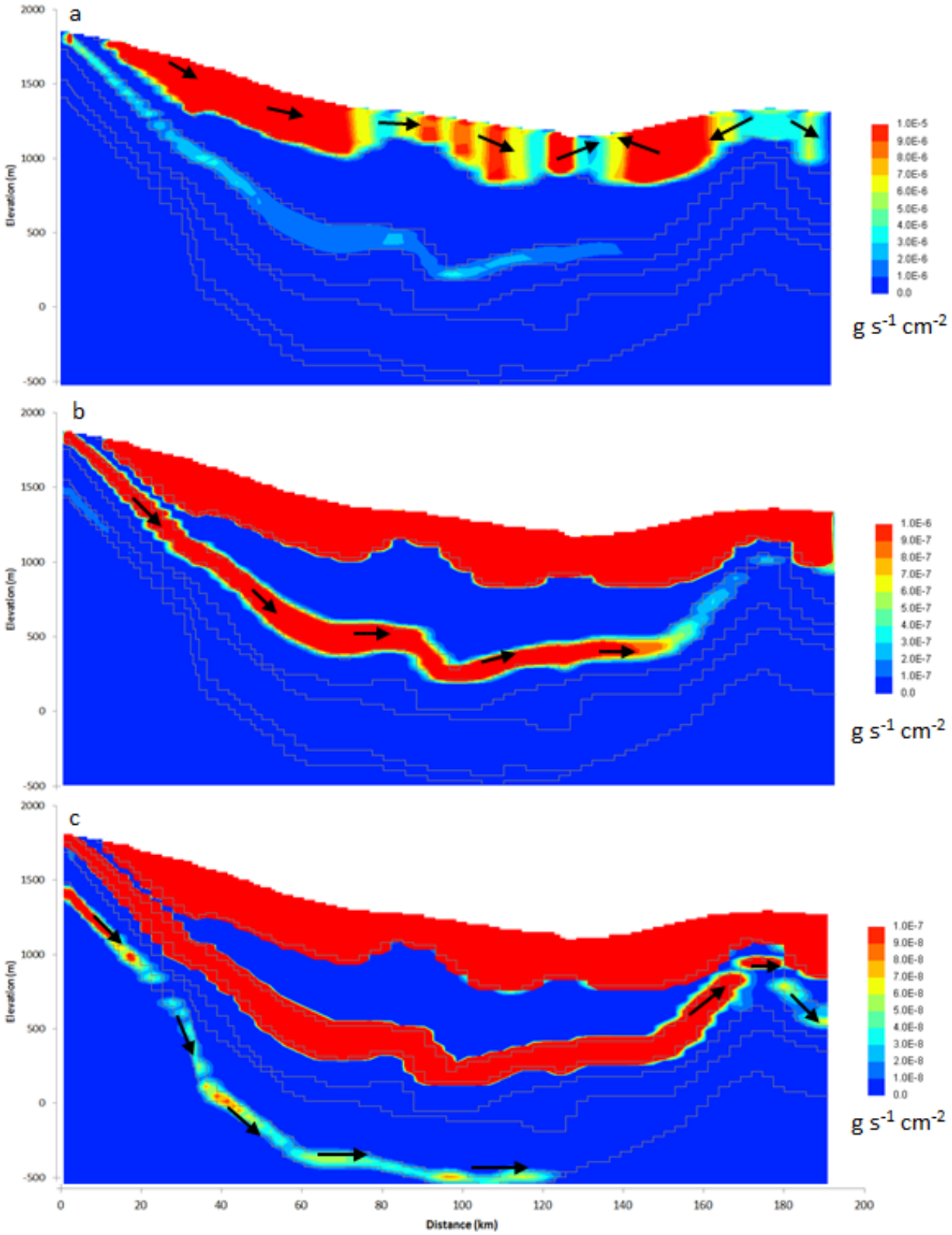

Figure 44. Simulated mass fluid flux rates for calibrated model.

that several previous hydrogeologic models of the Madison and Minnelusa regard both units as aquifers (McKaskey, 2013; Carter et al., 2001), while others designate the Minnelusa as a confining unit (Jorgensen et al, 1993; Signor et al., 1996). In this study the calculated harmonic mean permeability for the Minnelusa was relatively low with respect to the Madison and lower Cretaceous aquifers, effectively designating it as a confining layer.

The thermal Peclet number (Eq. 24) is used to identify regions of the flow domain in which the magnitude of thermal energy transport due to fluid flow (advection) is higher than that due to conduction. Figure 45 shows the Peclet number calculated for the simulation domain over three orders of magnitude (omitting the 1 to 10 scale). Because the Peclet number is proportional to Darcy velocity (which is proportional to mass fluid flux), the patterns in Figure 45 bear a noticeable resemblance to those in Figure 44. Not shown in Figure 44 is the mass fluid flux value of 4×10^{-9} g s^{-1} cm^{-2} (Darcy velocities of 3.15×10^{-3} m yr^{-1}) in upward flow within the Cretaceous confining layer. The encircled region in Figure 45c highlights a calculated Peclet number range of 0.1 to 0.2 for this area of upward flow in the confining layer. This likely explains the peak of ~68 mW m^{-2} calculated for the simulated heat flow shown in Figures 42 and 43.

Two additional simulations were run to isolate the advective contributions of individual aquifers to the overall simulated heat flow profile. Figures 46 and 47 compare the calibrated heat flow results of those shown in Figure 42 to those produced by effective zero permeability values applied to the Dakota and Madison aquifers, respectively. Such comparisons reflect the changes in heat flux imposed by fluid flow in each aquifer to the thermal profile of the simulation domain. The comparison of the two profiles in Figure 46 is suggestive of a cooling effect of the Dakota Aquifer on the western flanks of the basin, results which are expected of the

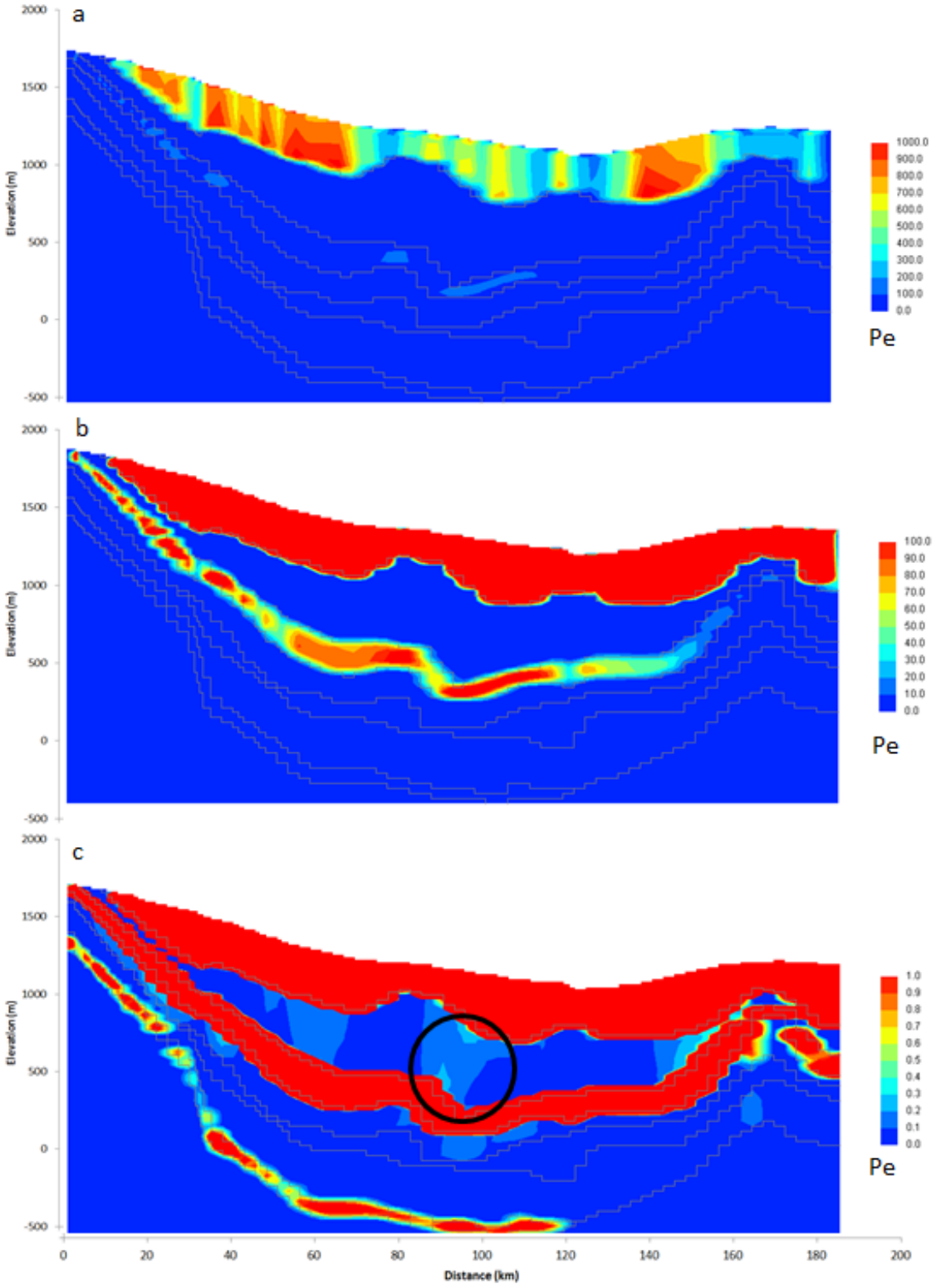

Figure 45. Peclet number calculated for calibrated simulation domain.

Figure 46. Results of zero permeability in Dakota aquifer compared to calibrated simulation. Simulated heat flow is calculated for the upper 200 meters of the model cross-section.

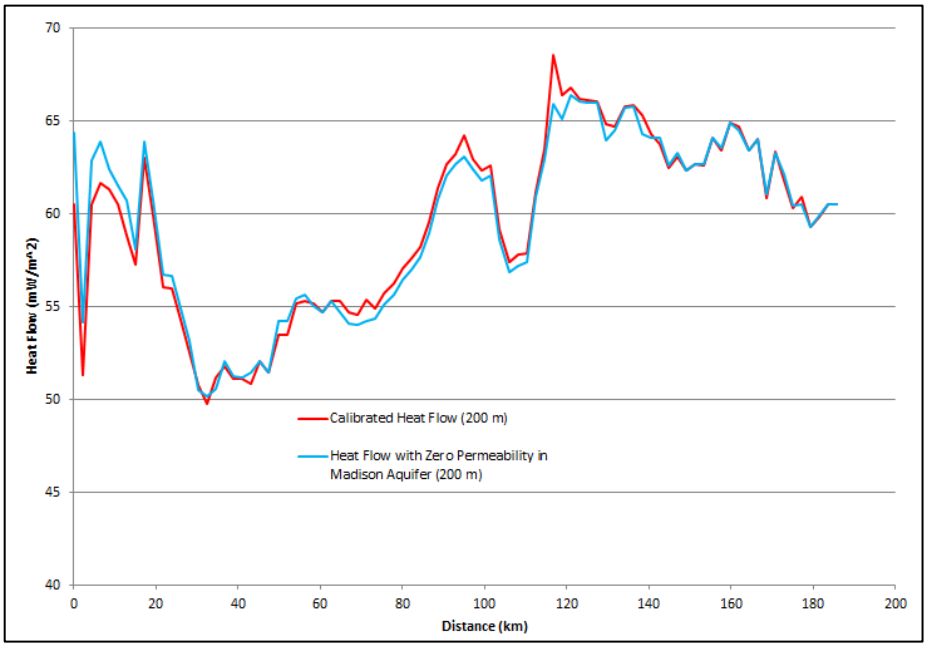

Figure 47. Results of zero permeability in Madison aquifer compared to calibrated simulation. Simulated heat flow is calculated for the upper 200 meters of the model cross-section.

margin of the basin that receives recharge in the Hartville Uplift area. Conversely, the same profile indicates a warming effect of the Dakota on the eastern margin of the basin, results characteristic of discharge zones or up-dip fluid flow.

The effects of reducing permeability in the Madison aquifer to zero are shown in Figure 47. Although an apparent cooling effect in the recharge margin of the basin (similar to that simulated for the Dakota aquifer) is exhibited by the Madison, the effects are far less pronounced. A slight warming effect is also attributed to the Madison in the trough of the basin and in the vicinity of the region where the Madison subcrops against the crystalline basement and overlying Minnelusa. Due to the absence of the Madison in the eastern portion of the transect, the heat flow profile in this area is virtually unchanged by the elimination of flow within the simulation rock unit.

Calibrated simulations appear to yield heat flow profiles consistent with baseline (non-anomalous) heat flow observations in the study transect (Figure 42). Several ranges of permeability and thermal conductivity values possible for the geologic units were also tested in an effort to calibrate simulations for both baseline and anomalous heat flow observations. These tests, however, indicate that anomalous heat flux may not be reproduced without distorting the baseline heat flux profile or invoking unrealistic parameters. The faults and lineament features documented in the study area by several authors (Cooley, 1986; Hildebrand and Kucks, 1985; Gott et al., 1974; Degraw, 1969) are herein considered to be possible explanations for the magnitude and patterns of anomalous heat flow observations. Hildebrand and Kucks (1985) provide geochemical data as evidence of upward fluid flux within faults in the southern Black Hills area. The authors suggest that such a mechanism is the primary control on the discharge of observed surface hot springs in the region.

The effects of a hypothetical, vertically-oriented linear fracture on the thermal profile of the study transect were tested in an experimental simulation, the results of which are shown in Figure 48. Although the results shown are those produced with a permeability value of 130 mD

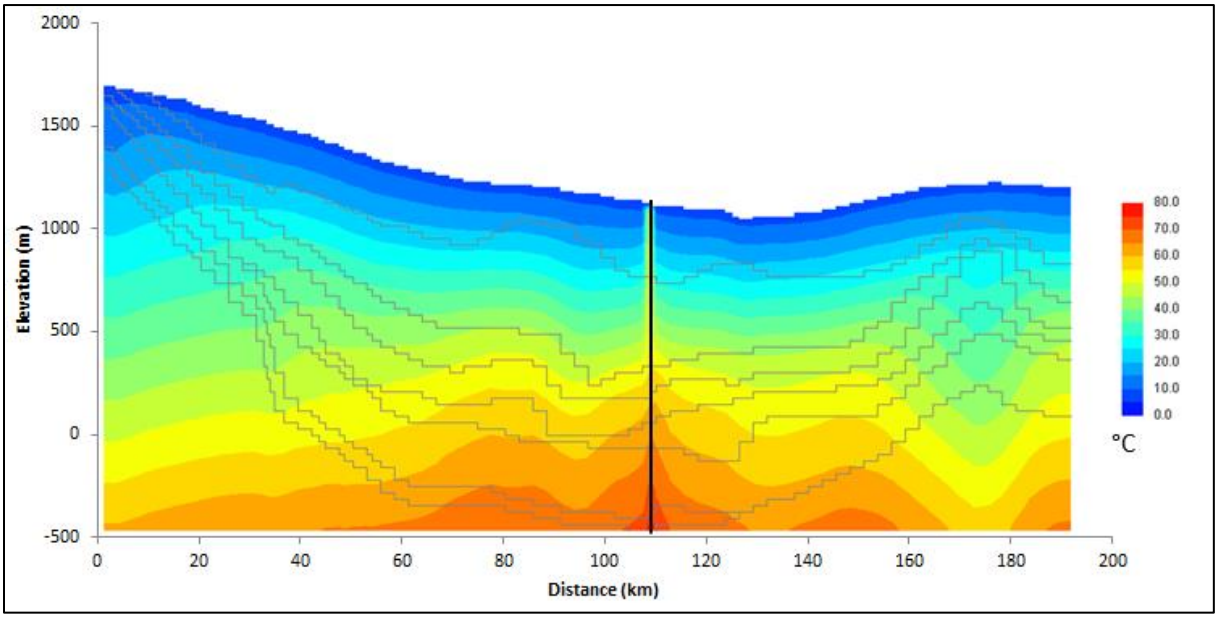

Figure 48. Simulated temperature distribution in study transect with hypothetical linear fracture (after 900,000 years). Width of fracture is exaggerated.

(after Cooley et al., 1986) assigned to the fracture, permeability over several orders of magnitude was tested and produced similar results. The resultant heat flow profile is compared to that of the original calibrated model and the transect of heat flow observations in Figure 49. Both figures indicate a noticeable disturbance of the thermal profile in proximity to the location of the fracture.

Aside from the area in closest proximity to the fracture, a decrease in heat flow across the majority of the profile is observed with the addition of the fracture. This effect is explained by the increase in flow on the western margin of the basin imposed on the aquifers by the presence of the fracture. The addition of the fracture creates an additional pathway for fluid flow in each

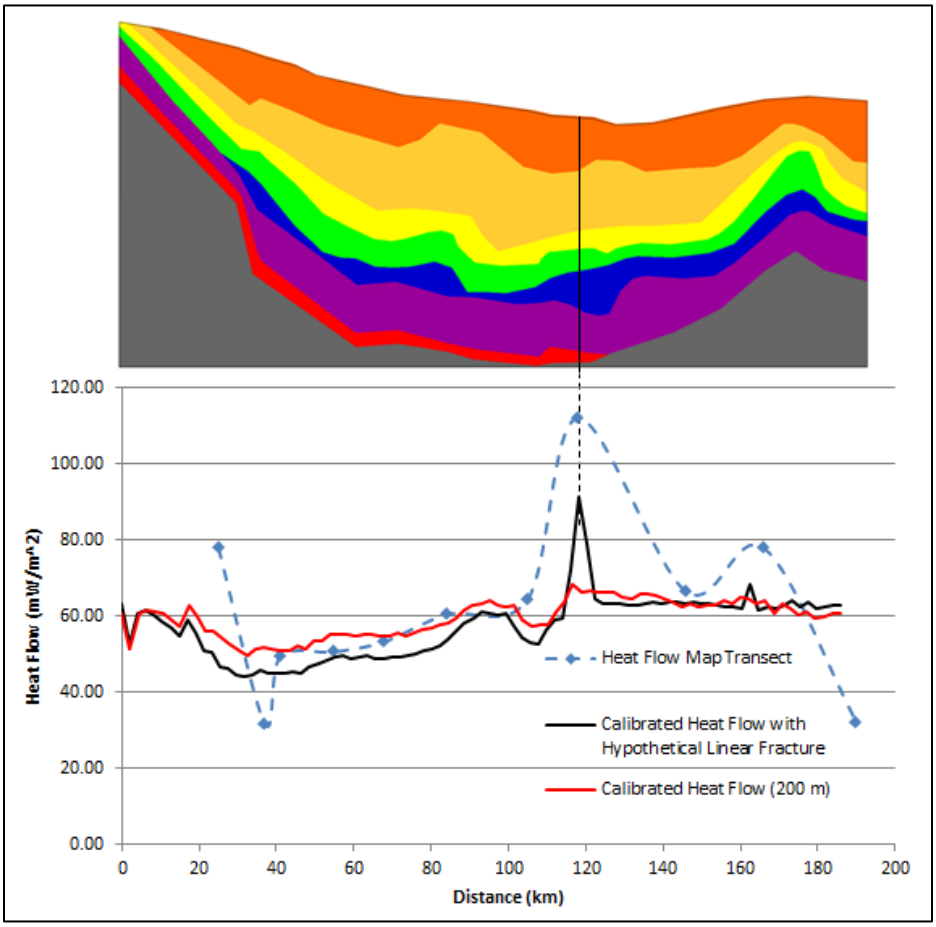

Figure 49. Compared heat flow profiles of observations, calibrated model, and calibrated model with added hypothetical linear fracture. Width of fracture is exaggerated.

aquifer, increasing flow rates on the down-dip margin of the flow domain. Additionally, lateral flow appears to be impeded as a result of fracture truncation, an effect discussed by Konikow (1976). These phenomena are illustrated in the contour plots of mass fluid flux in Figure 50. Figures 50a, 50b and 50c all capture the change in vertical flow rates within the fracture produced by the intersection of the Dakota Aquifer. Because transmissivity in the Dakota is significantly higher than that in the Madison, vertical flow in the portion of the fracture above the Dakota is substantially higher than the portion between the Madison and Dakota aquifers.

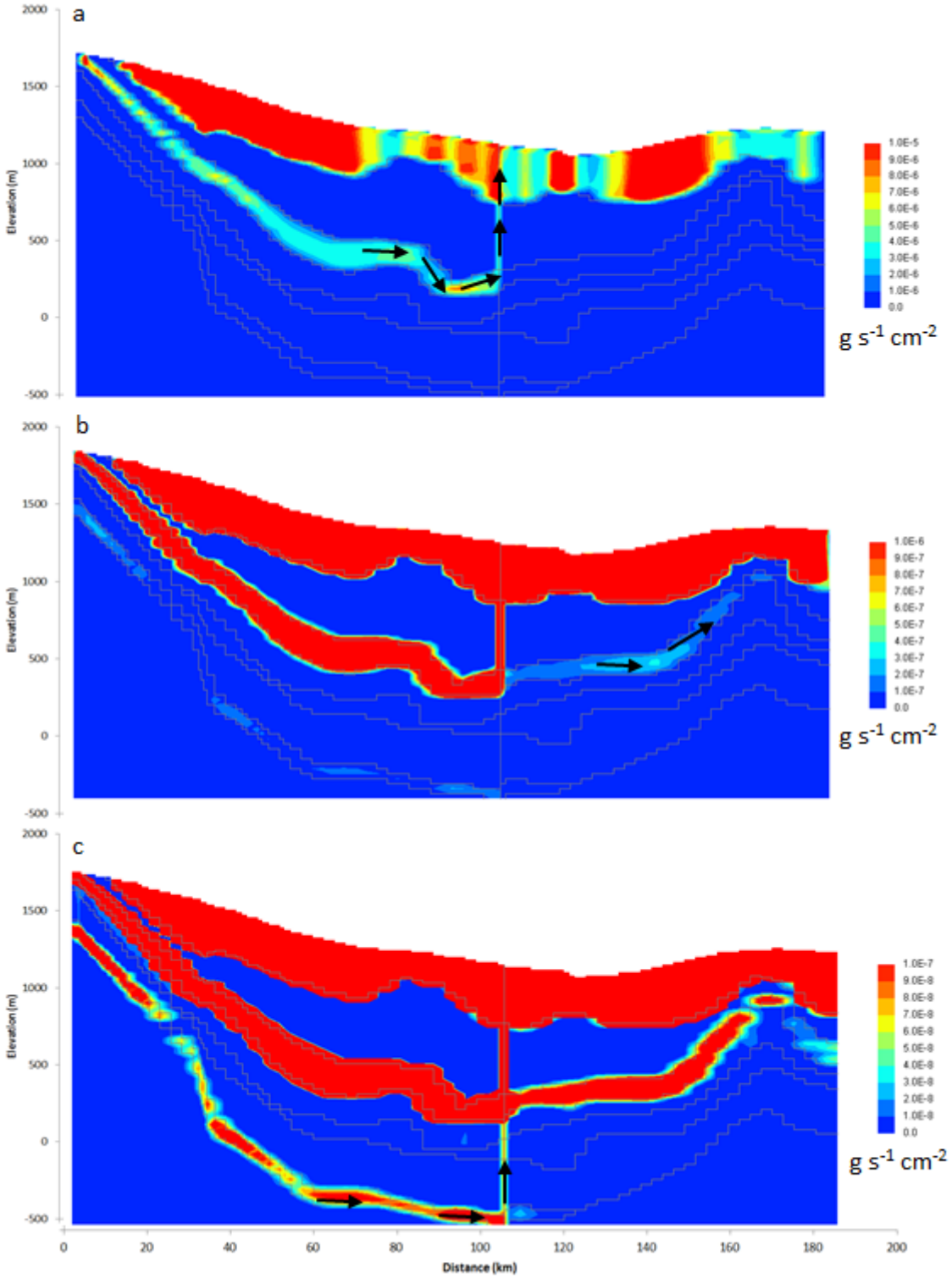

Figure 50. Simulated mass fluid flux rates for calibrated model with hypothetical linear fracture.

Like the calibrated simulations discussed earlier, the Peclet number can be used to delineate areas of the flow domain that exhibit different patterns of advective flow as a result of the addition of the hypothetical fracture. Excluding the 1 to 100 scale, Figure 51 shows three orders of magnitude of the Peclet number calculated for the flow domain after the addition of the vertical fracture. For both aquifers, heat transfer due to advection is increased on the western margin of the flow domain and is decreased east of the fracture. Referring to the definition of the Peclet number (Eq. 24), the mechanisms of advection do not necessitate the release of thermal energy by a fluid in a state of flux. In other words, advection allows for the absorption and desorption of thermal energy equally. Localized increases or decreases in temperature due to fluid flux are determined by the rate of flux, the thermal properties of the fluid and flow medium, and the three-dimensional temperature distribution. The Peclet number, therefore, does not necessarily represent a positive transfer of thermal energy by moving fluids into the surrounding medium. More appropriately it represents the degree to which the local temperature field is changed by fluid in motion compared to changes by pure conduction. The patterns in Figure 51 are appropriate explanations of the decrease in the majority of the heat flow profile of the calibrated simulation transect.

Gosnold (1988) models the vertical changes in heat flow along the profile of a simulated vertical fracture which serves as a conduit for upward fluid flow. In this simulation, heat flow is reduced at the bottom of the aperture in proximity to the heat source, and increased substantially at the point of discharge. The upward motion of fluid results in a redistribution of thermal energy in the direction of fluid flow. Such an effect is similar in areas subject to heat flow distortions due to up-dip flow in confined aquifers. Additionally, equilibrium temperature

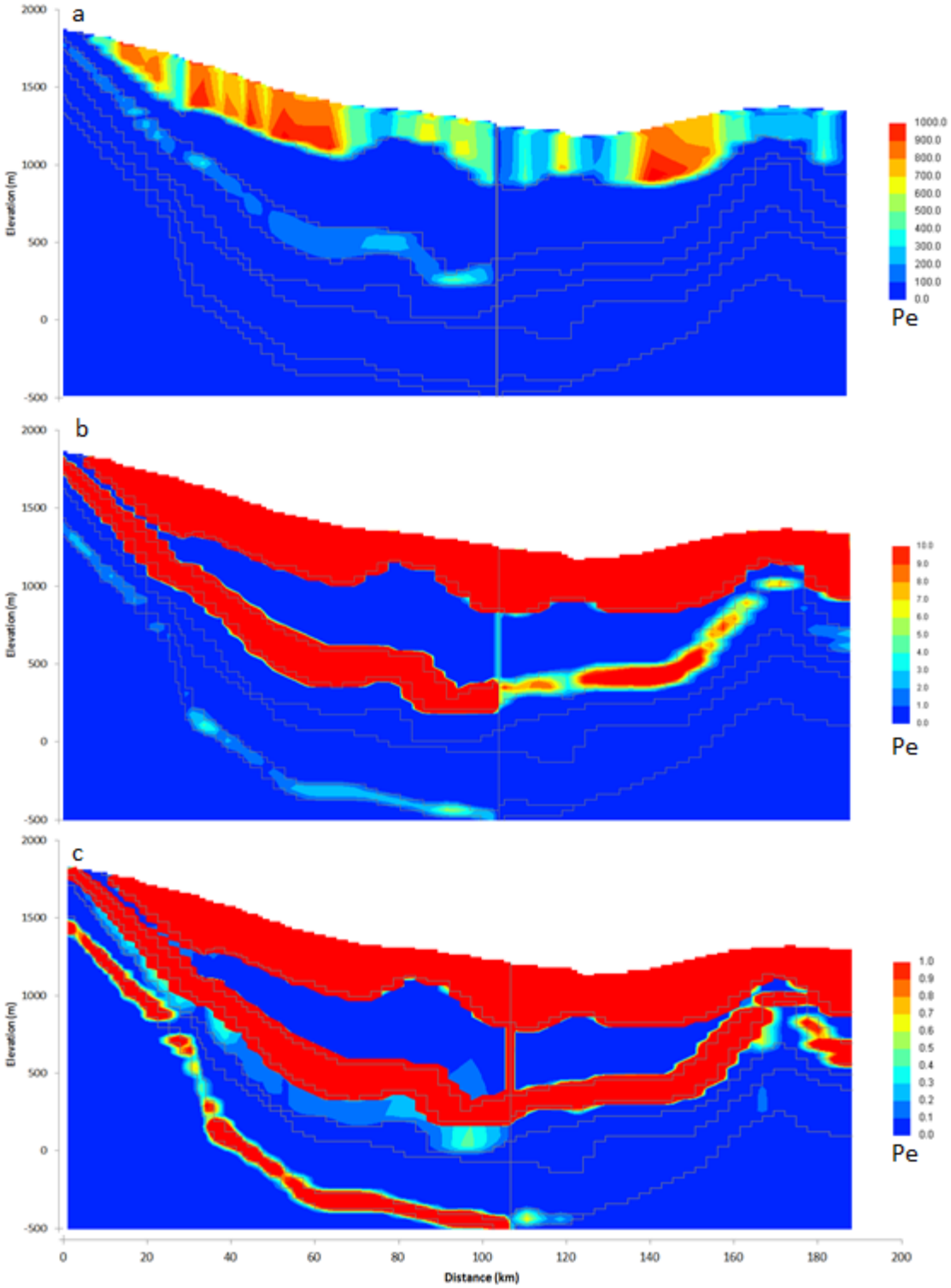

Figure 51. Peclet number calculated for calibrated model with hypothetical linear fracture.

gradient measurements used in the calculation of heat flow are commonly collected from shallow (< 500 m) wells. For these reasons, heat flow profiles shown in Figures 42, 43, 46, 47, and 49 are calculated using simulated temperature gradient data and empirical thermal conductivity data representative of the upper 200 m of the simulation cross-section (adjusted for topography). The simulated heat flow profiles presented herein are therefore representative of variations in surface heat flux due to advection within the underlying aquifers and hypothetical fractures.

Interpretations

To the knowledge of the author, no evidence of significant structural changes to the geological (and therefore hydrothermal) state of the study area have occurred since Laramide activity (ca. 35 Ma) (Curtis, 1988). Therefore, because simulations reached steady-state conditions in approximately 900,000 years, it can be reasoned that the thermal and hydrological regime of the study area are currently under steady-state conditions. More appropriately, it is reasonable to assume that allowing simulations to reach steady-state conditions has produced accurate representations of the current hydrothermal conditions.

The apparent cooling and warming effect of the Dakota and Madison aquifers on the western and eastern margins of the basin (respectively) are consistent with patterns of confined, advective, basin-scale flow documented by numerous authors (Smith & Chapman, 1983; Gosnold, 1999; Saar, 2011; Anderson, 2005). In this manner, relatively cool fluid recharged along outcrops in the Hartville Uplift area reduces the temperature gradients in the recharge zone and areas of down-dip flow. As fluid crosses the trough of the basin, thermal energy is transported laterally and vertically as flow progresses up-dip along the Chadron Arch in Nebraska. Because the Madison aquifer subcrops in the trough of the basin, however, no up-dip flow or heat advection is attributed to the Madison. Additionally, because of the low upward

flow rates calculated in portion of the Minnelusa that overlies the Madison subcrop, observed heat flow anomalies that correlate geographically with the limits of the Madison cannot be attributed to upward leakage. Permeability in the Minnelusa is sufficiently low, and hydrostatic pressure within the Madison in this region is sufficiently low to restrict upward leakage to a rate that does not result in significant upward advection.

The combined effects of conduction through the stratigraphic section and advective flow within permeable aquifers are undoubtedly the primary controls on the patterns of heat flow in the study area. However, available geological, hydrogeological, and geothermal data do not account for localized areas of anomalous heat flow. In considering the possible effects of a simple, vertical fracture on the hydrologic and geothermal mechanisms of the local system, simulations yield better consistency with observations than those that do not acknowledge the presence of faults or fractures. It should be noted that no surface manifestations of hot-water discharge (like those near Hot Springs, SD) are observed in northwestern Nebraska. A possible mechanism proposed by Hildebrand & Kucks (1985), however, is that of subsurface discharge from vertical faults into highly permeable aquifers. Simulations herein that include a hypothetical fracture are best explained with such a mechanism.

Because of the published documentation of existing faults and lineament features in the area, the consideration of the results provided herein is plainly justified. To further illustrate this point, regions within the study area delineated as exhibiting high fracture permeability (associated with high lineament density and proximity to structural manifestations of brittle deformation) mapped by Cooley (1986) (Figure 4) were overlain with the map heat flow (Figure 39). A notable consistency is found between the patterns shown in Figure 52.

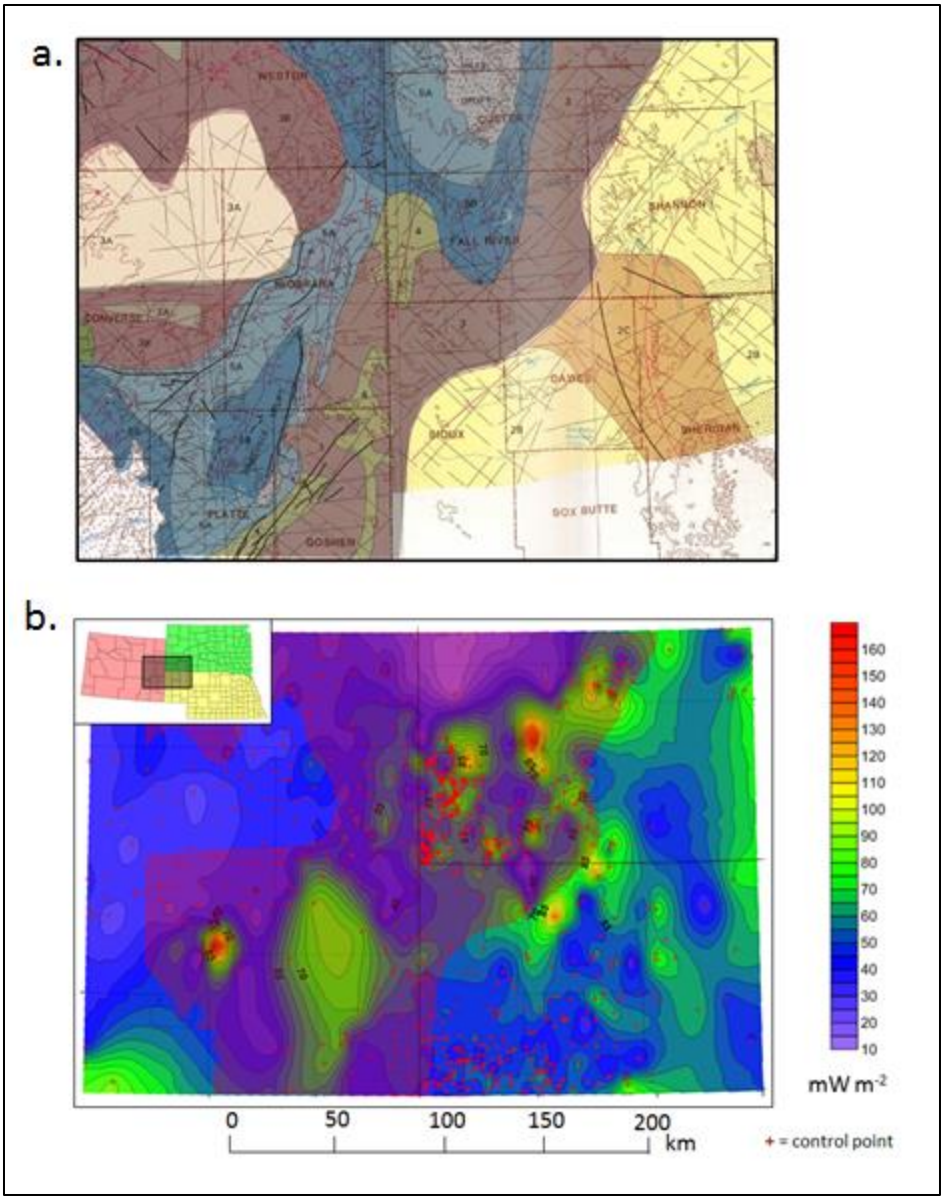

Figure 52. Correlation of heat flow patterns to observed lineaments in study area: a. Regions of highest inferred effect on permeability of structural lineaments (red and blue regions, from Cooley, 1986), and b. Overlay of inferred high-permeability regions (shaded purple) on thermal gradient map of study area.

CHAPTER V

CONCLUSIONS

The geothermal regime of the study area is one that is controlled by several mechanisms. Numerical solutions that incorporate a variety of geological data can be markedly useful in both identifying the mechanisms themselves, and quantifying their individual effects on the system. The simulations employed here have identified a system which is primarily defined by thermal conduction, but that is modified substantially by subsurface fluid flow. Although radiogenic heat production from the Precambrian basement may provide an influential amount of the heat energy on a regional basis, one would expect broader correlations of basement provinces to more extensive geothermal anomalies. This too is a reasonable expectation of advective transport in up-dipping substrata in basin-flank settings. Because of the localized nature of several of the observed thermal anomalies in the study area, the role of existing faults and fractures in controlling the geothermal setting ought not be dismissed or ignored.

Several conclusions are drawn from the simulation tests conducted on the Madison and Dakota aquifers: (1) Although advective flow within both the Dakota and Madison aquifers appears to control a measureable fraction of heat flow observed at the surface, heat transfer by means of conduction likely defines the underlying patterns of heat flow variation (shown in Figure 43). (2) The relative effects of advection are localized, both geographically and in terms of individual aquifers. Although isolation of heat transfer components (Fig. 43) indicate a net cooling effect of all fluid flow within the study transect, individual aquifers exhibit localized

warming depending primarily upon transmissivity and orientation of substrata. (3) The Dakota and Madison aquifers both produce a net cooling effect on the western margin of the basin due to the downward flow of recharged fluid. (4) Warming effects of the Dakota aquifer on the eastern flank of the basin are greater than those produced by the Madison aquifer, owing to the absence of the Madison in the east. (5) Low primary permeability in the Minnelusa does not permit upward leakage (or advective heat transport) from the underlying Madison in areas of subcrop at rates sufficient for producing the observed heat flow anomalies. (6) Because no significant discrepancies between observed and simulated heat flow profiles were calculated using empirical values of thermal conductivity and background heat flux, it is reasonable to assume that heat transfer occurs explicitly by means of conduction and advection within the vicinity of the simulation transect. More specifically, no evidence of neglected components of radiogenic heat production was detected during modelling experiments. (7) When incorporated into simulations, empirical geothermal, hydrogeological, and structural data yield temperature fields consistent with baseline (non-anomalous) observations, but do not account for localized observations of high heat flow.

The models which simulate the effects of a vertical, linear fracture on the heat flow patterns of the study transect yield a best-fit to observational data. These experiments, while theoretically representative of the structural and hydrothermal conditions of the study transect, are hypothetical without the empirical data to support them. Although vertical transport via faults and fractures is apparently a likely explanation for the patterns and magnitudes of observed surface heat flow anomalies, the construction of more definitive models would require the collection of data regarding specific fault characteristics (i.e. vertical and lateral extent, dip, bifurcation, permeability, etc.). It is therefore suggested that future studies include these data, as

well as additional data of every type. Refined models that invoke thermal conductivity anisotropy, three-dimensional flow patterns, and additional equilibrium temperature gradient data will undoubtedly aid in characterizing the system to a higher degree of detail.

APPENDICES

Appendix A
Locations of Well and Outcrop Sources of Samples Used

Source	API	UNL ID	Sample(s)	County	State	Lat (Deg.)	Long (Deg.)
Deans-1 Well	26045050230000	230031	4-10(1-1) to 27-9(1-1)	Dawes	NE	42.6279	-103.0747
Murray 17-24 Well	26161600010000	810010	M17-24	Sheridan	NE	42.7296	-102.6687
Kudrna Well	26045050130000	230016	K3567-85	Dawes	NE	42.5676	-102.8197
1a-GT-80 Well	-	-	(see Appdx. F)	Boyd	NE	42.9885	-99.0240
5-GT-80 Well	-	-	(see Appdx. F)	Wayne	NE	42.2289	-97.0443
9-GT-80 Well	-	-	(see Appdx. F)	Dawes	NE	42.7708	-103.2679
12-GT-80 Well	-	-	(see Appdx. F)	Garden	NE	41.4187	-102.4810
18-B-79 Well	-	-	(see Appdx. F)	Sheridan	NE	42.9137	-102.2098
Black Hills Outcrops	-	-	BHAO1	Lawrence	SD	44.5030	-103.9147
Black Hills Outcrops	-	-	BHAO3	Lawrence	SD	44.5030	-103.9147
Black Hills Outcrops	-	-	BHAO5	Lawrence	SD	44.4488	-103.9690
Derby Dome Outcrops	-	-	MS1 & MS2	Fremont	WY	42.701	-108.544

Appendix B
Lithology and Stratigraphic Nomenclature of Solid Samples

Top Depth (m)	Bottom Depth (m)	Sample ID	Lithology	Unit
960.7	961.6	4-10 (1-1)	very fine sandstone, gray to brown	Cheyenne/Lakota
961.6	962.6	4-11 (1-1)	siltstone, gray to tan, cross-laminated	Cheyenne/Lakota
1010.1	1011.0	5-10 (2-3)	sandstone, gray to tan, very fine, very porous	Cheyenne/Lakota
1010.1	1011.0	5-10 (3-3)	sandstone, gray to tan, very fine, very porous	Cheyenne/Lakota
1294.5	1295.4	6-7 (2-3)	red-orange shale, dense	Sumner (Middle Leonard)
1295.1	1296.0	6-8 (2-3)	red-orange sandstone, fine	Sumner (Middle Leonard)
1314.6	1315.5	7-10 (1-1)	anhydrite, gray-blue	Chase (Upper Wolfcamp)
1315.5	1316.4	7-11 (2-3)	argillaceous anhydrite, gray-blue to tan-brown	Chase (Upper Wolfcamp)
1340.8	1341.7	8-19 (1-1)	dark gray/brown shale, dense, dolomitic	Chase (Upper Wolfcamp)
1342.9	1343.9	9-2 (2-4)	dark gray/brown shale, dense, dolomitic	Chase (Upper Wolfcamp)
1342.9	1343.9	9-2 (3-4)	dark gray/brown shale, dense, dolomitic	Chase (Upper Wolfcamp)
1345.7	1346.6	9-5 (3-4)	dark gray to tan, argillaceous dolomite	Chase (Upper Wolfcamp)
1351.2	1352.1	9-11 (3-4)	white/gray sandstone, very slightly calcareous	Council Grove (Middle Wolfcamp)
1358.8	1359.7	10-1 (2-3)	blue-gray anhydrite, tan shale, no HCl	Council Grove (Middle Wolfcamp)
1358.8	1359.7	10-1 (3-3)	blue-gray anhydrite, tan shale, no HCl	Council Grove (Middle Wolfcamp)
1359.7	1360.6	10-2 (2-3)	gray/green/blue argillaceous, mottled anhydrite, no HCl	Council Grove (Middle Wolfcamp)
1359.7	1360.6	10-2 (3-3)	gray/green/blue argillaceous, mottled anhydrite, no HCl	Council Grove (Middle Wolfcamp)
1361.5	1362.5	10-4 (2-2)	gray & white, very fine sand, dolomitic	Council Grove (Middle Wolfcamp)
1364.3	1365.2	10-7 (2-4)	gray-brown l.s./dolo., argill., mottled, quartz cement fracture	Council Grove (Middle Wolfcamp)
1364.3	1365.2	10-7 (3-4)	gray-brown l.s./dolo., argill., mottled, quartz cement fracture	Council Grove (Middle Wolfcamp)
1368.9	1369.8	10-12 (2-3)	argillaceous limestone, gray-brown	Council Grove (Middle Wolfcamp)
1370.7	1371.6	10-14 (1-2)	mottled limestone (gray-brown) & anhydrite (white-gray)	Council Grove (Middle Wolfcamp)
1370.7	1371.6	10-14 (2-2)	mottled limestone (gray-brown) & anhydrite (white-gray)	Council Grove (Middle Wolfcamp)
1386.5	1387.4	12-2 (2-3)	anhydrite, gray	Council Grove (Middle Wolfcamp)
1416.4	1417.3	13-14 (1-2)	very fine sand, anhydrite, gray w/white fragments, no HCl react.	Broom Creek/Admire (Lower Wolfcamp)
1423.4	1424.3	14-2 (2-3)	dark gray mottled dolomite, siltstone & shale	Broom Creek/Admire (Lower Wolfcamp)
1435.3	1436.2	14-15 (2-2)	gray-brown mudstone/siltstone/shale & dolomite	Broom Creek/Admire (Lower Wolfcamp)
1442.6	1443.5	15-2 (2-3)	mottled dolo. (brown-gray) & anhydrite (blue-gray)	Broom Creek/Admire (Lower Wolfcamp)
1442.6	1443.5	15-2 (3-3)	mottled dolo. (brown-gray) & anhydrite (blue-gray)	Broom Creek/Admire (Lower Wolfcamp)

Appendix B (cont.)

1443.5	1444.4	15-3 (2-2)	anhydrite, blue/white/gray	Broom Creek/Admire (Lower Wolfcamp)
1447.2	1448.1	15-7 (3-4)	interbedded/mottled limestone & green shale	Shawnee/Wendover (Virgil)
1448.1	1449.0	15-8 (1-1)	mottled limestone	Shawnee/Wendover (Virgil)
1454.5	1455.4	16-2 (2-2)	dolomite/limestone fragments/matrix, mottled, gray-tan	Shawnee/Wendover (Virgil)
1455.4	1456.3	16-3 (1-2)	limestone, & dolomite, mottled, tan, shale?	Shawnee/Wendover (Virgil)
1469.1	1470.1	16-18 (2-3)	limestone & light green mudstone	Shawnee/Wendover (Virgil)
1470.1	1471.0	16-19 (2-2)	dark gray dolomite	Shawnee/Wendover (Virgil)
1471.9	1472.5	17-1 (2-3)	sandy dolomite, tan	Shawnee/Wendover (Virgil)
1473.4	1474.3	17-3 (2-3)	mottled limestone & green shale	KC/Meek (Missouri)
1474.3	1475.2	17-4 (1-1)	calcareous red shale interbedded green shale & pebble congl.	KC/Meek (Missouri)
1477.1	1478.0	17-7 (2-4)	gray-green dolomite, calcite crystals	KC/Meek (Missouri)
1477.1	1478.0	17-7 (3-4)	gray-green dolomite, calcite crystals	KC/Meek (Missouri)
1482.5	1483.5	17-13 (2-3)	gray dolomite	KC/Meek (Missouri)
1485.3	1486.2	17-16 (1-1)	purple-red shale & l.s. fragments	KC/Meek (Missouri)
1488.0	1488.9	17-19 (3-3)	white limestone	KC/Meek (Missouri)
1496.6	1497.5	18-6 (2-2)	drk gry l.s. & shale, red (biogenic?) particles, pebble congl.	KC/Meek (Missouri)
1499.3	1500.2	18-9 (1-1)	limestone, green-gray	KC/Meek (Missouri)
1500.2	1501.1	18-10 (1-1)	l.s. conglomerate? White-pink clasts in green-gray matrix	KC/Meek (Missouri)
1504.8	1505.7	18-15 (1-1)	white lime/dolo., not strong react w/ HCl	KC/Meek (Missouri)
1508.5	1509.4	18-19 (2-4)	dark gray limestone & shale, red particles (biogenic?)	Marmaton/Hayden (Upper DesMoines)
1508.5	1509.4	18-19(3-4)	dark gray limestone & shale, red particles (biogenic?)	Marmaton/Hayden (Upper DesMoines)
1511.2	1512.1	19-2 (2-2)	limestone, gray-green	Marmaton/Hayden (Upper DesMoines)
1513.9	1514.9	19-5 (2-3)	dolomite, gray-green	Marmaton/Hayden (Upper DesMoines)
1513.9	1514.9	19-5(3-3)	dolomite, gray-green	Marmaton/Hayden (Upper DesMoines)
1518.5	1519.4	19-10 (2-2)	limestone, white-gray, hard, fine sandstone	Marmaton/Hayden (Upper DesMoines)
1520.3	1521.3	19-12 (1-3)	dolomite, gray	Marmaton/Hayden (Upper DesMoines)
1520.3	1521.3	19-12 (2-3)	dolomite, gray	Marmaton/Hayden (Upper DesMoines)
1523.1	1524.0	19-15 (2-4)	lime & dolo., purple to gray-blue/green	Marmaton/Hayden (Upper DesMoines)
1523.1	1524.0	19-15 (3-4)	lime & dolo., purple to gray-blue/green	Marmaton/Hayden (Upper DesMoines)
1525.8	1526.7	19-18 (2-4)	white/green dolomite	Marmaton/Hayden (Upper DesMoines)

Appendix B (cont.)

1525.8	1526.7	19-18 (3-4)	white/green dolomite	Marmaton/Hayden (Upper DesMoines)
1531.0	1531.9	20-4d (2-2)	mottled red shale and limestone	Cherokee/Rountop (Lower DesMoines)
1531.0	1531.9	20-4u (2-3)	limestone, some mottled red shale	Cherokee/Rountop (Lower DesMoines)
1533.8	1534.7	20-7 (2-3)	red siltstn & gray-grn lime/dolostone	Cherokee/Rountop (Lower DesMoines)
1534.7	1535.6	20-8 (2-2)	gray to blue-grn mud/siltstn, slightly calcareous	Cherokee/Rountop (Lower DesMoines)
1542.9	1543.8	21-6 (1-1)	purple shale matrix w/ light green shale rip-up clasts	Lower Roundtop (Upper Atoka)
1563.0	1563.9	25-1 (2-4)	mottled red shale	Fairbank (Morrow)
1564.8	1565.8	25-3 (1-1)	dark red fine sandstone	Fairbank (Morrow)
1568.8	1569.7	26-2 (2-4)	sandy red shale, dolo. fragments	Fairbank (Morrow)
1568.8	1569.7	26-2 (3-4)	sandy red shale, dolo. fragments	Fairbank (Morrow)
1571.5	1572.5	26-5 (2-2)	sandy red shale, dolo. fragments	Fairbank (Morrow)
1575.2	1576.1	26-9d (4-5)	red shale fragments, dolomite	Fairbank (Morrow)
1577.9	1578.9	26-12 (1-2)	pink dolomite	Madison
1579.8	1580.7	27-14 (1-2)	limestone, yellow dolo.	Madison
1579.8	1580.7	27-14 (2-2)	limestone, yellow dolo.	Madison
1581.9	1582.2	27-1 (1-1)	pink dolomite, v.f. sand	Madison
1584.0	1585.0	27-4 (1-2)	yellow dolomite	Madison
1584.0	1585.0	27-4 (2-2)	yellow dolomite	Madison
1585.9	1586.8	27-6 (2-2)	dolomite, congl., shale	Englewood
1588.6	1589.5	27-9 (1-1)	Granite	Precambrian
922.3	922.6	M17-24	hornblende garnet gneiss, w/ quartzitic streaks	Precambrian
1087.2	1092.7	K3567-85	schist, weathered, very brittle	Precambrian
-	-	BHAO1	interbedded red shale & limestone, thinly laminated	Upper Goose Egg
-	-	BHAO3	limestone, gray, dense	Minnekahta (Lower Goose Egg)
-	-	BHAO5	calcareous red shale, white limestone rip-up clasts	Nippewalla (Upper Leonard)
-	-	MS1	fossiliferous limestone/coquina w/ bivalves	Sundance

Appendix C
Dimensions, Mass and Density Measured for Solid Samples

Top Depth (m)	Bottom Depth (m)	Sample ID	Avg. Diameter (mm)	Diameter St. Dev.	Diameter RSD (%)	Avg. Thick (mm)	Thickness St. Dev.	Thickness RSD (%)	Mass (g)	Density (g cm^{-3})
960.7	961.6	4-10 (1-1)	38.61	0.04	0.10	22.93	0.03	0.12	54.08	2.01
961.6	962.6	4-11 (1-1)	38.52	0.07	0.18	21.65	0.01	0.03	57.37	2.27
1010.1	1011.0	5-10 (2-3)	38.34	0.05	0.14	16.16	0.09	0.57	35.01	1.88
1010.1	1011.0	5-10 (3-3)	38.29	0.09	0.23	17.95	0.06	0.32	39.65	1.92
1294.5	1295.4	6-7 (2-3)	38.59	0.08	0.22	22.03	0.06	0.28	59.75	2.32
1295.1	1296.0	6-8 (2-3)	38.24	0.31	0.81	18.56	0.05	0.25	40.03	1.88
1314.6	1315.5	7-10 (1-1)	32.12	0.26	0.82	13.65	0.05	0.36	32.01	2.89
1315.5	1316.4	7-11 (2-3)	38.60	0.06	0.16	23.93	0.04	0.18	81.76	2.92
1340.8	1341.7	8-19 (1-1)	38.60	0.06	0.16	18.71	0.05	0.28	53.23	2.43
1342.9	1343.9	9-2 (2-4)	38.65	0.05	0.12	16.43	0.09	0.54	48.81	2.53
1342.9	1343.9	9-2 (3-4)	38.63	0.03	0.07	15.37	0.08	0.50	45.41	2.52
1345.7	1346.6	9-5 (3-4)	44.60	0.07	0.15	23.14	0.07	0.29	90.89	2.51
1351.2	1352.1	9-11 (3-4)	44.16	0.52	1.17	14.70	0.28	1.91	41.49	1.84
1358.8	1359.7	10-1 (2-3)	44.66	0.05	0.11	23.91	0.06	0.24	106.53	2.84
1358.8	1359.7	10-1 (3-3)	44.57	0.05	0.12	24.32	0.03	0.11	109.05	2.87
1359.7	1360.6	10-2 (2-3)	44.65	0.03	0.06	16.21	0.04	0.23	66.57	2.62
1359.7	1360.6	10-2 (3-3)	44.60	0.05	0.12	16.28	0.03	0.16	66.58	2.62
1361.5	1362.5	10-4 (2-2)	38.71	0.09	0.23	22.07	0.03	0.13	68.74	2.65
1364.3	1365.2	10-7 (2-4)	44.62	0.05	0.12	12.64	0.08	0.65	41.72	2.11
1364.3	1365.2	10-7 (3-4)	44.67	0.06	0.12	12.52	0.03	0.20	42.36	2.16
1368.9	1369.8	10-12 (2-3)	44.49	0.04	0.09	21.98	0.05	0.21	85.07	2.49
1370.7	1371.6	10-14 (1-2)	50.33	0.04	0.09	21.15	0.05	0.23	116.93	2.78
1370.7	1371.6	10-14 (2-2)	50.36	0.04	0.08	13.98	0.05	0.36	75.39	2.71
1386.5	1387.4	12-2 (2-3)	50.35	0.05	0.11	19.29	0.02	0.09	110.19	2.87
1416.4	1417.3	13-14 (1-2)	50.35	0.04	0.07	22.84	0.06	0.26	119.47	2.63
1423.4	1424.3	14-2 (2-3)	50.00	0.04	0.09	14.15	0.07	0.50	68.05	2.45
1435.3	1436.2	14-15 (2-2)	38.61	0.07	0.19	23.05	0.04	0.16	70.53	2.61
1442.6	1443.5	15-2 (2-3)	44.60	0.05	0.10	11.51	0.12	1.08	50.49	2.81
1442.6	1443.5	15-2 (3-3)	44.57	0.08	0.17	13.63	0.04	0.31	59.70	2.81

Appendix C (cont.)

1443.5	1444.4	15-3 (2-2)	38.59	0.03	0.08	14.61	0.04	0.31	50.15	2.94
1447.2	1448.1	15-7 (3-4)	38.62	0.04	0.10	12.95	0.11	0.85	40.00	2.64
1448.1	1449.0	15-8 (1-1)	38.66	0.10	0.25	21.06	0.02	0.10	65.83	2.66
1454.5	1455.4	16-2 (2-2)	38.64	0.09	0.24	23.36	0.01	0.05	73.31	2.68
1455.4	1456.3	16-3 (1-2)	38.63	0.04	0.11	19.68	0.02	0.11	62.56	2.71
1469.1	1470.1	16-18 (2-3)	31.86	0.11	0.34	19.99	0.02	0.11	36.27	2.28
1470.1	1471.0	16-19 (2-2)	38.53	0.13	0.33	9.36	0.06	0.65	28.01	2.57
1471.9	1472.5	17-1 (2-3)	38.77	0.08	0.20	20.03	0.06	0.30	53.08	2.25
1473.4	1474.3	17-3 (2-3)	38.59	0.05	0.14	11.98	0.06	0.46	37.14	2.65
1474.3	1475.2	17-4 (1-1)	38.54	0.07	0.18	31.60	0.09	0.27	96.60	2.62
1477.1	1478.0	17-7 (2-4)	31.56	0.03	0.08	17.64	0.12	0.66	36.75	2.66
1477.1	1478.0	17-7 (3-4)	31.45	0.07	0.24	17.80	0.10	0.57	35.81	2.59
1482.5	1483.5	17-13 (2-3)	38.58	0.07	0.18	23.49	0.07	0.31	73.05	2.66
1485.3	1486.2	17-16 (1-1)	38.63	0.08	0.20	18.52	0.04	0.20	58.33	2.69
1488.0	1488.9	17-19 (3-3)	31.69	0.05	0.15	17.11	0.12	0.68	33.56	2.49
1496.6	1497.5	18-6 (2-2)	44.60	0.08	0.18	24.15	0.25	1.06	99.90	2.65
1499.3	1500.2	18-9 (1-1)	44.61	0.05	0.10	22.09	0.17	0.78	81.56	2.36
1500.2	1501.1	18-10 (1-1)	38.65	0.09	0.24	20.22	0.05	0.23	63.51	2.68
1504.8	1505.7	18-15 (1-1)	38.57	0.08	0.22	22.75	0.20	0.87	66.16	2.49
1508.5	1509.4	18-19 (2-4)	38.59	0.11	0.28	11.68	0.21	1.79	36.75	2.69
1508.5	1509.4	18-19(3-4)	38.65	0.09	0.24	12.84	0.22	1.72	40.40	2.68
1511.2	1512.1	19-2 (2-2)	38.53	0.10	0.25	17.35	0.13	0.75	53.55	2.65
1513.9	1514.9	19-5 (2-3)	38.64	0.10	0.27	15.47	0.14	0.91	43.89	2.42
1513.9	1514.9	19-5(3-3)	38.57	0.04	0.11	16.31	0.18	1.09	46.59	2.44
1518.5	1519.4	19-10 (2-2)	38.74	0.09	0.23	21.13	0.07	0.31	64.72	2.60
1520.3	1521.3	19-12 (1-3)	38.60	0.05	0.12	19.04	0.04	0.21	61.84	2.78
1520.3	1521.3	19-12 (2-3)	38.62	0.09	0.23	18.47	0.09	0.47	59.62	2.76
1523.1	1524.0	19-15 (2-4)	31.51	0.04	0.12	18.56	0.11	0.62	34.40	2.38
1523.1	1524.0	19-15 (3-4)	31.54	0.04	0.13	18.47	0.08	0.46	36.51	2.53
1525.8	1526.7	19-18 (2-4)	44.55	0.09	0.20	14.54	0.19	1.28	59.46	2.62

Appendix C (cont.)

1525.8	1526.7	19-18 (3-4)	44.60	0.07	0.16	14.32	0.09	0.61	58.69	2.62
1531.0	1531.9	20-4d (2-2)	38.31	0.22	0.58	16.45	0.12	0.71	45.46	2.40
1531.0	1531.9	20-4u (2-3)	38.39	0.07	0.18	12.52	0.02	0.17	36.82	2.54
1533.8	1534.7	20-7 (2-3)	44.49	0.08	0.18	23.93	0.21	0.89	94.31	2.54
1534.7	1535.6	20-8 (2-2)	44.45	0.12	0.27	17.47	0.18	1.03	68.90	2.54
1542.9	1543.8	21-6 (1-1)	38.63	0.05	0.14	11.25	0.05	0.47	34.66	2.63
1563.0	1563.9	25-1 (2-4)	38.54	0.08	0.21	15.44	0.03	0.21	43.94	2.44
1564.8	1565.8	25-3 (1-1)	38.20	0.09	0.23	20.84	0.03	0.13	51.75	2.17
1568.8	1569.7	26-2 (2-4)	31.30	0.09	0.30	11.70	0.25	2.11	22.12	2.46
1568.8	1569.7	26-2 (3-4)	31.38	0.08	0.24	12.17	0.06	0.48	23.84	2.53
1571.5	1572.5	26-5 (2-2)	44.57	0.05	0.11	11.42	0.18	1.62	42.13	2.36
1575.2	1576.1	26-9d (4-5)	44.62	0.04	0.08	7.88	0.26	3.30	32.31	2.62
1577.9	1578.9	26-12 (1-2)	31.49	0.08	0.26	19.52	0.11	0.58	32.13	2.11
1579.8	1580.7	27-14 (1-2)	44.66	0.13	0.29	15.76	0.06	0.35	56.89	2.30
1579.8	1580.7	27-14 (2-2)	44.58	0.05	0.11	14.40	0.05	0.33	48.25	2.15
1581.9	1582.2	27-1 (1-1)	44.63	0.07	0.16	22.88	0.09	0.40	88.38	2.47
1584.0	1585.0	27-4 (1-2)	44.66	0.08	0.18	17.45	0.35	1.99	60.78	2.22
1584.0	1585.0	27-4 (2-2)	44.65	0.11	0.25	16.26	0.10	0.59	54.65	2.15
1585.9	1586.8	27-6 (2-2)	44.39	0.15	0.34	15.30	0.27	1.75	59.37	2.51
1588.6	1589.5	27-9 (1-1)	50.45	0.09	0.19	23.44	0.06	0.26	123.73	2.64
922.3	922.6	M17-24	31.96	0.06	0.18	15.84	0.05	0.32	35.97	2.83
1087.2	1092.7	K3567-85	44.48	0.04	0.10	11.03	0.14	1.29	37.54	2.19
-	-	BHAO1	38.68	0.05	0.13	14.76	0.07	0.44	46.17	2.66
-	-	BHAO3	38.64	0.10	0.27	21.51	0.05	0.24	67.97	2.70
-	-	BHAO5	38.57	0.09	0.22	13.72	0.03	0.23	40.70	2.54
-	-	MS1	38.60	0.09	0.24	18.45	0.06	0.35	57.03	2.64

Appendix D
Thermal Conductivity, Porosity and Density Measured for Solid Samples
(* = samples not saturated)

Top Depth (m)	Bottom Depth (m)	Sample ID	Avg. λ (W m^{-1} K^{-1})	λ St. Dev.	λ RSD (%)	N	Porosity (%)	Density (g cm^{-3})
960.7	961.6	4-10 (1-1)	3.781	0.319	8.443	4	24.21	2.01
961.6	962.6	4-11 (1-1)	2.969	0.375	12.649	2	15.34	2.27
1010.1	1011.0	5-10 (2-3)	2.921	0.059	2.033	2	17.58	1.88
1010.1	1011.0	5-10 (3-3)	1.714*	0.147	8.586	4	N/A*	1.92
1294.5	1295.4	6-7 (2-3)	2.687	0.093	3.459	4	15.13	2.32
1295.1	1296.0	6-8 (2-3)	1.118*	0.055	4.920	4	N/A*	1.88
1314.6	1315.5	7-10 (1-1)	4.631	1.348	29.120	4	0.00	2.89
1315.5	1316.4	7-11 (2-3)	5.345	0.523	9.793	4	0.00	2.92
1340.8	1341.7	8-19 (1-1)	2.554	0.091	3.570	4	11.10	2.43
1342.9	1343.9	9-2 (2-4)	1.911	0.088	4.626	2	4.57	2.53
1342.9	1343.9	9-2 (3-4)	1.665	0.107	6.455	2	6.66	2.52
1345.7	1346.6	9-5 (3-4)	2.098	0.151	7.211	4	8.82	2.51
1351.2	1352.1	9-11 (3-4)	2.078	-	-	1	16.53	1.84
1358.8	1359.7	10-1 (2-3)	4.364	0.521	11.946	4	0.16	2.84
1358.8	1359.7	10-1 (3-3)	4.580	0.469	10.251	4	0.00	2.87
1359.7	1360.6	10-2 (2-3)	4.621	0.346	7.496	4	3.94	2.62
1359.7	1360.6	10-2 (3-3)	4.520	0.467	10.338	4	4.52	2.62
1361.5	1362.5	10-4 (2-2)	5.127	0.624	12.164	4	3.00	2.65
1364.3	1365.2	10-7 (2-4)	2.314	0.278	12.016	3	22.42	2.11
1364.3	1365.2	10-7 (3-4)	2.505	0.093	3.697	4	22.28	2.16
1368.9	1369.8	10-12 (2-3)	2.235	0.061	2.721	3	7.20	2.49
1370.7	1371.6	10-14 (1-2)	3.273	0.203	6.211	4	0.14	2.78
1370.7	1371.6	10-14 (2-2)	2.876	0.250	8.709	4	1.29	2.71
1386.5	1387.4	12-2 (2-3)	4.440	0.530	11.938	4	0.00	2.87
1416.4	1417.3	13-14 (1-2)	4.853	0.270	5.572	4	3.10	2.63
1423.4	1424.3	14-2 (2-3)	2.304	0.213	9.238	3	11.77	2.45
1435.3	1436.2	14-15 (2-2)	2.469	0.080	3.245	5	6.63	2.61
1442.6	1443.5	15-2 (2-3)	3.235	0.258	7.978	6	1.06	2.81
1442.6	1443.5	15-2 (3-3)	4.235	0.255	6.017	5	1.22	2.81
1443.5	1444.4	15-3 (2-2)	5.221	0.213	4.088	3	0.00	2.94
1447.2	1448.1	15-7 (3-4)	1.990	0.299	15.022	3	1.38	2.64
1448.1	1449.0	15-8 (1-1)	3.007	0.093	3.092	3	2.31	2.66
1454.5	1455.4	16-2 (2-2)	2.909	0.119	4.102	3	2.12	2.68
1455.4	1456.3	16-3 (1-2)	2.880	0.066	2.295	3	2.25	2.71
1469.1	1470.1	16-18 (2-3)	3.305	0.287	8.671	4	13.18	2.28

1470.1	1471.0	16-19 (2-2)	2.484	0.451	18.162	5	6.87	2.57
1471.9	1472.5	17-1 (2-3)	3.703	0.318	8.593	3	12.39	2.25
1473.4	1474.3	17-3 (2-3)	2.292	0.282	12.306	5	1.00	2.65
1477.1	1478.0	17-7 (2-4)	3.287	0.367	11.168	5	3.91	2.66
1477.1	1478.0	17-7 (3-4)	3.353	0.316	9.415	5	6.80	2.59
1482.5	1483.5	17-13 (2-3)	2.944	0.006	0.207	3	4.91	2.66
1485.3	1486.2	17-16 (1-1)	2.795	0.112	4.009	3	0.28	2.69
1488.0	1488.9	17-19 (3-3)	2.610	0.250	9.584	5	9.56	2.49
1496.6	1497.5	18-6 (2-2)	2.212	0.025	1.151	2	2.31	2.65
1499.3	1500.2	18-9 (1-1)	2.687	0.095	3.538	3	13.96	2.36
1500.2	1501.1	18-10 (1-1)	2.757	0.138	4.991	3	0.34	2.68
1504.8	1505.7	18-15 (1-1)	2.298	0.233	10.119	5	12.34	2.49
1508.5	1509.4	18-19 (2-4)	1.808	0.259	14.347	5	1.32	2.69
1508.5	1509.4	18-19(3-4)	1.935	0.279	14.423	5	1.59	2.68
1511.2	1512.1	19-2 (2-2)	2.207	0.016	0.734	3	1.43	2.65
1513.9	1514.9	19-5 (2-3)	3.879	0.182	4.701	3	12.12	2.42
1513.9	1514.9	19-5(3-3)	3.439	0.474	13.787	5	10.91	2.44
1518.5	1519.4	19-10 (2-2)	3.704	0.162	4.362	5	1.85	2.60
1520.3	1521.3	19-12 (1-3)	3.597	0.127	3.517	3	1.84	2.78
1520.3	1521.3	19-12 (2-3)	3.641	0.195	5.367	3	2.91	2.76
1523.1	1524.0	19-15 (2-4)	2.225	0.193	8.676	5	15.61	2.38
1523.1	1524.0	19-15 (3-4)	2.342	0.206	8.777	3	10.60	2.53
1525.8	1526.7	19-18 (2-4)	2.673	0.175	6.536	5	5.60	2.62
1525.8	1526.7	19-18 (3-4)	3.078	0.138	4.493	3	4.74	2.62
1531.0	1531.9	20-4u (2-3)	3.533	0.328	9.269	4	5.11	2.54
1533.8	1534.7	20-7 (2-3)	3.212	0.114	3.540	3	4.38	2.54
1534.7	1535.6	20-8 (2-2)	1.864	0.319	17.095	3	7.67	2.54
1542.9	1543.8	21-6 (1-1)	1.528	-	-	1	2.96	2.63
1563.0	1563.9	25-1 (2-4)	2.897	0.330	11.401	2	11.55	2.44
1564.8	1565.8	25-3 (1-1)	1.848*	0.126	6.834	3	N/A*	2.17
1568.8	1569.7	26-2 (2-4)	2.232	0.083	3.698	3	10.44	2.46
1568.8	1569.7	26-2 (3-4)	2.841	0.387	13.638	3	6.48	2.53
1571.5	1572.5	26-5 (2-2)	2.035	0.423	20.765	3	10.55	2.36
1575.2	1576.1	26-9d (4-5)	1.914	0.201	10.526	3	1.79	2.62
1577.9	1578.9	26-12 (1-2)	2.539	0.304	11.987	3	18.42	2.11
1579.8	1580.7	27-14 (1-2)	2.672	0.292	10.909	3	13.41	2.30
1579.8	1580.7	27-14 (2-2)	2.648	0.251	9.476	3	20.78	2.15

Appendix D (cont.)

1581.9	1582.2	27-1 (1-1)	3.672	0.267	7.276	3	11.18	2.47
1584.0	1585.0	27-4 (1-2)	2.981	0.133	4.447	3	18.76	2.22
1584.0	1585.0	27-4 (2-2)	2.639	0.201	7.599	3	22.00	2.15
1585.9	1586.8	27-6 (2-2)	2.442	-	-	1	10.43	2.51
1588.6	1589.5	27-9 (1-1)	2.471	0.156	6.334	3	0.45	2.64
922.3	922.6	M17-24	2.621	0.424	16.178	4	0.00	2.83
-	-	BHAO1	2.904	0.265	9.112	4	0.98	2.66
-	-	BHAO3	3.123	0.256	8.192	4	0.16	2.70
-	-	BHAO5	4.041	0.355	8.795	4	4.18	2.54
-	-	MS1	2.853	0.201	7.041	4	1.90	2.64

Appendix E
Thermal Conductivity Measured for Unconsolidated Samples

Well	Sample ID	Avg. Conductivity (W m^{-1} K^{-1})	St Dev	RSD (%)	N
Deans-1	1-3cr	1.504	0.009	0.580	3
Deans-1	2-12cr	1.335	0.087	6.549	3
Deans-1	3-11u-cr	1.799	0.018	1.009	3
Deans-1	4-10 (1-1)cr	2.351	0.118	5.033	3
Deans-1	4-11 (1-1)cr	1.955	0.042	2.127	3
Deans-1	5-3cr	1.485	0.071	4.750	3
Deans-1	5-10 (2-3)&(3-3)cr	2.554	0.129	5.044	3
Deans-1	6-7 (2-3)cr	1.866	0.107	5.754	3
Deans-1	8-19 (1-1)cr	1.721	0.021	1.242	3
Deans-1	9-2 (2-4)&(3-4)cr	1.569	0.095	6.023	3
Deans-1	9-5 (3-4)cr	1.489	0.015	1.008	3
Deans-1	10-4 (2-2)cr	2.562	0.014	0.541	3
Deans-1	13-14(1-2)cr	2.581	0.131	5.086	3
Deans-1	14-2 (2-3)cr	1.848	0.082	4.416	3
Deans-1	14-15(2-2)cr	1.762	0.021	1.189	3
Deans-1	16-18 (2-3)cr	1.725	0.042	2.447	3
Deans-1	18-15 (1-1)cr	1.746	0.016	0.909	3
Deans-1	18-19 (2-4)&(3-4)cr	1.780	0.101	5.682	3
Deans-1	19-18 (3-4)cr	1.885	0.027	1.413	3
Deans-1	27-4 (1-2)cr	1.713	0.037	2.179	3
Deans-1	27-14(2-2)cr	1.513	0.110	7.243	3
Outcrop	MS2cr	1.477	0.096	6.515	3
18B79	10-15.5	1.148	0.027	2.360	3
18B79	100-105.8	1.141	0.033	2.920	3
18B79	170-173.5	1.197	0.028	2.339	3
18B79	190-200	1.159	0.081	6.952	3
18B79	253-256	1.240	0.038	3.030	4
18B79	297-300	1.070	0.010	0.973	4
12GT80	80-85	1.101	0.047	4.305	2
12GT80	230-235	1.005	0.023	2.323	2
12GT80	338-345	1.285	0.057	4.459	2
12GT80	548-555	0.942	0.024	2.552	2
12GT80	585-590	1.222	0.045	3.654	4
12GT80	610-615	1.245	0.032	2.596	4
9GT80	435_440	1.138	0.021	1.864	3
9GT80	440_445	0.987	-	-	1

9GT80	460_465	1.251	0.043	3.449	2
9GT80	495_500	0.971	-	-	1
9GT80	500_504	1.040	-	-	1
1aGT80	535-540	1.123	0.054	4.785	2
1aGT80	560-565	0.964	0.021	2.128	2
1aGT80	572-580	1.199	0.022	1.829	2
5GT80	235_240	1.190	-	-	1
5GT80	270_275	1.319	0.032	2.413	2
5GT80	350_355	1.071	0.014	1.320	2
5GT80	355_360	1.119	-	-	1
5GT80	360_370.5	1.183	-	-	1
5GT80	390_392.5	1.253	0.013	1.016	2
5GT80	426_430	1.189	0.008	0.654	2
5GT80	431.5_435	1.269	0.016	1.226	2
5GT80	435_440	1.289	0.024	1.865	2
5GT80	440_445	1.289	0.018	1.426	2
5GT80	445_450	1.147	-	-	1
5GT80	454_460	1.127	0.045	4.016	2
5GT80	460_461.5	1.290	0.005	0.384	2
5GT80	465_470	1.310	-	-	1
5GT80	482_485	1.266	0.014	1.117	2
5GT80	485_493	1.214	0.007	0.582	2
5GT80	493_495	1.150	-	-	1
5GT80	495_500	1.236	0.018	1.431	2

Appendix F
Lithology and Stratigraphic Nomenclature of Unconsolidated Samples

Well	Interval/ Sample ID	Unit	Lithology
18B79	10-15.5	Harrison	silt to siltstone, sandy, clayey, light yellowish to brown
18B79	100-105.8	Harrison	sand, very fine to fine, medium brown, calcareous
18B79	170-173.5	Monroe Creek	brown to yellowish brown calcareous silt, sand & clay
18B79	190-200	Monroe Creek	brown to yellowish brown calcareous silt, sand & clay
18B79	253-256	Gering	brown to yellowish brown sand to sandstone, v.f. to fine
18B79	297-300	Gering	Yellowish brown sandy and clayey silt
12GT80	80-85	Brule	siltstone to silt, light yellowish brown, clayey
12GT80	230-235	Brule	brown siltstone, clayey, contains reddish brown clay
12GT80	338-345	Brule	light brown to brown silt and siltstone, reddish brown clay
12GT80	548-555	Chadron	silt, pale olive, bentonitic, contains siltstones
12GT80	585-590	Chadron	claystone, light greenish gray
12GT80	610-615	Chadron	clay, brownish yellow
9GT80	435_440	Pierre	shale, dark gray to black
9GT80	440_445	Pierre	shale, dark gray to black
9GT80	460_465	Pierre	shale, dark gray to black
9GT80	495_500	Pierre	shale, dark gray to black
9GT80	500_504	Pierre	shale, dark gray to black
1aGT80	535-540	Niobrara	limestone, dark olive gray
1aGT80	560-565	Niobrara	limestone, dark olive gray
1aGT80	572-580	Niobrara	limestone, dark olive gray
5GT80	235_240	Carlile	shale, dark gray
5GT80	270_275	Carlile	shale, dark gray, very thinly bedded limestones
5GT80	350_355	Carlile	shale, dark gray, very thin sandy interbeds
5GT80	355_360	Carlile	shale, dark gray, very thin sandy interbeds
5GT80	360_370.5	Carlile	shale, dark gray, very thin sandy interbeds
5GT80	390_392.5	Greenhorn	limestone, dark grayish brown
5GT80	426_430	Graneros	shale, dark gray and limestone, dark olive gray
5GT80	431.5_435	Graneros	shale, dark gray and limestone, dark olive gray
5GT80	435_440	Graneros	shale, dark gray, limy

5GT80	440_445	Graneros	shale, dark gray, limy
5GT80	445_450	Graneros	shale, dark gray, limy
5GT80	454_460	Dakota	sand, dark olive gray, very fine, shaley
5GT80	460_461.5	Dakota	sandstone, dark olive gray, very fine, shaley
5GT80	465_470	Dakota	shale, dark olive gray, very fine sand
5GT80	482_485	Dakota	sandstone, dark grayish brown, very fine, shaley
5GT80	485_493	Dakota	sandstone, dark grayish brown, very fine, shaley
5GT80	493_495	Dakota	shale, dark olive gray, soft, sand to sandstone
5GT80	495_500	Dakota	shale, dark olive gray, soft, sand to sandstone

Appendix G
Specifications of Wells Used in Cross-Section Construction

API	State	County	Latitude	Longitude	TD m	Elevation (m)	Transect Distance (km)
2705014	WY	Niobrara	42.75386	-104.6956	486	1663.2936	0
2705022	WY	Niobrara	42.81784	-104.6097	475	1631.5944	8
2705012	WY	Niobrara	42.69329	-104.3223	1129	1495.6536	30
2720559	WY	Niobrara	42.80947	-104.262	1417	1568.196	35
2705040	WY	Niobrara	42.89307	-104.0975	1547	1328.3184	50
26165211150000	NE	Sioux	42.84538	-103.973	1579	1284.1224	60
26165211270000	NE	Sioux	42.85107	-103.8452	1551	1187.5008	70
26165050940000	NE	Sioux	42.85848	-103.6876	1591	1174.6992	83
26165050910000	NE	Sioux	42.8175	-103.6095	1686	1313.9928	90
26045210660000	NE	Dawes	42.85461	-103.4175	1570	1071.9816	106
26045050430000	NE	Dawes	42.84096	-103.348	1277	1073.5056	110
26045210220000	NE	Dawes	42.86272	-103.2296	1507	1051.56	120
26045210530000	NE	Dawes	42.85153	-103.2155	1514	1067.4096	121
26045210140000	NE	Dawes	42.86649	-103.1805	1486	1040.2824	124
26045050420000	NE	Dawes	42.83392	-103.0894	1370	1002.792	131
26045050390000	NE	Dawes	42.80836	-102.8395	1263	1106.424	152
26161050200000	NE	Sheridan	42.74564	-102.5984	930	1191.768	172
26161210320000	NE	Sheridan	42.8555	-102.4955	1062	1184.7576	180
26161050230000	NE	Sheridan	42.80527	-102.3733	1128	1150.3152	190

REFERENCES

Anderson, M.P. (2005). Heat as a ground water tracer. *Groundwater 43(6)*, 951-968.

Andrichuk, J.M. (1955). Mississippian Madison group stratigraphy and sedimentation in Wyoming and southern Montana. *AAPG Bulletin, 39(11)*, 2170-2210.

Antriasian, A.M. (2010). The Portable Electronic Divided Bar (PEDB): a tool for measuring thermal conductivity of rock samples. *Proceedings World Geothermal Congress, Bali, Indonesia, 25-29 April 2010*, 7 p.

Anna, L.O. (1986). Geologic framework of the ground-water system in Jurassic and Cretaceous rocks in the northern Great Plains, in parts of Montana, North Dakota, South Dakota, and Wyoming. *U.S. Geological Survey Professional Paper 1402-B*, 36 p.

Bartram, J.G. (1940). The stratigraphy and structure of eastern Wyoming and the Black Hills area. *Kansas Geological Society, Western South Dakota and Eastern Wyoming: Guidebook, 14th Annual Field Conference*, 113-120.

Bass, N.W. (1958). Subsurface geology of the Dakota sandstone in the oil-fields area of the Denver Basin, Colorado and Nebraska. *U.S. Geological Survey Open File Report 58-10*, 23 p.

Beardsmore, G.R. & Cull, J.P. (2001). Crustal heat flow: a guide to measurement and modelling. *Cambridge University Press, 2001, New York, NY*.

Blackstone, D.L. Jr. (1996). Structural geology of the Laramie Mountains, southeastern Wyoming and northeastern Colorado. *Wyoming State Geological Survey Report of Investigations No. 51*, 36 p.

Bredehoeft, J.D., Neuzil, C.E., and Milley, P.C.D. (1983). Regional flow in the Dakota aquifer: a study of the role of confining layers. *U.S. Geological Survey Water Supply Paper 2237*, 45 p.

Breyer, J. (1975). The classification of Ogallala sediments in western Nebraska. In Smith, G.R., & Friedland, N.E. (eds.)*, Studies on Cenozoic paleontology and stratigraphy, Claude W. Hibbard Memorial, v. 3: Museum of Paleontology, University of Michigan, Papers on Paleontology no. 12*, p. 1-8.

Brown, D.L., Blankennagel, R.K., MacCary, L.M., & Peterson, J.A. (1984). Correlation of paleostructure and sediment deposition in the Madison Limestone and associated rocks in parts of Montana, North Dakota, South Dakota, Wyoming, and Nebraska. *U.S. Geological Survey Professional Paper 1273-B*, 32 p.

Burchett, R.R. (1969). Geologic bedrock map of Nebraska. Nebraska Geological Survey, 1:1,000,000 scale map.

Burchett, R.R. (1982). Thickness and structure maps of the Pennsylvanian and Permian rocks in Nebraska. *Conservation and Survey Division, University of Nebraska—Lincoln, Report of Investigations No. 7*, 15 p.

Burk, C.A., & Thomas, H.D. (1956). The Goose Egg formation (Permo-Triassic) of eastern Wyoming. *The Geological Survey of Wyoming Report of Investigations No. 6*, 11 p.

Cardinal, D.F. & Holmes, K.H. (1984). Lower Permian and Pennsylvanian stratigraphy and structure of the tri-state area, southeastern Wyoming, western Nebraska and southwestern South Dakota. *Thirty-Fifth Annual Field Conference: Wyoming Geological Association Guidebook*, 333-340.

Carlson, M. P. (1963). Mississippian system in northwestern Nebraska. *Rocky Mountain Association of Geologists, 14th Field Conf.,* 31-35.

Carlson, M.P. (1970). Distribution and subdivision of Precambrian and lower and middle Paleozoic rocks in the subsurface of Nebraska. *Conservation and Survey Division, University of Nebraska—Lincoln, Report of Investigations No. 3*, 23 p.

Carlson, M.P. (1993). Geology, geologic time and Nebraska. *Nebraska Geological Survey Centennial, Educational Circular No. 10*, 60 p.

Carlson, M.P. (1999) Transcontinental Arch; a pattern formed by rejuvenation of local features across central North America. In *Tectonics of Continental Interiors, Tectonophysics, v. 305*, 225-233.

Carlson, M.P. (2007). Precambrian accretionary history and Phanerozoic structures—A unified explanation for the tectonic architecture of the Nebraska region, USA. In Hatcher, R.D., Carlson, M.P., McBride, J.H., and Catalán, J.R.M. (eds.)*, 4-D Framework of Continental Crust, Geological Society of America Memoir 200*, 321-326.

Carter, J.M., Driscoll, D.G., Hamade, G.R., and Jarrell, G.J. (2001). Hydrologic budgets for the Madison and Minnelusa aquifers, Black Hills of South Dakota and Wyoming, water years 1987-96. *U.S. Geological Survey Water-Resources Investigations Report 01-4119*, 53 p.

Condra, G. E., Reed, E. C., & Scherer, O. J. (1940). Correlation of the formations of the Laramie Range, Hartville Uplift, Black Hills, and western Nebraska. *Nebraska Geological Survey Bulletin 13,* 50 p.

Condra, G.E. & Reed, E.C. (1959). The geological section of Nebraska. *Nebraska Geological Survey Bulletin Number 14A*, 82 p.

Cooley, M.E. (1986). Divisions of potential fracture permeability based on distribution of structures and linear features in sedimentary rocks, northern Great Plains—Rocky Mountains region of Montana, North Dakota, South Dakota,Wyoming, and northern Nebraska. *U.S. Geological Survey Miscellaneous Investigations Map 1-1687, scale 1:1,000,000, 1 sheet*.

Cooley, R.L., Konikow, L.F., & Naff, R.L. (1986). Nonlinear-regression groundwater flow modeling of a deep regional aquifer system. *Water Resources Research 22(13)*, 1759-1778.

Crowell, A.M., Ochsner, A.T., & Gosnold, W.D. (2012). Correcting bottom-hole temperatures in the Denver Basin: Colorado and Nebraska. *GRC Transactions, 36*, 201-206.

Crowell, A.M. and Gosnold, W.D. (2013). GIS-based geothermal resource assessment of the Denver Basin: Colorado and Nebraska. *GRC Transactions, 37*, 941-943.

Crowell, A.M. (2014). Personal communication with A.T. Ochsner on May 16, 2014.

Curtis, B.F. (1988). Sedimentary rocks of the Denver basin. In Sloss, L.L. (ed.)*, Sedimentary Cover—North American Craton, U.S. Geological Society of America, The Geology of North America, v. D-2, ch. 8*, 182-196.

Dahl, P.S., Holm, D.K., Gardner, E.T., Hubacher, F.A., & Foland, K.A. (1999). New constraints on the timing of Early Proterozoic tectonism in the Black Hills (South Dakota), with implications for docking of the Wyoming province with Laurentia. *Geological Society of America Bulletin, 111(9)*, 1335-1349.

Dahlstrom, D.J. & Fox, J.E. (1995). Fluvial architecture of the lower Cretaceous Lakota formation, southwestern flank of the Black Hills uplift, South Dakota. *U.S Geological Survey Bulletin 1917-S*, 20 p.

Degraw, H.M. (1969). Subsurface relations of the Cretaceous and Tertiary in western Nebraska. *M.S. Thesis, University of Nebraska-Lincoln*, 137 p.

Deming, D. (1994). Estimation of the thermal conductivity anisotropy of rock with application to the determination of terrestrial heat flow. *Journal of Geophysical Research*, 99(B11), 22087-91.

Denison, R.E., Lidiak, E.G., Bickford, M.E., & Kisvarsanyi, E.B. (1984). Geology and geochronology of Precambrian rocks in the Central Interior region of the United States. *U.S. Geological Survey Professional Paper 1241-C*, 26 p.

Downey, J.S. (1984). Geohydrology of the Madison and associated aquifers in parts of Montana, North Dakota, South Dakota, and Wyoming. *U.S. Geological Survey Professional Paper 1273-G*, 47 p.

Downey, J. S. (1986). Geohydrology of bedrock aquifers in the northern great plains in parts of Montana, North Dakota, South Dakota, and Wyoming. *U.S.Geological Survey Professional Paper 1402-E*, E1-E87, 95 p.

Downey, J.S. & Dinwiddie, G.A. (1988). The regional aquifer system underling the northern Great Plains in parts of Montana, North Dakota, South Dakota, and Wyoming—Summary. *U.S. Geological Survey Professional Paper 1402-A*, 64 p.

Duebendorfer, E.M., & Houston, R.S. (1987). Proterozoic accretionary tectonics at the southern margin of the Archean Wyoming craton. *Geological Society of America Bulletin, 98(5)*, 554-568.

Fetter, C.W. (2001). Applied Hydrogeology: Fourth Edition, Prentice-Hall, Inc., Upper Saddle River, NJ.

Fischer, D.W., LeFever, J.A., LeFever, R.D., Helms, L.D., Sorensen, J.A., Smith, S.A., Steadman, E.N., & Harju, J.A. (2005). Skull Creek formation outline. *Report compiled for the Plains CO_2 Reduction (PCOR) Partnership, Energy & Environmental Research Center, University of North Dakota*, 8 p.

Förster, A. and Merriam, D.F. (1995). A bottom-hole temperature analysis in the American midcontinent (Kansas): implications to the applicability of BHTs in geothermal studies. *World Geothermal Congress (Florence, Italy, 1995)*, 777-782.

Gosnold, W.D., Eversoll, D.A. & Carlson, M.P. (1981). Geothermal investigations in Nebraska: methods and results. *Geothermal Direct Heat Program, State Coupled Geothermal Resource Assesment Program: Glenwood Springs Technical Conference Proceedings, Volume I*, 187-203.

Gosnold, W.D., Eversoll, D.A. & Carlson, M.P. (1982). Three years of geothermal research in Nebraska. *Report to the U.S. Department of Energy State-Coupled Resource Assessment Meeting, Salt Lake City, UT, April 1982*, p. 142-157.

Gosnold, W.D. and Eversoll, D.A. (1983). An inventory of geothermal resources in Nebraska. *United States Department of Energy publication of work performed under contract No. AS07-79ET27205*, 291 p.

Gosnold, W.D. (1984). Heat flow and ground water movement in the central Great Plains. *in DG. Jorgensen and D.C. Signor (eds.), Geohydrology of the Dakota Aquifer, First C.V. Theis Conference on Geohydrologogy, National Water Well Association, Worthington, OH*, 176-181.

Gosnold, W.D. (1988). Analysis of heat flow and groundwater flow in the South Dakota geothermal anomaly. GRC Transactions 12, 251-255.

Gosnold, W.D. (1990). Heat flow in the great plains of the United States. *Journal of Geophysical Research 95(B1)*, 353-374.

Gosnold, W.D. Todhunter, P.E., & Schmidt, W. (1997). The borehole temperature record of climate warming in the mid-continent of North America. *Global and Planetary Change 15*, 33-45.

Gosnold, W.D. (1999). Basin-scale groundwater flow and advective heat flow: an example from the northern great plains. In Forster, A. & Marriam, D.F. (eds.), Computer Applications in the Earth Sciences: Geothermics in Basin Analysis, 99-116.

Gosnold, W.D., Majorowicz, J. Klenner, R., & Hauch, S. (2011). Implications of post-glacial warming for northern hemisphere heat flow. *GRC Transactions 35*, 795-799.

Gosselin, D.C., Papike, J.J., Zartman, R.F., Peterman, Z.E., & Laul, J.C. (1988). Archean rocks of the Black Hills, South Dakota: reworked basement from the southern extension of the Trans-Hudson orogen. *Geological Society of America Bulletin 100(8)*, 1244-1259.

Gott, G.B., Wolcott, D.E., & Bowles, C.G. (1974). Stratigraphy of the Inyan Kara Group and localization of uranium deposits, southern Black Hills, South Dakota and Wyoming. *U.S. Geological Survey Professional Paper 763*, 57 p.

Gries, J.P. (1977). Geothermal applications on the Madison (Pahasapa) aquifer system in South Dakota. Report prepared for the Department of Energy Division of Geothermal Energy and Idaho Operations Office under contract no. EY-76-C-07-1570, 102 p.

Gutentag, E.D., Heimes, F.J., Krothe, N.C., Luckey, R.R., & Weeks, J.B. (1984). Geohydrology of the High Plains aquifer in parts of Colorado, Kansas, Nebraska, New Mexico, Oklahoma, South Dakota, Texas, and Wyoming. U.S. Geological Survey Professional Paper 1400-B, 72 p.

Harrison, W.E., Prater, M.L., & Cheung, P.K. (1982). Geothermal assessment in Oklahoma. *In C.A. Ruscetta (ed.), Geothermal Direct Heat Program Roundup Technical Conference Proceedings, Vol. 1*, 187-204.

Helgesen, J.O. & Hansen, C.V. (1989). Description of data files compiled for the Central Midwest Regional Aquifer-System Analysis. U.S. Geological Survey Open File Report 89-42, 41 p.

Helgesen, J.O., Leonard, R.B., and Wolf, R.J. (1993). Hydrology of the Great Plains aquifer system in Nebraska, Colorado, Kansas, and adjacent areas. *U.S. Geological Survey Professional Paper 1414-E*, 80 p.

Hildebrand, T.G., and Kucks, R.P. (1985). Model of the geothermal system in southwestern South Dakota from gravity and aeromagnetic studies. in Hinze, W.J. (ed.), *The Utility of Regional Gravity and Magnetic Anomaly Maps: Soc. Expl. Geophys.*, 258-266.

Hoyt, J.H. (1963). Permo-Pennsylvanian correlations and isopach studies in the northern Denver Basin. In P. J. Katich and D. W. Bolyard, (eds.), *Geology of the northern Denver Basin and adjacent uplifts: 14th Annual Field Conference Rocky Mountain Association of Geologists*, 68-83.

Huan, J.D., & Barlow, J.A. (1962). Lower Cretaceous stratigraphy of Wyoming. In Enyert, R.L., & Curry, W.H. (eds.), *Symposium on Early Cretaceous Rocks of Wyoming and Adjacent Areas, 17th Annual Field Conference Guidebook*, Wyoming Geological Association, 15-22.

Huan, J.D. (1963). Stratigraphy of Dakota Group and relationship to petroleum occurrence, northern Denver Basin. In Bolyard, D.W., & Katisch, P.E. (eds.), *Geology of the northern Denver Basin and adjacent uplifts: 14th Annual Field Conference Guidebook, Rocky Mountain Association of Geologists*, 119-134.

Jorgensen, D.G., Helgesen, J.O., & Imes, J.L. (1993). Regional aquifers in Kansas, Nebraska, and parts of Arkansas, Colorado, Missouri, New Mexico, Oklahoma, South Dakota, Texas, and Wyoming—Geohydrologic framework. *U.S. Geological Survey Professional Paper 1414-B*, 72 p., 25 pl. in separate volume.

Kipp, K.L. Jr., Hsieh, P.A., & Charlton, S.R. (2008). Guide to the revised ground-water flow and heat transport simulator: HYDROTHERM—Version 3. *U.S. Geological Survey, Techniques and Methods 6-A25*, 178 p.

Kitely, L.W. (1977). Shallow marine deposits in the upper Cretaceous Pierre shale of the northern Denver Basin and their relation to hydrocarbon accumulation. *Rocky Mountain Association of Geologists 1977 Symposium, Exploration Frontiers of the Central and Southern Rockies*, 197-211.

Klasner, J.S., & King, E.R. (1986). Precambrian basement geology of North and South Dakota. *Canadian Journal of Earth Science, 23(8)*, 1083-1102.

Konikow, L.F. (1976). Preliminary model of ground-water flow in the Madison Group, Powder River Basin and adjacent areas, Wyoming, Montana, South Dakota, North Dakota, and Nebraska. *U.S. Geological Survey Water-Resources Investigations 63-75*, 44 p.

LaGarry, H.E. (1998). Lithostratigraphic revision and redescription of the Brule Formation (White River Group) of northwestern Nebraska. In Terry, D.O. (ed.), LaGarry, H.E. (ed.), & Hunt, R.M. Jr. (ed.), *Depositional Environments, Lithostratigraphy, and Biostratigraphy of the White River and Arikaree Groups (Late Eocene to Early Miocene, North America), Geological Society of America, Special Paper 325*, 63-91.

Love, J.D., & Christiansen, A.C. (1985). Geologic map of Wyoming. United State Geologic Survey, 1:500,000 scale map.

Lugn, A.L. (1934). Pre-Pennsylvanian stratigraphy of Nebraska. *AAPG Bulletin, 18(12)*, 1597-1631.

MacFadden, B.J., and Hunt, R.M. (1998). Magnetic polarity stratigraphy and correlation of the Arikaree Group, Arikareean (late Oligocene-early Miocene) of northwestern Nebraska. In *Terry, D.O. (ed.), LaGarry, H.E. (ed.), & Hunt, R.M. Jr. (ed.). Depositional Environments, Lithostratigraphy, and Biostratigraphy of the White River and Arikaree Groups (Late Eocene to Early Miocene, North America), Geological Society of America, Special Paper 325*, 143-165.

MacLachlan, J.C., and Bieber, A. (1963). Permian and Pennsylvanian geology of the Hartville Uplift—Alliance Basin—Chadron Arch area. In Bolvard, D.W., and Katich, P.J. (eds.), *Geology of the northern Denver Basin: 14th Annual Field Conference*, Rocky Mountain Association of Geologists, p. 84–94.

Martin, C.A. (1965). Denver Basin. *AAPG Bulletin 49(11),* 1908-1925.

Martin, J.E., Sawyer, J.F., Fahrenbach, M.D., Tomhave, D.W., & Schulz, L.D. (2004). Geologic map of South Dakota. *South Dakota Geological Survey General Map 10*, 1:500,000 scale map.

Maughn, E.K. (1967). Eastern Wyoming, eastern Montana, and the Dakotas. In McKee, E.D., Oriel, S.S., et al. (eds.), *Paleotectonic Investigations of the Permian System in the United States, Geological Survey Professional Paper 515*, 125-152.

McCormick, K.A. (2010). Precambrian basement terrane of South Dakota. *University of South Dakota and Department of Environment and Natural Resources Geological Survey Program, Bulletin 41*, 37 p.

McCoy, A.W. (1953). Tectonic history of Denver Basin. *AAPG Bulletin 37(8)*, 1873-1893.

McCrae, R. O. (1956). Subsurface stratigraphy of the pre-Niobrara formations in the Julesburg Basin, southeastern Wyoming. In Burk, C.A., Anderman, G.G., Berg, R.R., et al. (eds.), *Wyoming Stratigraphy, Part 1: Subsurface Stratigraphy of the Pre-Niobrara Formations in Wyoming*, Wyoming Geological Association 85-89.

McGregor, D.J. (state geologist; no author cited). (1972). Geologic map of the Black Hills. *South Dakota Geological Survey Educational Series Map Five*.

McKaskey, J.D.R.G. (2013). Hydrogeologic framework for the Madison and Minnelusa Aquifers in the Black Hills area. *Master of Science Thesis, South Dakota School of Mines and Technology, Rapid City, South Dakota*, 56 p.

Moore, V. A. & Nelson, R. B. (1974) Effect of Cambridge-Chadron structural trend on Paleozoic and Mesozoic thickness, western Nebraska. *American Association of Petroleum Geologists Bulletin 58 (2), February 1974*, 260-268.

Momper, J. A. (1963). Nomenclature, lithofacies and genesis of Permo-Pennsylvanian rocks; northern Denver Basin. In Bolvard, D.W., and Katich, P.J. (eds.), *Guidebook to the Geology of the Northern Denver Basin and Adjacent Uplifts: 14th Annual Field Conference, Rocky Mountain Association of Geologists*, 41–47.

Montgomery, S.L., Goolsby, S., & Pierini, D. (1998). Permian (Wolfcampian) Admire "C": new exploratory potential in the northern Denver Basin. *AAPG Bulletin 82(12)*, 2173-2191.

Morgan, P. & Gosnold, W.D. (1972). Heat flow and thermal regimes in the continental United States. *Geological Society of America Memoir 172*, 493-522.

Mudge, M.R. (1967). Central midcontinent region. In McKee, E.D., Oriel, S.S., et al. (eds.), *Paleotectonic Investigations of the Permian System in the United States, Geological Survey Professional Paper 515*, 97-123.

Naus, C.A., Driscoll, D.G., and Carter, J.M. (2001). Geochemistry of the Madison and Minnelusa aquifers in the Black Hills area, South Dakota. *U.S. Geological Survey Water-Resources Investigations Report 01-4129*, 118 p.

Nolan, B.T., Healy, R.W., Taber, P.E., Perkins, K., Hitt, K.J., & Wolock, D.M. (2007). Factors influencing ground-water recharge in the eastern United States. *Journal of Hydrology 332*, 187-205.

Oldham, D.W. (1996). Permian salt in the Northern Denver Basin: controls on occurrence and relationship to oil and gas production from Cretaceous reservoirs. In M.W. Longman & M.D. Sonnenfeld (eds.), *Paleozoic Systems of the Rocky Mountain Region, Rocky Mountain Section, SEPM (Society for Sedimentary Geology)*, 335-354.

Peterson, J.A. (1984). Stratigraphy and sedimentary facies of the Madison limestone and associated rocks in parts of Montana, Nebraska, North Dakota, South Dakota, and Wyoming. *U.S. Geological Survey Professional Paper 1273-A*, 32 p.

Petty, D.M. (2003). Sequence stratigraphy of the Pahasapa Formation (Madison Group) in the Northeastern Black Hills: insights from regional correlations. *The Mountain Geologist, 40(2)*, 19-34.

Pipiringos, G.N., & O'Sullivan, R.B. (1978). Principal unconformites in Triassic and Jurassic rocks, Western Interior United States—A preliminary survey. *U.S. Geological Survey Professional Paper 1035-A*, 29 p.

Prichard, G.E. (1975). Nebraska and adjoining parts of South Dakota and Wyoming. *in* MecKee, E.D. and Crosby, E.J., coordinators, *Introduction and regional Analyses of the Pennsylvanian System in the United States, U.S. Geological Survey Professional Paper 853, pt. 1*, 115-126.

Randall, A.G. (1963). Catalog of formation names for northern Denver Basin and adjacent areas. In P. J. Katich and D. W. Bolyard, (eds.), *Geology of the northern Denver Basin and adjacent uplifts: 14th Annual Field Conference Rocky Mountain Association of Geologists*, 6-22.

Robertson, E.C. (1988). Thermal properties of rocks. *U.S. Geological Survey Open-File Report 88-441*, 106 p.

Robinson, C.S., Mapel, W.J., & Bergendahl, M.H. (1964). Stratigraphy and structure of the northern and western flanks of the Black Hills uplift, Wyoming, Montana, and South Dakota. *U.S. Geological Survey Professional Paper 404*, 134 p.

Rothrock, E.P. (1949). *Structures south of the Black Hills. South Dakota Geological Survey Report of Investigations No. 62*, 52 p.

Rothrock, D.P. (1960). Devonian and Mississippian systems in Colorado. *Guide to the Geology of Colorado, Rocky Mountain Association of Geologists*, 17-22.

Roy, R.F., Blackwell, D.D. & Decker, E.R. (1972). Continental heat flow. *In E.C. Robertson (ed.), The Nature of the Solid Earth, Ch. 19*, 506-544.

Sando, W.J. & Sandberg, C.A. (1987). New interpretations of Paleozoic stratigraphy and history in the northern Laramie Range and vicinity, southeast, Wyoming. *U.S. Geological Survey Professional Paper 1450*, 39 p.

Saar, M.O. (2011). Review: geothermal heat as a tracer of large-scale groundwater flow and as a means to determine permeability fields. *Hydrogeology Journal 19*, 31-52.

Sass, J.H., Lacenbruch, A.H., & Munroe, R.J. (1971a). Thermal conductivity of rocks from measurements on fragments and its application to heat flow determinations. *Journal of Geophysical Research*, 76(14), 3391-4301.

Sass, J.H., Lacenbruch, A.H., & Munroe, R.J. (1971b). Heat flow in the western United States. *Journal of Geophysical Reasearch, 76(26)*, 6376-6413.

Schultz, L.G., Tourtelot, H.A., Gill, J.R., & Boerngen, J.G. (1980). Composition and properties of the Pierre Shale and equivalent rocks, northern Great Plains region. *U.S. Geological Survey Professional Paper 1064-B*, 114 p.

Schoon, R.A. & McGregor, D.J. (1974). Geothermal potentials in South Dakota. *South Dakota Geological Survey, Report of Investigations No. 110*, 79 p.

Signor, D.C., Helgesen, J.O., Jorgensen, D.G., and Leonard, R.B. (1996). Geohydrology and simulation of steady-state flow conditions in regional aquifer systems in Cretaceous and older rocks underlying Kansas, Nebraska, and parts of Arkansas, Colorado, Missouri, New Mexico, Oklahoma, South Dakota, Texas, and Wyoming. *U.S. Geological Survey Professional Paper 1414-C*, 105 p.

Sims, P.K. and Day, W.C. (1999). Geologic map of Precambrian rocks of the Hartville Uplift, southeastern Wyoming. *U.S. Geological Survey Pamphlet to Accompany Geologic Investigations Series I-2661*, 30 page pamphlet and 1: 48,000 scale map.

Sims, P.K., Finn, C.A. & Rystrom, V.L.(2001). Preliminary Precambrian basement map showing geologic—geophysical domains, Wyoming. *U.S. Geological Survey Open-File Report 2001-199*, 12 p.

Sims, P.K. & Petermar, Z.E. (1986). Early Proterozoic Central Plains orogeny: a major buried structure in the north-central United States. *Geology*, 14(6), 488-491.

Schmitt, G.T. (1953). Regional stratigraphic analysis of middle and upper marine Jurassic in northern Rocky Mountains—Great Plains. *AAPG Bulletin 37(2)*, 355-393.

Smith, L., & Chapman, D.S. (1983). On the thermal effects of groundwater flow. *Journal of Geophysical Research, 88(1)*, 593-608.

Sonnenberg, S.A., and Weimer, R.J. (1981). Tectonics, sedi-mentation, and petroleum potential, northern Denver Basin, Colorado, Wyoming, and Nebraska. *Colorado School of Mines Quarterly, 76(2)*, 45 p.

Stach, R.L. (1972). Mineralogy and stratigraphy of the Niobrara formation, South Dakota. University of South Dakota, *M.S. Thesis*, 53 p.

Stanton, J.S., Qi, S.L., Ryter, D.W., Falk, S.E., Houston, N.A., Peterson, S.M. Westonbroek, S.M., & Christenson, S.C. (2011). Selected approaches to estimate water-budget components of the High Plains, 1940 through 1949 and 2000 through 2009. U.S. Geological Survey Scientific Investigations Report 2011-5183, 79 p.

Stix, J. (1982). Seasat satellite investigation of the structure of western Nebraska and its application to the evaluation of geothermal resources. *U.S. Department of Energy Publications, Los Alamos National Laboratory*, 15 p.

Tenney, C.S. (1965). Pennsylvanian and lower Permian deposition in Wyoming and adjacent areas. *AAPG Bulletin, 50(2)*, 227-250.

Terry, D.O. (1998). Lithostratigraphic revision and correlation of the lower part of the White River Group: South Dakota to Nebraska. In Terry, D.O. (ed.), LaGarry, H.E. (ed.), & Hunt, R.M. Jr. (ed.), *Depositional Environments, Lithostratigraphy, and Biostratigraphy of the White River and Arikaree Groups (Late Eocene to Early Miocene, North America), Geological Society of America, Special Paper 325*, 15-37.

Tromp, P.L., Cardinal, D.F., & Steidmann, J.R. (1981). Stratigraphy and depositional environments of the "Leo Sands" in the Minnelusa formation, Wyoming and South Dakota. *Thirty-Second Annual Field Conference, Wyoming Geological Association Guidebook*, 11-22.

USGS, 2013, Jan 15, Geologic Unit: Englewood, National Geologic Map Database (NGMDB), Geologic Names Lexicon (GEOLEX), retrieved February 24, 2014, from http://ngmdb.usgs.gov/Geolex/NewUnits/unit_7638.html.

Waage, K.M. (1959). Stratigraphy of the Inyan Kara group in the Black Hills. *U.S. Geological Survey Bulletin 1081-B*, 90 p.

Weimer, R.J. (1978). Influence of Transcontinental Arch on Cretaceous marine sedimentation: a preliminary report. In Pruit, J.D., & Coffin, P.E. (eds.) *Energy Resources of the Denver Basin*, Rocky Mountain Association of Geologists 1978 Symposium, 211-222.

Wilson, J.M. (1978). Permo-pennsylvanian of the west-central Nebraska panhandle. In Pruit, J.D. and Coffin, P.E. (eds.), *Energy Resources of the Denver Basin: Denver Rocky Mountain Association of Geologists*, 129-140.